

FORUM HOLZBAU INTERNATIONAL

26th International Wood Construction Conference (IHF)

Master Colloquium

Volume III December 1, 2022

Practical experience – Practical application

BETH BIEL
TH ROSENHEIM
UNI AALT OHELSINKI
TU MUNICHEN
UNBC PRINCE GEORGE
TU WIEN

Content MASTER COLLOQUIUM

Lateral Load Transfer in Multi-story Timber Modular Buildings	4
<i>Lukas Kotrbaty, Sweco Structural Engineering, Aalto University, Helsinki, Finland</i>	
Experimental determination of the rotational stiffness and moment capacity of connections in CLT buildings	14
<i>Jenny Abrahamsson, Linnaeus University, Halmstad, Sweden</i>	
<i>Filip la Fleur, Linnaeus University, Växjö, Sweden</i>	
Investigation of the Impact of Micro Structuring on Bonding Behaviour of Beechwood	26
<i>Destin B. Moanda, Bern University of Applied Sciences, Biel/Bienne, Switzerland</i>	
Investigation of Fleural Properties of Glued Laminated Timber Composed of Oil Palm Wood	40
<i>Martin Hackel, Technische Hochschule Ostwestfalen-Lippe, Lemgo, Germany</i>	
Real-time digital collaboration interphases for timber structure analysis and calculation	52
<i>Matias Penroz, Bern University of Applied Sciences, Biel/Bienne, Switzerland</i>	
Analysis and evaluation of mass data for production planning and system configuration	66
<i>Niki Karatza, Rosenheim Technical University of Applied Sciences /holzbau.tech, Rosenheim, Germany</i>	
b-CTC	
Bent-Computational Tooth Construction - ITECH Masterthesis	73
<i>Miro Bannwart, Bern University of Applied Sciences, Biel/Bienne, Switzerland</i>	
Degrees of Parametrization:	
Rewiring design-to-construction for prefab modular products	86
<i>Alejandro Arruñada, Rosenheim Technical University of Applied Sciences, Rosenheim, Germany</i>	

Moderation and welcome

Gertiser Christa

Bern University of Applied Sciences
Solothurnstrasse 102
2500 Biel/Bienne, Schweiz
+41 32 344 02 50
christa.gertiser@bfh.ch

Prof. Heinzmann Andreas

Rosenheim Technical University
of Applied Sciences
Hochschulstrasse 1
83024 Rosenheim, Deutschland
+49 8031 805 23 08
andreas.heinzmann@fh-rosenheim.de

Prof. Dr. Sigrist Christophe

Bern University of Applied Sciences
Solothurnstrasse 102
2500 Biel/Bienne, Schweiz
+41 32 344 03 76
christophe.sigrist@bfh.ch

Speakers

Abrahamson Jenny

Linnaeus University
Lückligsplats 1
35195 Växjö, Schweden
+46 708 18 34 25
nennyabrahamsson@gmail.com

Arrunada Alejandro

Rosenheim Technical University
of Applied Sciences
Hochschulstrasse 1
83024 Rosenheim, Deutschland
+1 210 214 5025
aj.arrunada@gmail.com

Bannwart Miro

University Stuttgart
Keplerstrasse 11
70174 Stuttgart, Deutschland
+41 32 344 02 24
miro.bannwart@bfh.ch

Hackel Martin

Technische Hochschule Ostwestfalen-Lippe
Campusallee 12
32657 Lemgo, Deutschland
+49 5261 702 50 62
martin.hackel@th-owl.de

Karatza Niki

Rosenheim Technical University
of Applied Sciences
Hochschulstrasse 1
83024 Rosenheim, Deutschland
+49 163 790 48 78
niki.karatza@holzbau.tech

Kotrbaty Lukas

Aalto University
Otakaari 1B
00076 Aalto, Finnland
+35 846 545 88 71
luk.kotrbaty@gmail.com

Ia Fleur Filip

Linnaeus University
Lückligsplats 1
35195 Växjö, Schweden
+46 736 42 66 24
filiplafleur97@gmail.com

Moanda Destin B.

Bern University of Applied Sciences
Solothurnstrasse 102
2500 Biel/Bienne, Schweiz
+41 32 344 17 37
destin.bamokinamoanda@bfh.ch

Penroz Matias

Bern University of Applied Sciences
Solothurnstrasse 102
2500 Biel/Bienne, Schweiz
+41 32 344 02 51
matias.penroz@bfh.ch

Lateral Load Transfer in Multi-story Timber Modular Buildings

Lukas Kotrbaty
Sweco Structural Engineering
Aalto University
Helsinki, Finland



Lauri Lepikonmäki
Sweco Structural Engineering
Tampere, Finland



Gerhard Fink
Aalto University
Espoo, Finland



Lateral Load Transfer in Multi-story Timber Modular Buildings

1. Introduction

Modular timber buildings are economical, time-efficient and, for countries with sustainable forestry, an environmentally friendly alternative to conventional constructions. Engineers, nowadays, look for an efficient way of using the high level of prefabrication in the multi-story buildings. This paper aims to contribute to the development of the multi-story timber modular buildings (MSTMBs) by investigating their reaction on lateral loads.

In multi-story buildings without an additional lateral load resisting system, wind and other horizontal loads must be safely transferred through intermediate floors and shear walls down to the foundations. The lateral load distribution to the shear walls is affected by the stiffness of the intermediate floors [1]. For the preliminary stage of design, building codes offer guidance whether to assume the intermediate floor as rigid or flexible (e.g. [2][3]). However, none of these approaches describe semirigid discontinuous behavior of intermediate floors, which is typical for MSTMBs. A couple of studies suggest simplified methods (e.g. [1][4][5]) applicable for the load transfer, yet none of them investigated MSTMBs specifically. In this paper, we introduce a 2D finite element model (FEM) and we demonstrate its application for the lateral load distribution analysis in MSTMBs.

The project was carried out as a Master thesis [6] at Aalto university in cooperation with Sweco Structural Engineering. Selected parts of the Master thesis are presented in this paper.

2. 2D FEM

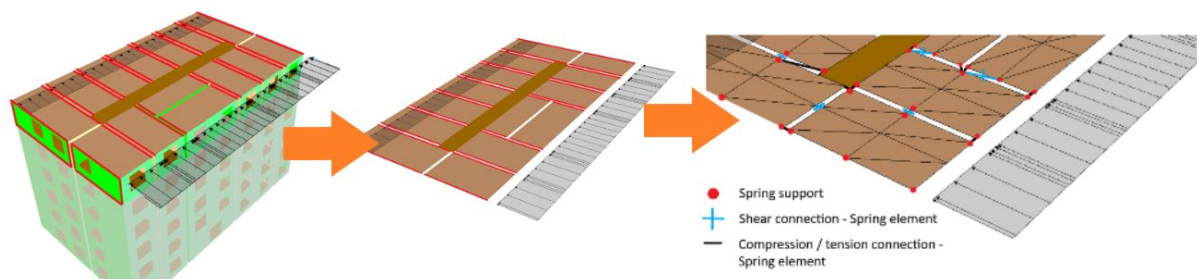


Figure 1: Modelling of MSTMB with the use of 2D FEM.

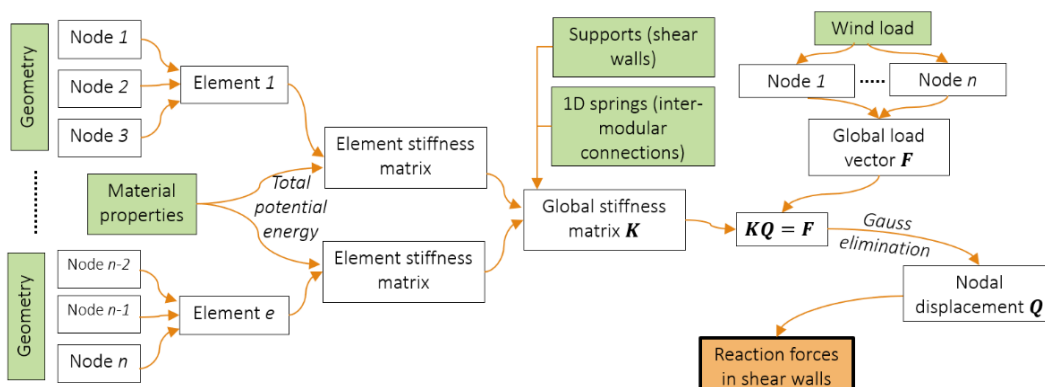


Figure 2: System of 2D FEM for lateral load distribution analysis. Input data in green cells, output in orange cell.

MSTMBs are modelled in 2D space, where the intermediate floor is represented by thin solid bodies (see Figure 1). These bodies, which represent both the individual modular plates and the corridor plates, are connected with 1D springs. The springs are analogous to the shear and compression/tension connections at the floor level. The plane model is supported by spring supports, which represent the shear walls.

The supporting spring can include not only the shear stiffness of the shear wall but also the effects of other possible stiffness contributions such as the bending deflection of the

shear wall, the stiffness of the wall-to-floor connection and the deformation of the vibration insulation. Each story of the building is modelled separately starting from the roof. In order to obtain maximum shear forces in the first floor, the forces from the upper floors are summed up. This linear analysis is carried out by plane stress considering elastic regions of deformation using constant strain triangular (CST) finite elements. The whole procedure from the input data to the results is outlined in Figure 2. The described 2D FEM can be implemented in any numerical-analysis software. For the purpose of this work, Microsoft Excel 2016 with VBA (Visual Basic for Applications) is used.

3. Reference building

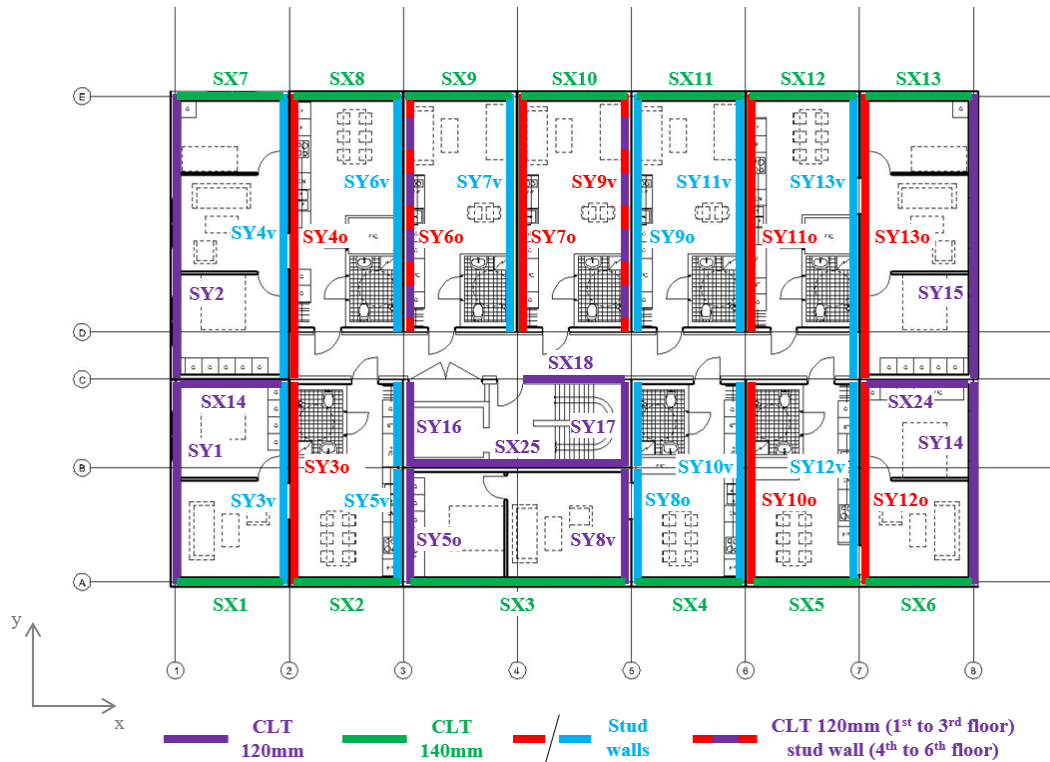


Figure 3: Positions and types of the shear walls in the studied MSTMB [7].

In this work, the lateral load distribution is studied on a 22,0 m high 6 story timber modular building (length 29.3 m, width 17.8 m) with a floor height of 3,15 m. All room modules are prefabricated volumetric elements. The vertical structures of the modules are either CLT or timber-gypsum stud walls. The positions and the types of the shear walls are illustrated in Figure 3. In this project, most of the walls are designed as shear walls, even though they are coupled (e.g. SY6o and SY6v). The MSTMB was designed according to Eurocode and Swedish national annexes EKS11 [8] and a detailed 3D FE model was created in RFEM 5.18 as a part of the design.

4. 2D FEM validation

As there are no measured data from site, the results obtained from 3D FEM (RFEM 5.18 model) represent the most precise available data of the lateral load distribution in the MSTMB and they are taken as a reference. Additionally, the 2D FEM is compared with two other simplified methods, which are used in engineering practice for the lateral load distribution. The results for the y direction are illustrated in this paper.

Table 1: Lateral load distribution by 3D FEM (left) and 2D FEM (right) in y direction, relative values.

Y	3D FEM [%]						2D FEM [%]					
	floor						floor					
	1st	2nd	3rd	4th	5th	6th	1st	2nd	3rd	4th	5th	6th
SY1	7	7	7	7	7	7	6	6	6	6	6	6
SY2	8	9	9	10	10	11	7	8	8	9	9	9
SY3v	1	1	1	1	1	1	2	1	1	1	1	1
SY3o	1	1	1	0	0	-2	2	2	1	1	1	1
SY4v	2	2	3	3	4	4	3	2	2	3	3	3
SY4o	2	2	2	2	3	3	2	2	2	2	2	2
SY5v	1	2	2	2	2	1	2	2	2	2	2	2
SY5o	6	5	4	3	3	3	6	6	6	5	5	5
SY6v	2	2	3	4	4	4	2	2	2	2	2	2
SY6o	9	8	8	6	4	4	7	8	8	8	8	7
SY7v	2	2	3	4	5	6	2	2	2	2	2	3
SY7o	2	2	3	4	4	5	2	2	2	2	2	3
SY8v	5	4	4	3	3	3	5	5	4	4	3	3
SY8o	2	2	1	1	1	0	2	2	2	2	2	2
SY9v	9	9	9	8	6	6	8	8	9	9	8	8
SY9o	3	3	3	3	3	4	2	2	2	2	3	3
SY10v	2	2	2	2	2	1	3	3	3	3	3	2
SY10o	2	2	2	2	1	1	3	3	3	3	3	2
SY11v	3	3	3	3	4	5	3	3	3	3	3	3
SY11o	3	3	3	3	3	3	3	3	3	3	3	3
SY12v	2	2	2	1	1	0	2	2	2	2	1	1
SY12o	2	2	2	2	2	2	2	2	2	1	1	1
SY13v	2	2	2	2	2	2	2	2	2	2	2	2
SY13o	2	3	3	3	3	4	3	3	3	3	3	3
SY14	8	7	7	7	7	8	6	6	6	6	7	7
SY15	8	9	9	10	10	11	8	9	9	9	10	10
SY16	3	2	2	1	1	0	3	3	3	3	2	2
SY17	2	2	2	3	4	3	4	4	3	3	3	3
SUM	100	100	100	100	100	100	100	100	100	100	100	100

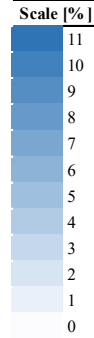
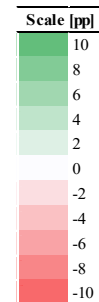


Table 2: Comparison of the simplified methods with the reference 3D FEM in y direction. Values in percentage points [pp] are obtained by subtraction of the 3D FEM results [%] from the given method results [%].

Δ [pp] = given method [%] - 3D FEM [%]												
Y	2D FEM [pp]						Tributary areas [pp]					
	floor						floor					
	1st	2nd	3rd	4th	5th	6th	1st	2nd	3rd	4th	5th	6th
SY1	-1	-1	-1	-1	-1	-1	-4	-4	-4	-4	-4	-4
SY2	-1	-1	-1	-1	-1	-1	-4	-5	-5	-6	-6	-7
SY3v	0	0	0	0	0	0	2	1	1	1	2	1
SY3o	0	1	1	1	1	3	2	2	2	3	3	5
SY4v	1	0	0	-1	-1	-2	2	2	2	1	1	0
SY4o	0	0	0	-1	-1	-1	2	2	2	2	1	1
SY5v	1	0	0	0	0	1	2	1	1	1	2	2
SY5o	0	1	2	2	2	2	1	2	2	2	3	3
SY6v	0	0	-1	-2	-2	-2	2	2	1	0	0	-1
SY6o	-2	-1	0	2	3	3	-7	-6	-5	-2	0	0
SY7v	0	0	0	-1	-2	-3	-1	-2	-2	-3	-5	-5
SY7o	0	0	0	-1	-2	-2	-1	-2	-2	-3	-4	-5
SY8v	0	1	1	0	0	0	2	3	3	2	3	3
SY8o	0	0	1	1	1	2	1	1	2	2	2	3
SY9v	-1	-1	-1	1	3	2	-6	-6	-6	-4	-2	-2
SY9o	-1	-1	-1	-1	-1	-1	1	1	1	1	1	1
SY10v	0	1	1	1	1	1	1	1	1	1	1	2
SY10o	0	1	1	1	1	1	1	1	1	2	2	2
SY11v	0	0	0	-1	-1	-2	1	1	1	0	0	-1
SY11o	0	0	0	0	0	0	1	1	1	1	1	1
SY12v	0	0	0	0	1	2	1	1	2	2	3	3
SY12o	0	0	0	0	0	-1	1	1	1	1	1	1
SY13v	0	0	0	0	0	0	2	2	2	2	2	2
SY13o	1	0	0	0	-1	-1	2	2	1	1	1	1
SY14	-2	-1	-1	-1	-1	-1	-4	-4	-4	-4	-4	-4
SY15	0	0	0	0	0	-1	-5	-5	-5	-6	-6	-7
SY16	1	1	1	1	1	2	2	3	3	3	3	4
SY17	2	1	1	0	-1	0	3	2	2	2	1	1



The 3D FEM is based on geometrically linear analysis. The target length of the finite elements is 0,3 m. All load-bearing walls, ceiling structures and floor structures are modelled as 2D plate elements. The intra-module connections are modelled with line hinges and the inter-module connections with 1D members. All structural elements as well as all joints are modelled with their actual stiffness properties. The lateral load is assigned as line load to each floor.

All input data for the 2D FEM imitate the input data for the 3D FEM. However, several deviations in the input data are observed as the 2D FEM represents simplified method. For instance, ceiling structures of the volumetric elements, as well as uplift connections are not considered in the 2D FEM. Also, the finite element mesh is sparser in the 2D FEM than in the 3D FEM. There are 8 finite elements per modular plate in the 2D FEM, which means 1,4 – 5,2 m long finite elements depending on the size of the modular plate.

In order to compare the results from the 2D FEM and the 3D FEM, the lateral load distribution is expressed in relative values considering that the sum of the lateral load in each floor is equal to 100 %. It can be observed that with both models the critical walls could be identified (see Table 1). The qualitative values are similar, the slight differences are caused by variations in the input data such as different stiffness properties of the walls (SY60 and SY9v), which change their materials over the floors. However, in both directions, the developed 2D FEM shows the same trend of the lateral load distribution as the 3D FEM.

The 2D FEM is compared to other methods. First, «tributary areas» method is based on an assumption of discontinuous and flexible intermediate floor. In that case, the lateral load is distributed to the shear walls based on the tributary areas. Second, a rigid intermediate floor with no inter-module connections in the floor level is assumed in «rigid floor» method. In both, only shear stiffness of the shear walls is taken into account. The results from all the simplified methods are expressed with deviations from the reference 3D FEM in Table 2.

The 2D FEM shows a wider agreement with the 3D FEM compared with the other simplified methods in y direction. In x direction, also the rigid floor method gives satisfactory results despite the several deviations. Anyhow, the wide agreement indicates that the presented 2D FEM is suitable for the lateral load distribution in the preliminary stage of MSTMBs projects.

5. Parameter study

Using the developed 2D FEM, five parameters that determine the lateral load distribution are studied: (i) stiffness of the inter-module connections, (ii) stiffness of the modular plates forming the intermediate floor, (iii) total stiffness of the shear walls, (iv) in-plane bending stiffness of the shear walls and (v) positions of the shear walls. The individual parameters are studied on different small layouts, although the input data, which are invariable in the parameter study, are taken from the reference building (chapter 3).

5.1. Stiffness of the inter-module connections

On a simple one-story layout consisting of 3 identical modules 3 x 6 m (Figure 4), the effect of stiffness of the inter-module compression/tension connections on the lateral load distribution is analysed. The LVL frame with OSB sheathing works as an intermediate floor transferring the lateral load into the shear walls. The shear walls are stud walls with timber studs 48 x 123 mm spacing 400 mm and gypsum sheathing.

A considerable effect, which could be amplified in more sophisticated layouts of MSTMBs, is noticed. If the stiffness of the inter-module connections is small compared to the stiffnesses of the structural elements, the lateral load is not substantially distributed to the modular plates, which are located further away from the lateral load action. This may lead to excessively large shear forces in the shear walls of the modules, which are directly exposed to the lateral load. In this example, for a stiffness of the inter-module connection 30kN/mm, the shear force in the shear walls of module 3 is about 1,5 times larger than the shear force in module 1. If the connection is designed with a smaller stiffness 10kN/mm, the shear force in module 3 is even 2,5 times larger than in module 1 (see Figure 4).

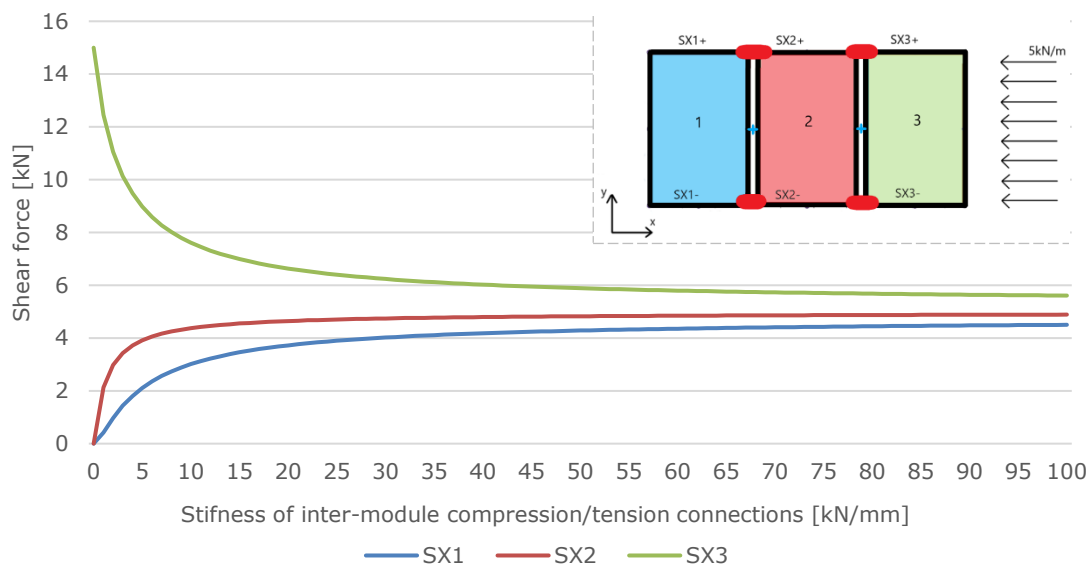


Figure 4: Effect of inter-module compression/tension connections on the lateral load distribution. The numbering of the shear walls corresponds to the numbering of the modules.

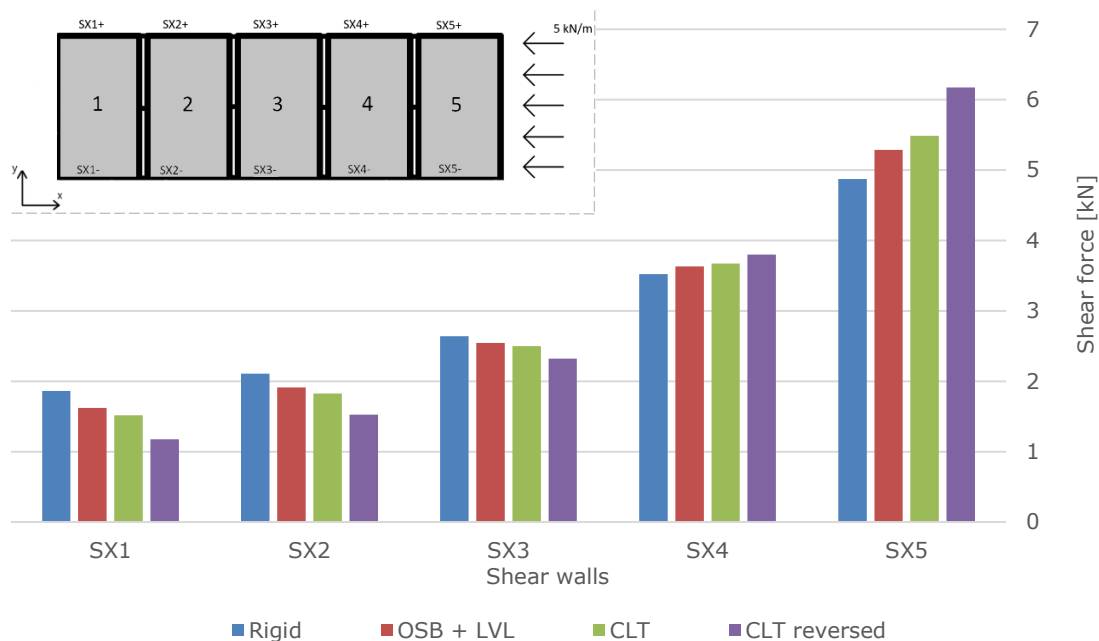


Figure 5: Effect of stiffness of the modular plates in the intermediate floor on the lateral load distribution. The numbering of the shear walls corresponds to the numbering of the modules.

5.2. Stiffness of the modular plates in the intermediate floor

Three different structural types of the intermediate floor are compared with the rigid assumption. The LVL frame with OSB sheathing taken from the reference building is studied together with 140 mm thick (40-20-20-20-40) CLT panels. CLT panels spanned in both directions are investigated. The building layout follows the same principle as in the previous example but with five identical modules 3 x 6 m placed behind each other (see Figure 5). The lateral load is assigned from the right side, thus, module 5 is the closest to the lateral load action.

If the floor is modelled as rigid (blue column in Figure 5), the shear force in the shear wall SX5 is 2.6x larger than in the SX1. While for the LVL frame and OSB sheathing, there is 3.2x more lateral load in the walls SX5 compared with the SX1. Thus, the importance of

taking into account the actual stiffness, instead of assuming the modular plates of the intermediate floor being rigid, is outlined. Furthermore, the study shows the differences in the lateral load distribution when comparing CLT panels spanned transversely.

5.3. Total stiffness of the shear walls

In order to study how the lateral load is distributed into two shear walls with different stiffnesses, a single module 6 x 3 m is analysed. The module is composed of LVL ceiling and 4 shear walls (see Figure 6). The total stiffness of one of the shear walls (SX1+) is taken as a variable, which varies from 0 to 50 kN/mm. The rest of the shear walls have constant stiffness 5 kN/mm.

The lateral load is distributed to the two parallelly positioned shear walls relatively evenly, although there is a significant difference in their stiffnesses (see Figure 6). The load distribution is dependent also on the stiffness of the transversely positioned shear walls, on the vertical connections between the walls (considered as rigid in this study), and on the stiffness of the intermediate floor. However, we can conclude, that the lateral load is not necessarily distributed to the shear walls in the exact proportion of their stiffnesses.

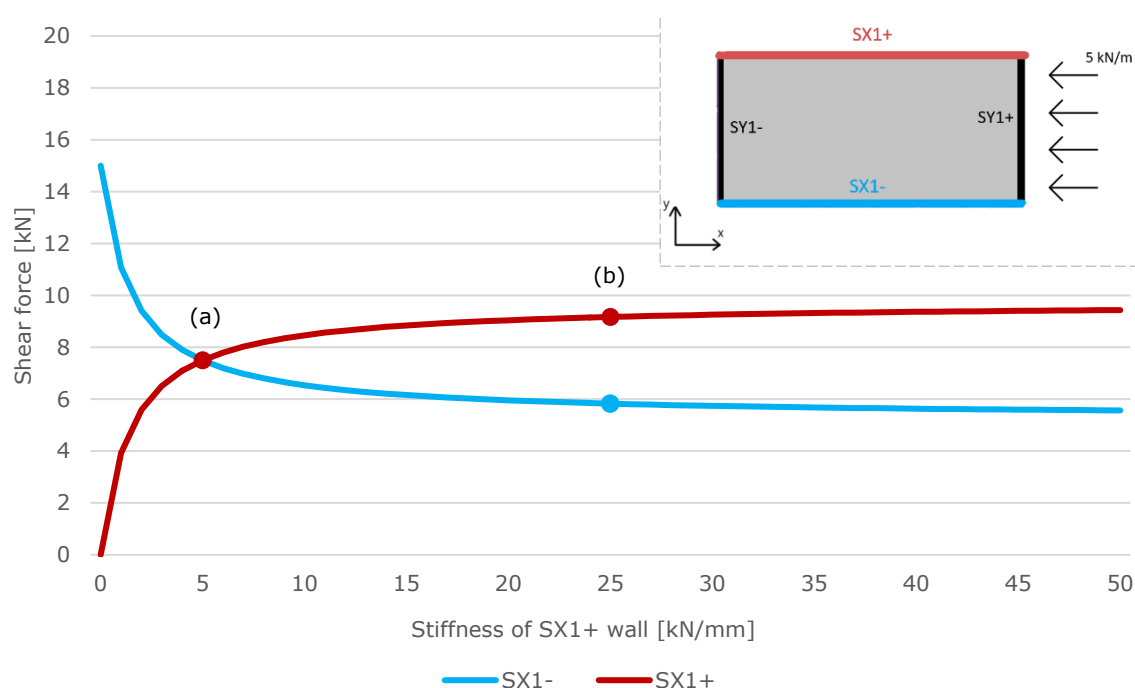


Figure 6: Effect of stiffness of the shear walls on the lateral load distribution. (a) Stiffness of SX1+ is equal to stiffness of SX1- (both walls as stud walls). (b) Stiffness of SX1+ is 5x larger than stiffness of SX1- (CLT 120 mm vs. stud wall).

5.4. In-plane bending stiffness of the shear walls

The in-plane bending stiffness depends on the height and the length of the shear walls [9]. Therefore, if some of the shear walls vary in their lengths, the load distribution should differ with the height of the building.

Three-module layout is drawn (Figure 7) so that the bottom half consists of two small (red) modules 2,85 x 3 m, whereas there is one large (blue) module 6 x 3 m at the top half. All the walls of all three modules are designed as CLT walls, and they all work as shear walls. Their stiffnesses, therefore, differ only because of their lengths and heights (number of floors). All the levels from the single-story (3,1 m high) to the six-story (6 x 3,1 m high) building are evaluated, meaning, six individual sub-analyses are carried out. The aim of this study is to find out the difference in the shear forces between the blue part (module 3) and the red part (modules 1,2).

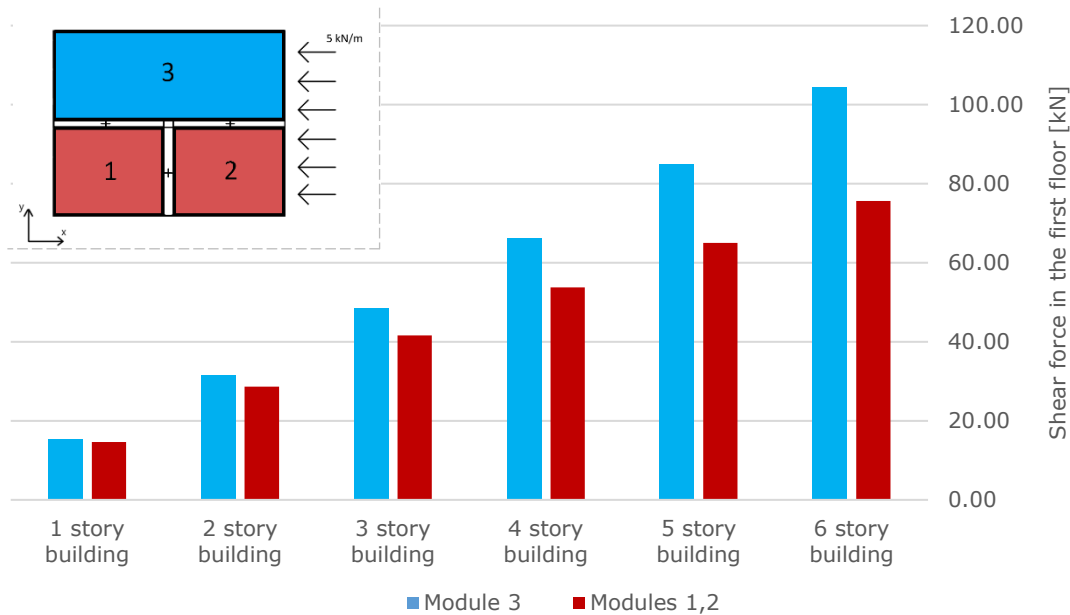


Figure 7: Effect of in-plane bending stiffness of the shear walls on the lateral load distribution.

If the studied three-module building has only one story, the difference between the load in the module 3 and the modules 1, 2 is neglectable (less than 5 %). However, in the 6-story building, the module 3 takes much more lateral load than the two smaller modules 1,2. In this example, the load transferred in module 3 is larger by 38 % than in the other half of the layout (see Figure 7).

We can see different load distribution for one-story and multi-story building, even though they have identical floor plan. Hence, the effect of in-plane bending stiffness of the shear walls on the lateral load distribution should not be neglected in designing and analysing MSTMBs.

5.5. Positions of the shear walls

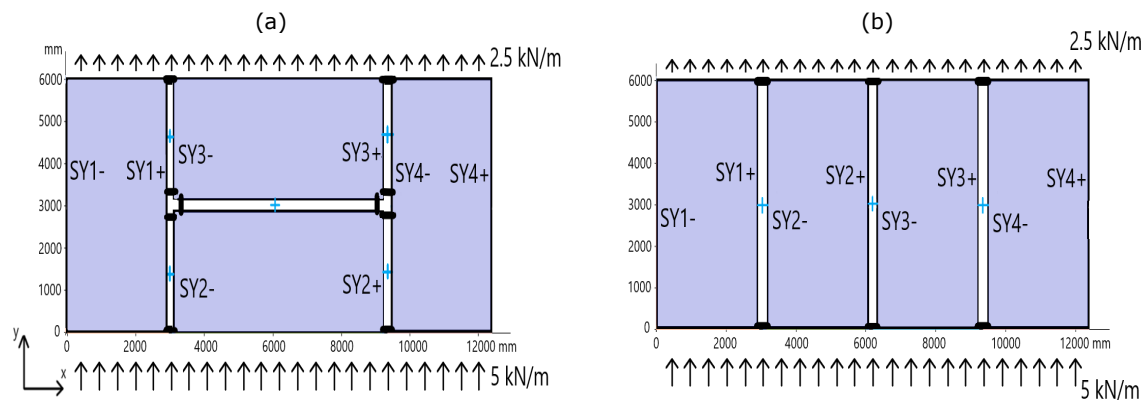


Figure 8: Two building layouts of the 6th story timber modular building compared with each other in terms of lateral load distribution.

Lastly, it is reported that only a small variation in the floor plans may considerably influence the uniformity of the lateral load distribution. Using layout (a) in Figure 8 lead to maximum shear forces 108,8 kN, comparing to maximum shear force 65,8 kN from layout (b).

Thus, it approves the potential of the presented 2D FEM to be used for the lateral load transfer assessment of different building layouts. The 2D FEM could help with optimization of MSTMBs by carrying out similar kind of analyses and searching for better modules' configurations.

6. Conclusions

This work proposes 2D FEM, which is suitable for obtaining the lateral load distribution from the intermediate floor to the shear walls in MSTMBs in the early stage of design. The lateral load distribution analysis is carried out on the reference MSTMB. The results obtained by the 2D FEM show similar trend as the reference 3D FEM. Moreover, the potential of using the 2D FEM in the preliminary stage of the projects is confirmed by obtaining the closest results to the reference 3D FEM in comparison with other commonly used simplified methods.

Various parameters, which affect the lateral load distribution, are individually studied by the 2D FEM on simple layouts. First, the importance of ensuring a sufficient stiffness of the inter-module connections in the intermediate floor is emphasized. Second, it is shown how the actual stiffness of the modular plates plays a role and how the lateral load distribution may differ, when the modular plates are considered as rigid instead of taking the actual stiffness into account. Third, the study of two shear walls with different stiffness gives evidence that the lateral load is not necessarily distributed to the shear walls in the exact proportion of their stiffnesses. Fourth, the in-plane bending stiffness of the shear walls is a significant attribute, which may cause the variations of the lateral load distribution. Fifth, the orientation of the shear walls might significantly influence the lateral load distribution.

Overall, it is proved that the stiffness of the intermediate floor as well as the stiffnesses and the positions of the shear walls play considerable roles in the load transfer. Thus, none of these parameters should be neglected in the preliminary calculations of MSTMBs design. However, the lateral load distribution is always dependent on several factors, which are linked to each other. It is not possible to express in a general way, which of the above-mentioned factors has the largest influence, as the effects vary on a case-by-case basis. The parameter study indicates a potential of using the 2D FEM in optimization process in terms of structural efficiency. The possibility to quickly observe the effect of the shear wall stiffness or the inter-module connection stiffness can help designers to optimize the load distribution by adapting these parameters.

Regarding a future work, it would be beneficial to conduct analyses, which would deal with the relations between individual factors so that their effects are known in the context of other attributes, e.g. ratio of the intermediate floor and the shear walls stiffnesses. Also, other factors such as uplift connections stiffness or plastic deformation of structural elements could be added in the list of input data for the 2D FEM. For a larger credibility of the 2D FEM, the load distribution should be analysed in several other MSTMBs and the results should be compared with the complex 3D FEM, or with the measured data from a site. Lastly, the utilization of the method could increase, if not only the load transfer, but also horizontal displacement and vibration analysis could be carried out by the similar approach.

7. References

- [1] D. Moroder, «Floor diaphragms in multi-storey timber buildings,» *Uni. of Canterbury, Christchurch*, 2016.
- [2] C. E. N. Eurocode, «8: Design of structures for earthquake resistance-Part 1: General rules, seismic actions and rules for buildings, EN 1998-1,» *European Committee for Standardization, Bruxelles*, 2004.
- [3] ASCE, «Minimum design loads and associated criteria for buildings and other structures, ASCE/SEI 7-16,» *American Society of Civil Engineers*, 2016.
- [4] S. Srisangeerthanan, M. J. Hashemi, P. Rajeev, E. Gad, and S. Fernando, «Numerical study on the effects of diaphragm stiffness and strength on the seismic response of multi-story modular buildings,» *Eng. Struct.*, vol. 163, pp. 25–37, 2018.
- [5] Z. Chen, Y. H. Chui, C. Ni, G. Doudak, and M. Mohammad, «Load distribution in timber structures consisting of multiple lateral load resisting elements with different stiffnesses,» *J. Perform. Constr. Facil.*, 2014.
- [6] L. Kotrbaty, «Analysis of lateral load transfer from intermediate floor to shear walls in multi-story timber modular buildings,» *Aalto University, Espoo*, 2020.
- [7] O. Takala, «Lehto Deco concept, Design report,» *Sweco Raken. Oy*, unpublished, 2020.
- [8] EKS 11, «Application of the European construction standards.» *Boverket, Karlskrona, Sweden*, 2019.
- [9] I. Lukacs, A. Björnfort, and R. Tomasi, «Strength and stiffness of cross-laminated timber (CLT) shear walls: State-of-the-art of analytical approaches,» *Eng. Struct.*, vol. 178, pp. 136–147, 2019.

Experimental determination of the rotational stiffness and moment capacity of connections in CLT buildings

Jenny Abrahamsson
Department of Building Technology,
Linnaeus University
Halmstad, Sweden



Filip la Fleur
Department of Building Technology,
Linnaeus University
Växjö, Sweden



Experimental determination of the rotational stiffness and moment capacity of connections in CLT buildings

1. Introduction

In Sweden, building with cross laminated timber (CLT) has become more favored during the last years. Due to the development of CLT-based building systems for multi-story buildings and due to higher loads, higher demands on the connections are required [1]. Since connections are used to transfer loads, connect members, and provide stiffness and ductility, the global structural behavior of a CLT structure is decisively affected by the behavior of the connections [2, 3, 4], especially in multi-story buildings.

In the structural analysis, of multi-story buildings, connections are commonly assumed to be pinned or rigid, even though the actual behavior is somewhere in between, i.e., semi-rigid [2]. For most structures adequate results can be achieved by assuming the connection to be rigid or pinned. This can however be a «problem» when designing taller CLT buildings where the stiffness in the connections is crucial [5]. Furthermore, the behavior of connections in timber structures can be described as ductile or brittle. Ductile behavior is characterized by the possibility to reach high deformations while still maintaining some of the strength in the connection, while for brittle behavior a sudden failure occurs at small deformations [6]. In CLT Buildings the ductile behavior is preferable [7].

Previous studies have focused on the compression perpendicular to the grain behavior [8], while knowledge about the rotational stiffness properties and the moment rotation behavior of wall-floor-wall connections in CLT-structures is currently limited and needs to be extended. Some work on the rotational stiffness and capacity of moment loaded steel to CLT contact connections was done in [9, 10]. Information on the rotational stiffness is crucial for a more efficient and reliable design of connections in CLT structures [2]. This research therefore focused on the rotational stiffness and moment capacity of common wall-floor-wall CLT connections in platform building systems.

2. Materials and methods

The rotational stiffness and moment capacity were studied through experimental investigations. The setup used in the experiments is shown in Figure 1 and the dimensions of the specimens for each series can be seen in Table 1. Different thicknesses of the CLT were used to investigate how the thickness of the wall and the floor specimens influence the stiffness and the moment capacity of the connection. In each of the four test series, eight replication tests were performed. The different CLT-layups used in the experimental campaign are shown in Table 2. Strength class C24 was used for all CLT elements. Prior to testing, specimens were stored in a climate room at constant temperature of 20 °C and a relative humidity of 65 %, resulting in a moisture content of about 12 %. The specimen was kept in the climate room until maximum one hour before testing of that specimen, in accordance to SS-EN 408 [11]. More information about specimen specifications and additional test series using screws and acoustic layers in the wall-floor-wall connection can be found in [12].

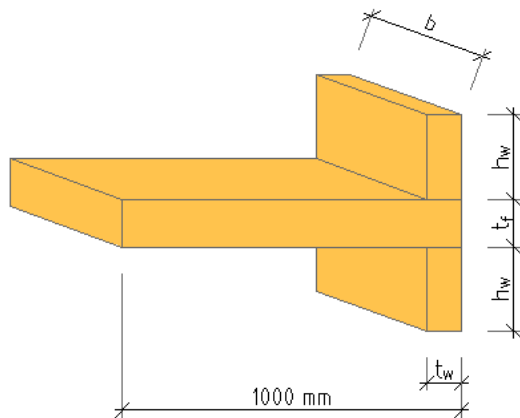


Figure 1: Nomenclature of dimensions for the CLT specimen. Corresponding values for t_w , h_w , t_f and b are given in Table 1.

Table 1: Dimensions of the CLT specimens in each test series.

Test series	t_f [mm]	t_w [mm]	h_w [mm]	b [mm]
A	120 (5-layers)	80 (3-layers)	250	350
C	120 (5-layers)	140 (5-layers)	300	350
E	140 (5-layers)	100 (5-layers)	250	350
G	120 (5-layers)	100 (5-layers)	250	350

Table 2: Cross sectional dimensions of each CLT-layup.

Total thickness [mm]	Layer thickness [mm]
80	20-40-20
100	20-20-20-20-20
120	30-20-20-20-30
140	40-20-20-20-40

2.1. Test setup

The setup used during the tests is shown in Figure 2. For the application of the loading on the CLT wall element, and the CLT floor element, two pistons were used within a steel load frame. The pistons were placed with a distance of 800 mm between the center of each piston. The test setup was realized within a steel load frame with hydraulic actuators. The piston for load application on the wall was an MTS load actuator with a nominal force capacity of 500 kN and the piston for the floor load was an MTS load actuator with a force capacity of 250 kN. For uniformly load introduction, and to get a good contact surface between the pistons and the specimen, steel plates were used. The steel plates were meant to represent the contact from the continuation of the wall and the load application on the floor.

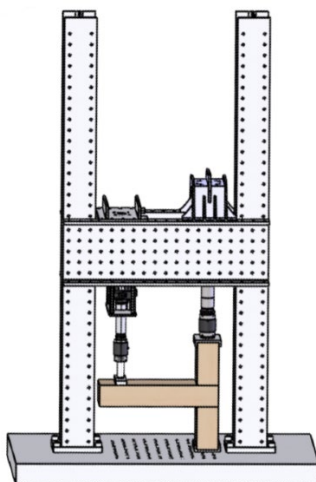


Figure 2: Test setup for the wall-floor-wall connection in the steel load frame.

The dimensions and the weight of the steel plates, which were located between the pistons and the CLT connection specimen, are given in Table 3. The steel plate used for load introduction on the CLT-floor element, to simulate a live load on the floor was a cuboid with a half-spherical hole on the upper side, providing the contact point for the piston. The reason for the spherical hole was used was to make sure that the steel plate was free to rotate at large displacements and thus to maintain contact with the floor specimen. Two sheets of teflon were put between the surface of the steel plate and the surface of the CLT floor specimen, to reduce friction and thus minimize horizontal load transfer between piston and CLT floor element (Figure 3).

Table 3: Dimensions of contact area and weight of steel plates used for load application.

	Weight [kg]	Length [mm]	Width [mm]
Floor	10.90	350	100
80 mm wall	15.64	350	80
100 mm wall	14.62	350	100
140 mm wall	12.34	350	140

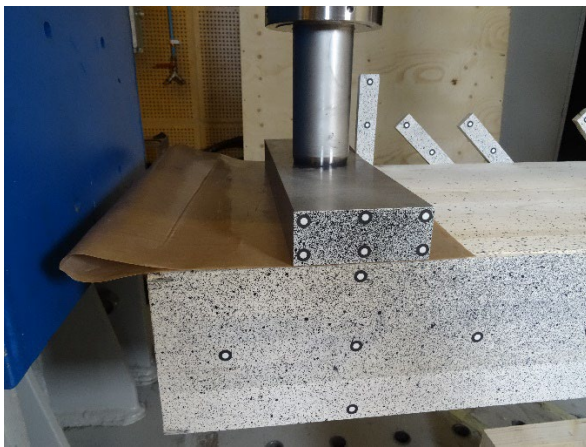


Figure 3: Teflon sheets in the test setup.

U-shaped steel plates were used for application of the pressure on the CLT wall element. The u-shaped allowed for horizontal stabilization, and thus to keep wall elements in place during assembly and testing of the CLT connections. The upper steel plate had a similar spherical hole on the top for load application through the piston, as it was used at the floor element. To secure the position of the CLT-elements, the plate for the lower wall had holes in the bottom, which were aligned to studs in the floor of the load frame.

2.2. Loading procedure

The same loading procedure was used for all tests (see Figure 4). As regards the loading on the wall, four different load levels were applied. These load levels corresponded to a contact pressure on the steel plate 0.5, 1.0, 1.5 and 2.0 MPa, corresponding to the weight of a different number of stories above the investigated wall-floor-wall connection. As soon as the force-controlled load level on the wall was applied, a relative displacement of 20 mm was applied on the floor element. The relative displacement started from the position of the floor piston after the load level on the wall was reached. During the test both pistons were always active. Hence, when the piston on the wall applied load, the floor piston kept a constant force, and vice versa when the floor piston moved displacement controlled to a certain displacement, the piston on the wall kept a constant force level.

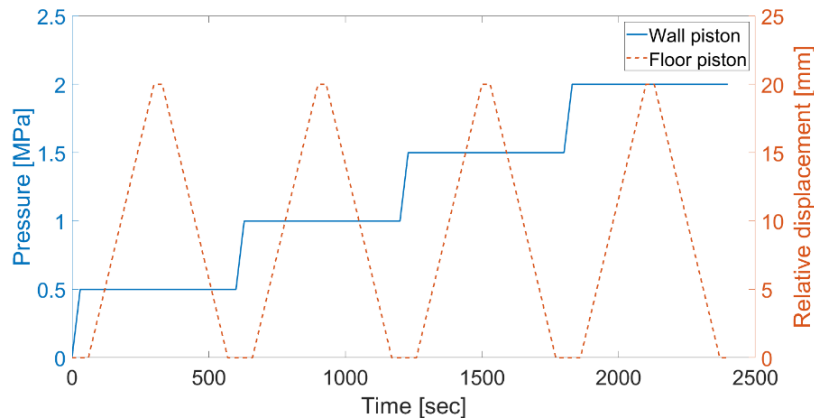


Figure 4: Loading procedure for the wall-floor-wall connection (idealized illustration).

At the start of the tests, pre-loads on the wall and floor element were applied. These pre-loads were small enough to not cause any damage to the specimen but still make the system stable. After the pre-loads had been applied and all the temporary supports had been removed, the test was started. Hence, the force on the wall was increased until the first load level of 0.5 MPa was reached. Thereafter the force was kept constant for 30 seconds to reduce the effect of creep deformations on the connection stiffness.

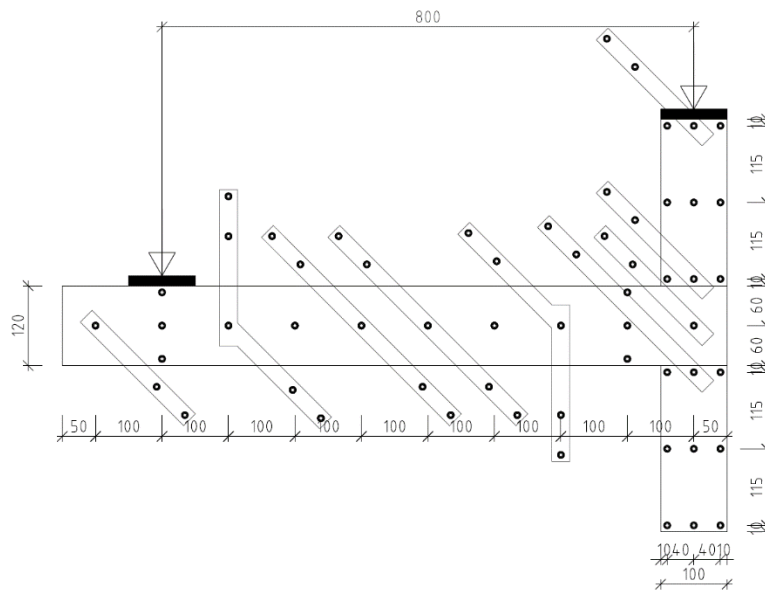
When the load on the wall was stable, i.e., after the 30 second holding phase, the piston on the floor started to move displacement controlled with displacement rate of 5 mm/min. After the 20 mm relative displacement had been reached there was a 30 second holding phase again to take the short-term creep into account and to reach stable load levels at the wall and floor piston. After these 30 seconds the unloading of the floor started. This was done with the same speed of 5 mm/min as for the loading phase. The unloading stopped when the load on the floor reached 100 N. Due to local plastic deformations in the material, the floor piston did not get back to the initial position. When 100 N had been reached in the unloading phase, there was once again a 30 second hold phase before the force on the wall was increased to a nominal stress of 1.0 MPa. After this the procedure was repeated for the four load steps.

All specimens used in the experimental part of the study were used twice. This was done to conduct as many tests as possible within the time frame of the research and with the available material. The wall elements were assumed to not be affected by the loading procedure since the wall was mainly loaded parallel to grain in the tests. The floor elements were also used twice as aforementioned. These elements were assumed to be affected in the contact area with the wall element, since loading was applied perpendicular to grain. Therefore, the floor elements were rotated 180° to be able to test both edges of the floor elements.

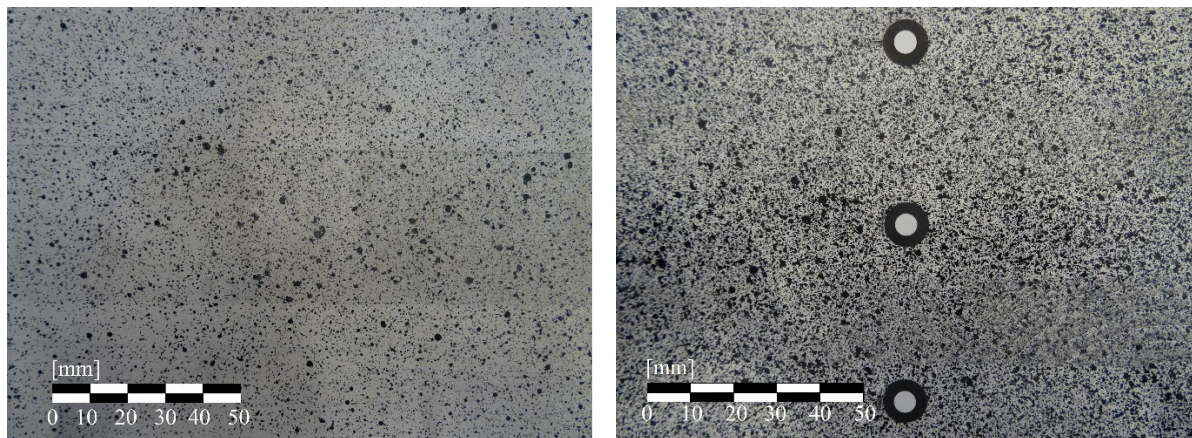
2.3. Load and deformation measurements

During each test, the deformations of the tested specimen were measured with a non-contact 3D optical measurement system, based on digital image correlation (DIC) (ARAMIS, GOM GmbH, Germany) [13]. The measurement system was used to document, analyze, and calculate the local material deformation. The deformations were further used to assess the displacement of specific points on the test specimen to be able to calculate the rotation of the floor. The applied forces from the pistons were measured by load cells of the MTS-hydraulic actuators and used as an analog input to the ARAMIS system. Detailed description of the ARAMIS setup can be seen in Section 3.4.3 in [12].

The displacement of specific points was measured with reference point markers placed on the specimen surface as shown in Figure 5. The reference point markers had an outer diameter of 10 mm including a white dot in the center with 5 mm in diameter. The placement of the markers was done in a symmetric pattern to be able to use the same marker when testing the other side of the floor specimen. On the backside of the specimen plywood sticks were attached with screws. These sticks had reference point markers on them to measure the displacement of the backside of the specimen. This was done to account for any torsional rotation of the floor specimen during testing. Figure 5 shows the position



To get access to the local strains on the CLT surface in the connection area, a stochastic spray pattern was sprayed onto the front side of both the floor and wall specimens. The stochastic spray pattern and a detailed picture of the reference point markers are shown in Figure 6.



2.4. Determination of moment capacity and rotational stiffness

Instead of estimating the maximum compressive load, the maximum moment capacity was estimated. This estimation was set to start at a moment corresponding to a rotation of 0.02 rad. 10 % and 40 % of the estimated maximum moment capacity were then calculated to find the intersections points on the moment-rotation curve. A straight line was then drawn through these two intersection points and a parallel line was drawn with a distance of 0.01 rad along the rotational axis. This distance was assumed from the calculations of a 6 meter span beam with hinged connections and with a deflection of $L/300$.

The calculated maximum moment capacity was then determined by the intersection point of the second line with the moment-rotation curve. If the calculated value of the maximum moment capacity was within the tolerance of 0.5 % of the estimated value, the calculated value was then used to determine the maximum moment capacity. Otherwise, the procedure was repeated until a value of the maximum moment capacity was within the tolerance.

3. Results

3.1. Series A

In Figure 7 the moment-rotation curves for test series A are shown. Test series A was the test setup with 80 mm wall thickness and 120 mm floor thickness. The inclination of the curves change depending on the load level applied on the wall. A higher load level resulted in a higher inclination of the curve, and thus, in a higher rotational stiffness.

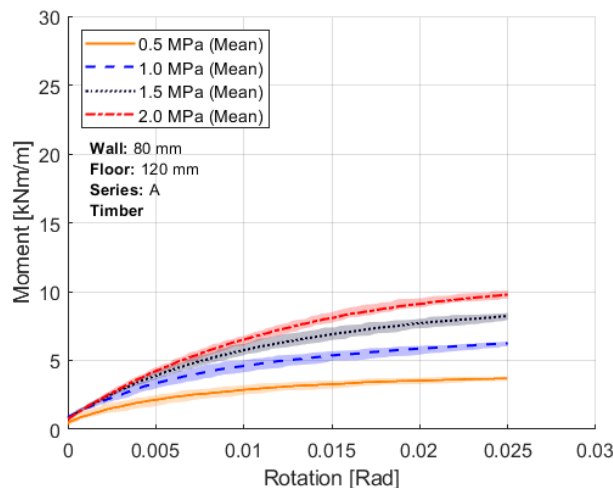


Figure 7: Moment-rotation curve for the four load levels in test series A. The shaded area behind the mean curves represents the interval between the minimum and maximum values of the individual tests.

In Table 4 the calculated mean moment capacity, rotational stiffness and the coefficient of variation (CV) for the different load levels in series A are summarized. The capacity and stiffness values are given per meter CLT wall/floor depth ($b = 1$ m). The capacity between load level 0.5 and 1.0 MPa increased with almost 70 % and the stiffness with just below 30 %. Between these two loads is the largest jump in percentage between two load levels. The increase from the lowest to the highest load level is for the capacity 175 % and for the stiffness 62 %.

Table 4: Moment capacity and rotational stiffness for the different load levels in series A. The capacity calculated, based on the 0.01 rad offset.

Load level	Capacity [kNm/m]	CV [%]	Stiffness [kNm/rad/m]	CV [%]
0.5 MPa	3.42	4.90	434.86	31.64
1.0 MPa	5.78	3.40	565.06	16.57
1.5 MPa	7.76	2.36	667.97	7.83
2.0 MPa	9.43	2.05	706.29	3.93

An explanation for the CV for the rotational stiffness was thought to be because the moment-rotation curve levels out to almost a horizontal curve and therefore the same capacity from two tests can be found at very different rotations. This can also be seen as the variation is almost 10 times lower for the rotational stiffness of the 2.0 MPa load level compared to the 0.5 MPa load level. But at the same time the variation of the capacity only differs by a factor of approximately 2.5 between the two load levels.

3.2. Series C

In Figure 8 the moment-rotation curve for test series C are presented. Test series C was the setup with 140 mm wall thickness and 120 mm floor thickness. In this test setup the thickest walls of this study were used. This means that higher moments were needed to rotate the floor. Also, in this test series the inclination of the curves change depending on the load level applied on the wall. The curves in this test series do not end at the same rotation because of the bending of the floor element. For load levels of 1.5 MPa and 2.0 MPa the connection was stiff enough to cause significant bending deformations in the floor instead of almost pure rotation in the connection as it was seen for the lower load levels.

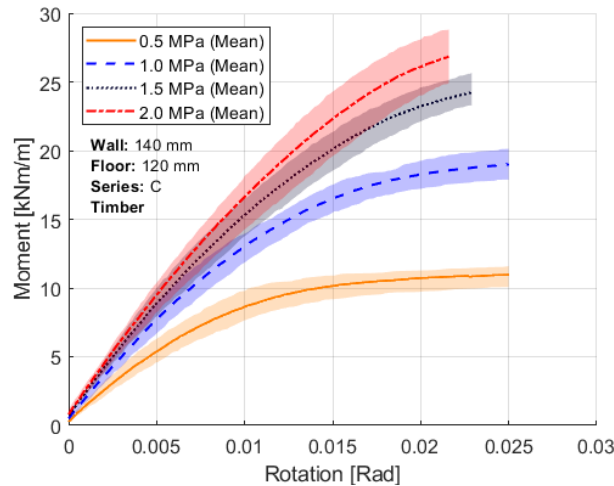


Figure 8: Moment-rotation curve for the four load levels in test series C. The shaded area behind the mean curve represents the interval between the minimum and maximum values of the individual tests.

In Table 5 the calculated mean moment capacity, rotational stiffness, and the CV for the different load levels in series C can be seen. Here the increase of both capacity and stiffness between the first and second load level are 75 % and 38 %, respectively. The increase from load level 0.5 to 2.0 MPa are 147 % and 62 % for the capacity and stiffness, respectively.

Table 5: Moment capacity and rotational stiffness for the different load levels in series C. The capacity calculated, based on the 0.01 rad offset.

Load level	Capacity [kNm/m]	CV [%]	Stiffness [kNm/rad/m]	CV [%]
0.5 MPa	10.71	5.19	1035.72	19.34
1.0 MPa	18.69	4.12	1426.30	12.52
1.5 MPa	23.69	4.81	1587.89	11.36
2.0 MPa	26.46	6.57	1678.46	9.98

In Figure 8 it can be seen, that just like for series A, there develops kind of a geometrical plasticity on the load level of 0.5 MPa. A thicker wall means that a greater moment was needed on the floor to lift the wall even if the same pressure was applied as for the 80 mm wall in series A.

3.3. Series E

In Figure 9 the moment-rotation curve for test series E can be seen. Test series E was the setup with 100 mm wall thickness and 140 mm floor thickness. The inclination of the curves change depending on the load level applied on the wall for this series as well. The moment-rotation curve shows a larger increase in the capacity between the load level of 0.5 and 1.0 MPa than it does between the other load levels, as it was seen for the previous series. The «geometrical plasticity» on the load level of 0.5 MPa can also be seen for this series.

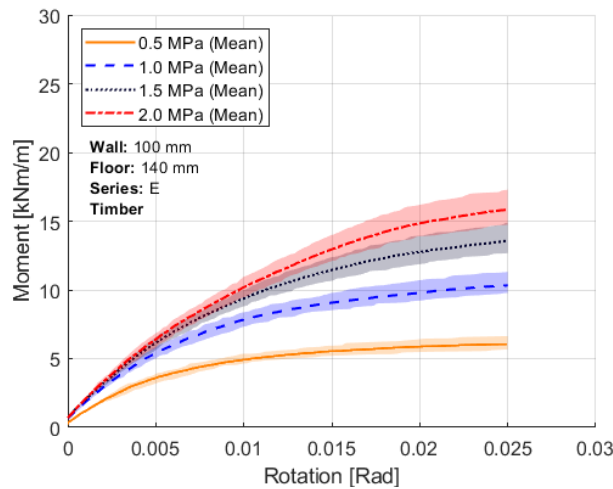


Figure 9: Moment-rotation curve for the four load levels in test series E. The shaded area behind the mean curve represents the interval between the minimum and maximum values of the individual tests.

In Table 6 the calculated mean moment capacity, rotational stiffness and the CV for the different load levels in series E can be seen. In this series the increase in capacity and stiffness between the load level of 0.5 and 2.0 MPa were 172 % and 47 %, respectively.

Table 6: Moment capacity and rotational stiffness for the different load levels in series E. The capacity calculated, based on the 0.01 rad offset.

Load level	Capacity [kNm/m]	CV [%]	Stiffness [kNm/rad/m]	CV [%]
0.5 MPa	5.69	5.29	756.63	11.68
1.0 MPa	9.63	4.86	1029.89	6.97
1.5 MPa	12.92	5.52	1104.38	7.51
2.0 MPa	15.49	5.91	1112.41	7.82

The increase in stiffness between the load levels in this series align with the results from series A and C. In this series the variations are in general lower than compared with previous mentioned series. This could be because the bending stiffness in the specimen was higher than the other series and therefore does not influence the moment rotation curve as much.

3.4. Series G

In Figure 10 the moment-rotation curve for test series G can be seen. Test series G was the setup with 100 mm wall thickness and 120 mm floor thickness. In this series only four tests were used. As noticed in previous tests the connection stiffness depends on the load level and increase with higher load.

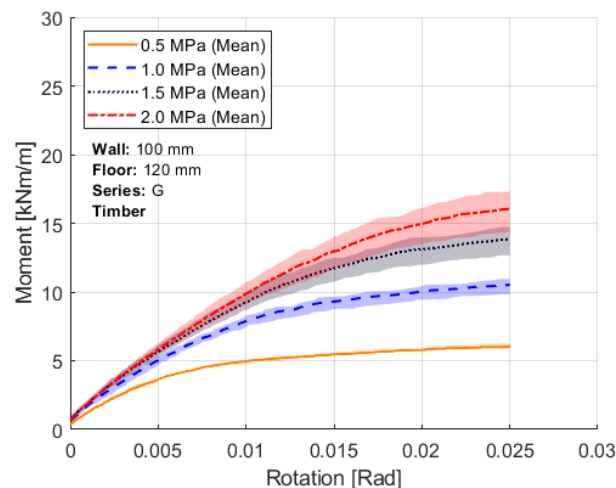


Figure 10: Moment-rotation curve for the four load levels in test series G. The shaded area behind the mean curve represents the interval between the minimum and maximum values of the individual tests.

In Table 7 the calculated mean moment capacity, rotational stiffness and the CV for the different load levels in series G can be seen. The increase in capacity and stiffness between the load level 0.5 and 1.0 MPa are in this series 81 % and 21 %, respectively. The total increase from load level 0.5 and 2.0 MPa for the stiffness and capacity are 175 % and 32 %, respectively.

Table 7: Moment capacity and rotational stiffness for the different load levels in series G. The capacity calculated, based on the 0.01 rad offset.

Load level	Capacity [kNm/m]	CV [%]	Stiffness [kNm/rad/m]	CV [%]
0.5 MPa	5.58	2.66	741.13	7.64
1.0 MPa	10.09	4.43	898.09	7.79
1.5 MPa	13.40	6.40	955.87	6.61
2.0 MPa	15.39	5.43	977.16	7.12

For more details on the result, the reader is referred to [12]. Furthermore [12, 14] include numerical models to calculate the stiffness of the tested connection.

3.5. Comparison

Two main things that can be noticed between the four series is that the biggest impact on the stiffness and capacity is the width of the wall. The wider the wall the higher capacity and stiffness of the connection. When looking at the influence from the thickness of the floor on the stiffness and capacity series E and series G were compared. Where the floor thicknesses were 120 and 140 mm, respectively. The difference is very small when looking at the capacity of the connection and only just above 10 % increase of the stiffness between the two floor thicknesses.

In Figure 11 a comparison between the capacity and stiffness depending on the thickness of the wall can be seen. In the graphs the blue line, line drawn between the boxplots, represent the mean value between the different test series. The red line in each box is the median of that specific series. Furthermore, the values inside the boxes represent the values between the 25 and 75 percentiles. Finally, the outer lines represent the maximum and minimum values. Linear regression was used to create the equations based on the results. A coefficient of determination (R^2) was calculated for all the linear regressions. The R^2 show how strong the linear relationship between the variables is, in this case the thickness of the wall and moment capacity or rotational stiffness. For all the load levels the moment capacity can be considered linear depending on the thickness of the wall.

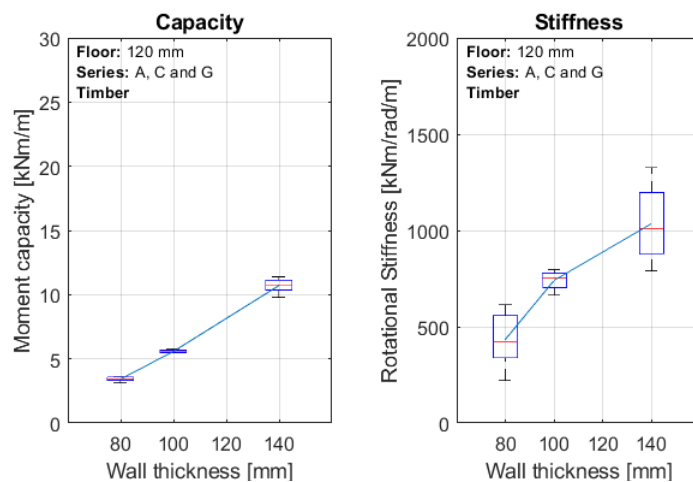


Figure 11: Box plot of the moment capacity and rotational stiffness depending on the thickness of the walls for load level 0.5 MPa.

For load level 0.5 MPa both the moment capacity and rotational stiffness were given equations to estimate the moment capacity and rotational stiffness based on the thickness of the wall. The equations for the estimations can be seen in Eq. 1 and 2, respectively.

$$M_{R,0.5} = 0.122t_w - 6.424, \quad (1)$$

$$K_{R,0.5} = 9.784t_w - 320.2, \quad (2)$$

where $M_{R,0.5}$ is the moment capacity in kNm/m, $K_{R,0.5}$ is the rotational stiffness in kNm/rad/m and t_w is the thickness of the walls in mm. For Eq. (1) and (2) the R^2 values are 0.988 and 0.755, respectively.

The other main result that can be seen throughout the four test series is that the load level impact both the capacity and the stiffness. The capacity had an increase with around 150 % or higher in all four series and the stiffness had an increase between 32 and 62 %. The variation between the tests was in general lower for the capacity than it was for the stiffness in all of the series.

4. Conclusions

In the study 28 tests in four different series were performed. The series differed with different wall thicknesses and floor thicknesses. The testing procedure was the same for all of the four series and included for different load levels on the wall and a 20 mm deformation of the floor element.

The two main factors, influencing the behavior of the connection was the load level on the wall and the thickness of the wall. For the series with 80 mm wall and 120 mm floor the increase in capacity and stiffness was 175 % and 62 % respectively when increasing the load from 0.5 MPa to 2.0 MPa. For the difference between the wall thickness an increase in capacity and stiffness of 213 % and 137 % could be seen when comparing the 80 and 140 mm walls when looking at a load of 0.5 MPa.

It was also seen that the connection showed a ductile behavior. This was seen by the large deformations that were achieved in the test series, without and brittle failure.

5. References

- [1] M. Izzi, A. Polastri, and M. Fragiaco. Modelling the mechanical behaviour of typical wall-to-floor connection systems for cross-laminated timber structures. *Engineering structures*. vol. 162, pp. 270–282, 2018. [Dataset]. Available: <http://doi.org/10.1016/j.engstruct.2018.02.045>.
- [2] G. Flatscher. Evaluation and approximation of timber connection properties for displacement-based analysis of CLT wall systems. *Timber Engineering Technology*. vol. 6, 2017. [Dataset]. Available: <http://dx.doi.org/10.3217/978-3-85125-557-7>.
- [3] I. Gavric M. Fragiaco A. Ceccotti. Cyclic behavior of typical screwed connections for cross-laminated (CLT) structures. *European Journal of Wood and Wood Products*. vol. 73, pp. 179–191, 2015. [Dataset]. Available: <https://doi.org/10.1007/s00107-014-0877-6>.
- [4] R. Brandner et al. Cross laminated timber (CLT): overview and development. *European Journal of Wood and Wood Products*. vol. 74, pp. 331–351, 2016. [Dataset]. Available: <https://doi.org/10.1007/s00107-015-0999-5>.
- [5] S. Tulebekova, K. A. Malo, A. Rönquist, and P. Nævik. Modeling stiffness of connections and non-structural elements for dynamic response of taller glulam timber frame buildings. *Engineering Structures*, 261:114209, jun 2022. ISSN 01410296. doi: 10.1016/j.engstruct.2022.114209. URL <https://linkinghub.elsevier.com/retrieve/pii/S014102962200339X>.
- [6] A. Jorissen and M. Fragiaco. General notes on ductility in timber structures. *Engineering Structures*. vol. 33, pp 2987–2997, 2011. [Dataset]. Available: <http://dx.doi.org/10.1016/j.engstruct.2011.07.024>.
- [7] H. J. Blaß and P. Schädle. Ductility aspects of reinforced and non-reinforced timber joints. *Engineering structures*. vol. 33, pp. 3018–3026, 2011. [Dataset]. Available: <https://doi.org/10.1016/j.engstruct.2011.02.001>.
- [8] M. Schweigler et al. An experimental study of the stiffness and strength of cross-laminated timber wall-to-floor connections under compression perpendicular to the grain. *Engineering Structures*. vol. 271, 114850, 2022. [Dataset]. Available: <https://doi.org/10.1016/j.engstruct.2022.114850>.
- [9] M. Schweigler, T.K. Bader, and S. Sabaa. Design of moment loaded steel contact connections at the narrow face and side face of CLT panels. In: *9th INTER Proceedings: International Network on Timber Engineering Research, 55-7-7, Bad Aibling, Germany, August 22-25, 2022*.
- [10] M. Schweigler et al. Non-uniform compressive loading of cross-laminated timber (CLT) perpendicular to the grain. In *Proceedings of the World Conference on Timber Engineering (WCTE 2021)*, [Online]. 2021.
- [11] *SS-EN 408:2010+A1:2012: Timber structures – Structural timber and glued laminated timber – Determination of some physical and mechanical properties*. Swedish Standards Institute (SIS), Stockholm, Sweden, 2012.
- [12] J. Abrahamsson and F. la Fleur. The impact of connection stiffness on the global structural behavior in a CLT building. M.S. Thesis, Dep. of Building Technology, Linnaeus University, Växjö, Sweden, 2021. [Online]. <https://www.diva-portal.org/smash/get/diva2:1570139/FULLTEXT01.pdf>.
- [13] *GOM. GOM Correlate Professional – V8 SR1 Manual Basic*. Braunschweig, Germany: GOM GmbH. 2015. [Dataset]. Available: http://213.8.45.88/PDF/gom_correlate_prof_basic_v8.pdf. (Visited on 04/08/2021).
- [14] S.T. Akter, T.K. Bader, and E. Serrano. Stiffness of cross-laminated timber (CLT) wall-to-floor-to-wall connections in platform-type structures. In *Proceedings of the World Conference on Timber Engineering (WCTE 2020)*, [Online]. 2021.

Investigation of the Impact of Micro Structuring on Bonding Behaviour of Beechwood

D. B. Moanda
Bernern Fachhochschule Architektur Holz und Bau
Biel/Bienne, Schweiz



Investigation of the Impact of Micro Structuring on Bonding Behaviour of Beechwood

1. Einleitung

In der Schweiz wird der grösste Teil des Holzes, das jährlich für verschiedene Anwendungen im Holzbau verarbeitet wird, aus Nadelholz gewonnen. Während die Buche einen jährlichen Zuwachs von rund 2 Millionen Kubikmetern, verzeichnet, dominiert die Fichte mit einem Zuwachs von 5 Millionen Kubikmetern deutlich. Diese Dominanz lässt sich gleichermassen auf den Baumarkt übertragen, wobei in der Schweiz für jede Million Kubikmeter Fichtenholz nur knapp 36 000 Kubikmeter Buchenholz verwendet [1] werden. Dieser bemerkenswerte Unterschied ist hauptsächlich auf die Ausrichtung der Holzindustrie zurückzuführen.

Darüber hinaus motiviert die Tatsache, dass Fichtenholz eine begrenzte Ressource ist, die Forschung zur Entwicklung von Bearbeitungstechniken für die optimale Nutzung von Laubholz. Die hervorragenden mechanischen Eigenschaften der Buche und die grossen Reserven in der Schweiz machen sie zum idealen Kandidaten für den Versuch, den Baumarkt wieder ins Gleichgewicht zu bringen. Aufgrund der geringen Nutzung von Laubholz in Mitteleuropa haben die Bearbeitungstechniken noch keinen ähnlichen technologischen Entwicklungsstand erreicht wie die für Nadelholz.

Die Verklebung ist sicherlich eine wichtige Herausforderung, die zu bewältigen ist. Es ist selbstverständlich, dass die Verwendung von Holzwerkstoffen in Holzbauanwendungen durch Verklebung ermöglicht wird. Daher ist eine effiziente Verklebung von Laubhölzern ausschlaggebend für den Markteintritt wettbewerbsfähiger Produkte aus Laubholz.

Um Buchenholz (*Fagus Sylvatica* L.) mit den gängigen Klebstoffen zu verkleben, muss eine geschlossene Wartezeit eingehalten werden und im Falle von 1K-PUR-Klebstoffen muss die zu verklebende Oberfläche zunächst mit einem Primer vorbehandelt werden. Die geschlossene Wartezeit kann bis zu einer Stunde betragen [2]. Beide Anforderungen erhöhen die Produktionskosten und/oder verringern die Produktivität, da die Rentabilität nur durch den Einsatz sehr grosser und/oder spezialisierter Produktionsanlagen erreicht werden kann.

Vor diesem Hintergrund wird in der vorliegenden Arbeit untersucht, welche Möglichkeiten zur Verbesserung der Verklebung von Buchenholz durch Strukturhobeln bestehen. In mehreren Studien wurde die Möglichkeit untersucht, die Verklebungsfestigkeit durch Stirnfräsen zu verbessern. Die vorliegende Arbeit wurde im Rahmen einer Machbarkeitsstudie der Innosuisse durchgeführt. In Vorarbeiten wurde ein positiver Einfluss der Mikrostrukturierung auf die Verklebungsqualität von Buchenholz festgestellt [3]. Aufgrund der durch diese Verklebung erreichten Stabilität gekoppelt mit der hohen Steifigkeit von Laubholz, können Beton und Stahl durch Laubholz ersetzt werden.

Auf europäischer Ebene ist es für die Zukunft wichtig, die Verarbeitung von Laubholz zu beherrschen (optimieren), da eine Verschiebung von nadelholzdominierten Wäldern hin zu Wäldern mit einem höheren Anteil an Laubholzarten absehbar ist. Die Verbesserung der Technologien für Laubholzverarbeitung kann der Holzindustrie helfen, einen möglichen Rohstoffmangel zu überstehen [4].

Im Gegensatz zur Fichte fördert die Buche anatomisch bedingt ein tiefes Eindringen von Klebstoff. Dieses Eindringungsverhalten kann zur Bildung von sehr dünnen Klebefugen führen [5][6][7]. Hass, [8] konnte das komplexe Gefässnetzwerk der Buche mittels röntgentomographischer Synchrotronstrahlungsmikroskopie aufklären. Bis dahin wurde das Eindringungsverhalten eines Klebstoffs nur mit Hilfe der maximalen Eindringtiefe beschrieben. Er zeigte auch die Liste der wichtigsten Faktoren, die das Eindringen des Klebstoffs in das Holz beeinflussen. Im Falle von sehr dünnen Klebefugen ist die Haftfestigkeit gering. Dies zeigt, dass es irreführend sein kann, sich nur auf die Klebstoffpenetration zu verlassen, um die Qualität einer Verklebung zu beurteilen [3]. Buchenholz hat eine starke volumetrische Schwindung, die bis zu 18 % betragen kann [9]. Dies schränkt die Anzahl der verwendbaren Klebstoffe ein, da höhere mechanische Eigenschaften erforderlich sind, um

den inneren Spannungen des Holzes standzuhalten. Bei der Delaminierungsprüfung muss der Klebstoff die durch diese besonders starke Schwindung verursachten Kräfte aufnehmen. Die Verwendung von Klebstoffen, die ursprünglich für Nadelhölzer (wie Fichte, Kiefer und Tanne) entwickelt wurden, erfordern für die Verklebung von Laubhölzern (wie Buche, Esche und Eiche) aufgrund der zuvor genannten Faktoren eine Anpassung der Prozessparameter. Die Dichte einer Holzart ist ein guter Faktor zur groben Einschätzung ihrer Verklebbarkeit. Tanne und Balsa gehören beispielsweise in die Kategorie «leicht zu verkleben¹», während Buche und Esche in die Kategorie «zufriedenstellend zu verkleben²» fallen, wie Frihart und Hunt, [10] es darlegen. Eine hohe Dichte entspricht dickeren Zellwänden und kleineren Lumina, die das Eindringen des Klebstoffs in das Holzgewebe erschweren. Diese komplizierte Klebstoffeindringung führt dazu, dass die mechanische Verriegelung auf weniger als zwei Zellen Tiefe begrenzt ist. Bei Holzarten mit hoher Dichte (Laubholz oder dichtes Nadelholz) ist ein stärkeres Quellen und Schwinden zu beobachten. Die Holzporosität ergibt sich aus der Holzdichte und der holzartbezogenen Anatomie.

Knorz *et al.* [11] und Luedtke *et al.* [12] untersuchten den Einfluss der Oberflächenvorbereitung auf die Verklebungsqualität von Massivholz und die erzielte Verbundfestigkeit. In dem nachfolgenden Abschnitt wird der aktuelle Stand der Technik zu diesem Thema zusammengefasst. Hobeln, Schleifen und Planfräsen wurden in vielen Forschungsarbeiten berücksichtigt [13][14][15].

Beim Hobeln hat die Schärfe der Hobelmesser einen Einfluss auf die Oberflächenqualität [14][16]. Singh *et al.* [16] beschreibt anhand mikroskopischer Analysen, wie stumpfe Messer das Eindringen von Klebstoff in das Holz beschweren. Kläusler *et al.* [14] bestätigten die Ergebnisse von Singh *et al.* [16], da sie berichteten, dass mit scharfen Messern gehobelte Oberflächen die Zugscherprüfung bestanden [17][18]. Das Schleifen unterscheidet sich von den anderen Oberflächenvorbereitungsmethoden durch die Schneidengeometrie [19][20]. Beim Schleifen ist die Korngrösse ausschlaggebend für die Verklebbarkeit der erzeugten Oberflächen. Feine Körnung führt zu einer Verbesserung des Adhäsionsverhaltens [14][17]. Grobe Körnung wird dagegen mit schlechter Verklebung assoziiert [21]. B. Moanda *et al.* [22] gaben einen Überblick über aktuelle Erkenntnisse zum Hobeln und Schleifen im Zusammenhang mit der Holzhaftung.

Die Rauheit ist ein quantitativer Parameter, der zur Charakterisierung einer Oberflächenbehandlungsmethode verwendet wird [15]. Es gibt Studien, die einen positiven Einfluss der Rauheit auf die Holzverklebung feststellen [14][23]. Dieser positive Einfluss wird auf die vergrösserte Klebefläche zurückgeführt. Allerdings sind die mit stumpfen Messern gehobelten Oberflächen rauer als die mit scharfen Messern gehobelten, und die Verklebungsleistung ist schlechter [24]. Andererseits können zu raue Oberflächen einen idealen Kontakt zum Substrat verhindern. Es gibt verschiedene Methoden zur Bestimmung der Rauheit. Aufgrund der Anisotropie des Holzes messen die meisten Studien die Oberflächenrauheit quer zur Faser [14][15][25]. Die durch die Oberflächenbearbeitung verursachten Schäden auf mikroskopischer Ebene scheinen geringer zu sein als die daraus resultierende Vergrösserung der für die Verklebung zur Verfügung stehenden Fläche, wie Murmanis, *et al.* [26] mit Hilfe der Fluoreszenzmikroskopie an geschliffenen und gehobelten Oberflächen nachweisen konnten.

Um eine erfolgreiche Verklebung von Hartholz zu erreichen, ist bei der Verwendung von Melamin-Formaldehyd-Klebstoffen (MUF- oder MF-Systemen) eine lange geschlossene Wartezeit erforderlich. Diese Wartezeit kann bei der Verwendung von MUF sogar länger als eine Stunde sein [2][27]. Bei der Verwendung von Einkomponenten-Polyurethanklebstoffen (1K PUR) war es nicht möglich, die Delaminierungsprüfung nach EN 302-2 ohne chemische Vorbehandlung der Oberfläche zu bestehen [12].

Die Mikrostrukturierung hat ihre Wurzeln im Bereich der Oberflächenbeschichtung. Es hat sich gezeigt, dass durch Strukturhobeln der zu beschichtenden Oberfläche die Dauerhaftigkeit der Beschichtung erhöht werden kann [28]. Es wurden Untersuchungen an Nadelhölzern für Aussenanwendungen durchgeführt, bei denen eine bessere Haltbarkeit der Haftung zwischen Holz und Beschichtung erforderlich ist.

¹ Sehr leichtes Verbinden mit Klebstoffen unterschiedlichster Eigenschaften und unter verschiedensten Klebebedingungen

² zufriedenstellende Verklebung mit qualitativ hochwertigen Klebstoffen unter gut kontrollierten Klebebedingungen

Lehmann and Volkmer, [3] untersuchten die Verklebungsqualität von mikrostrukturierten Oberflächen für Harthölzer. Sie verwendeten drei verschiedene Holzarten: Esche (*Fraxinus excelsior* L.), Buche (*Fagus Sylvatica* L.) und Fichte (*Picea Abies* Karst.). Die auf der Oberfläche bearbeitete Mikrostruktur wurde mit Hilfe der Lichtmikroskopie beobachtet. Die Profiltiefe wurde mit 43 µm angegeben. Es wurden Untersuchungen an Klebefugen durchgeführt, die mit 1K-PUR (ohne Primer) und MUF ausgeführt wurden. Diese Serien wurden einem Delaminierungstest gemäss EN 302-2 unterzogen. Die Ergebnisse zeigten, dass bei MUF das einseitige Mikrostrukturhobeln der Proben einen vielversprechenden Einfluss auf die Klebequalität hatte. Sie berichteten, dass keine geschlossene Wartezeit erforderlich war, um die Delaminierungsanforderungen für MUF zu erfüllen. Andererseits war der Einfluss der Mikrostrukturierung bei den mit PUR geklebten Proben immer noch sichtbar, die Delaminationswerte lagen jedoch weit über dem akzeptierten Grenzwert. Der Einsatz von 1K-PUR ohne Primer für die Verklebung von Laubholz wies eine tiefe Verbundsqualität auf. Es wurde auch beobachtet, dass die einseitige Mikrostrukturierung bessere Ergebnisse liefert als die beidseitige Mikrostrukturierung. Die 1K-PUR-Proben konnten weder den Niedrig- noch den Hochtemperaturprozess der Norm EN 302-2 erfüllen. Der Brettschichtholzaufbau dieses Experiments führte zu mikrostrukturierten und normal gehobelten Oberflächen innerhalb derselben Platte. Dies könnte die Ergebnisse ebenfalls beeinflusst haben, denn sobald die schwächste Klebefuge versagt, werden die anderen Klebefugen entlastet und es kommt zu weniger Delamination. Auch der Formfaktor kann in Betracht gezogen werden. Es ist bekannt, dass eine kleinere Probengrösse für die Delaminierung mit Hartholz die Testergebnisse verbessern kann[29].

Ziel dieser Studie war es, den Einfluss der Oberflächenbeschaffenheit auf die Verklebbarkeit von Buchenholz zu untersuchen. Durch die Charakterisierung der strukturierten Hobelflächen und die Verwendung verschiedener Klebstoffe mit unterschiedlichen Prozessparametern sollten Erkenntnisse über das Ausmass der positiven Wirkung des Strukturhobelns gewonnen werden, die bereits in früheren Studien beobachtet werden konnten.

2. Methodik

2.1. Ausführung der Zugscherprüfung

Bei allen durchgeführten Klebeverbindungen wurde Buchenholz (*Fagus sylvatica* L.) verwendet. Für den Zugscherversuch lag der Jahrringwinkel zwischen 60° und 85°, um die Auswirkungen des Holzes auf die Ergebnisse zu verringern. Es ist bekannt, dass ein flacher Jahrringwinkel mit einer niedrigen Zugscherfestigkeit im nassen Zustand verbunden ist [30][31]. Die Buchenbretter wurden im Normalklima (20 °C / 65 % relative Luftfeuchtigkeit) konditioniert, bis die Gleichgewichtsfeuchte von 12 % erreicht war. Unter diesen Bedingungen betrug die durchschnittliche Dichte ρ der Bretter $700 \frac{\text{kg}}{\text{m}^3}$. Fünf verschiedene Oberflächenvorbereitungen wurden verglichen: scharfes Hobeln, Hobeln mit stumpfen Messern, Schleifen, Strukturhobeln mit grobem und feinem Muster. Um den Einfluss der Oberflächenvorbereitung auf die Verklebungsqualität zu beurteilen, wurde ein Zugscherversuch nach EN 302-1 [32] durchgeführt. Die verschiedenen hergestellten Oberflächen sind in Tabelle 1 zusammenfassend dargestellt.

Tabelle 1: geprüfte Oberflächenbeschaffenheiten

Oberflächenbearbeitung	Werkzeug	Beschreibung	Code
Hobeln	scharfe Messer	Hobeln (normal)	N
Hobeln	stumpfe Messer	Hobeln (stumpf)	P
Hobeln	grobstrukturierte Messer	Strukturhobeln	S1
Hobeln	feinstrukturierte Messer	Strukturhobeln	S2
Schleifen	P100 Schleifband	Schleifen	B

Der Klebstoff wurde einseitig mit einer auf 125 g/m^2 eingestellten Auftragsmenge mit einem Holzspachtel aufgetragen. Als Klebstoff für die vorgefertigten Bretter wurde ein Einkomponenten-Polyurethan verwendet. Dabei handelt es sich um einen Einkomponenten-Klebstoff mit einer Verarbeitungszeit von 30 Minuten (Offenzeit), der für tragende Anwendungen mit Nadelholz verwendet wird. Durch den Verzicht auf Primer bei 1K-PUR wurde ein Adhäsionsversagen erzielt, um den Einfluss der Holz Auswahl auf das Ergebnis zu eliminieren, da der Holzbruchanteil auf ein Minimum reduziert wird.

Die strukturgehobelten, vorgefertigten Bretter weichen von den Normen (EN 205 [33]) ab, da die Faltung nicht eingehalten werden konnte, um einseitig strukturierte, gehobelte Verbindungen zu gewährleisten. Wie zuvor erwähnt ist bekannt, dass eine einseitige Strukturierung bessere Ergebnisse erzielt [3]. Das Brett wurde jedoch gedreht, um ein Fischgrätmuster zu erhalten. Aus produktionsbedingten Gründen waren die strukturgehobelten vorgefertigten Platten³ 20 mm dick und mussten nach der Verklebung auf einer normalen Dickenhobelmaschine auf 10 mm abgehobelt werden (mit einem gleichmässigen Abtrag von 5 mm auf jeder Seite). Die Verklebungsparameter sind in **Tabelle 2.** aufgeführt.

Tabelle 2: Verklebungsparameter

Klebstoff	Geschlossene Wartezeit [min]	Jahringlage Lamellen [°]	Presszeit [min]	Pressdruck [Mpa]	Auftragsmenge [g/m ²]	Auftragsmittel
1K PUR	0	60-85	75	0.8	125	Holzspachtel

Die Rauheitsmessung erfolgte innerhalb von 24 Stunden nach der Bearbeitung. Der Oberflächenrauheitsparameter R_a (arithmetisches Mittel der absoluten Ordinatenwerte) wurde auf einer Messlänge von 4 mm, mit einer Abschnittslänge von 0,5 mm bei einer Messgeschwindigkeit von $0,5 \text{ mm s}^{-1}$ bestimmt. Die Messung wurde mit dem SurfTest SJ 210 Rauheitsmessgerät in Übereinstimmung mit DIN EN ISO 4287:2010 [34] durchgeführt.

2.2. Delaminierungsprüfung

Um die Verklebungsqualität strukturgehobelter Lamellen zu vergleichen, wurden Delaminierungstests an Buchenholz (*Fagus Sylvatica L.*) durchgeführt. Das ausgewählte Holz hatte einen flachen Jahringwinkel, wie in der Norm EN 302-2 [35] vorgegeben. Das Holz wurde zunächst im Normalklima (20 °C / 65 % relative Luftfeuchtigkeit) klimatisiert, bis die Gleichgewichtsfeuchte von 12 % erreicht war. Die gemessene durchschnittliche Dichte ρ der Bretter betrug $(687 \pm 27) \text{ kg/m}^3$. Das Holz wurde nach der Dichte sortiert und die Dichteklassen wurden wie folgt definiert:

- C1 ($627 - 662 \text{ kg/m}^3$)
- C2 ($662 - 697 \text{ kg/m}^3$)
- C3 ($697 - 732 \text{ kg/m}^3$)

Die ersten beiden Bretter stammen aus der Klasse C1, das mittlere Brett paar aus der Klasse C3 und das letzte Paar aus der Klasse C2. Dieser Aufbau wurde für alle Delaminierungsprüfkörper eingehalten. Aufgrund der Produktionskapazität war die Länge des Brettschichtholzes auf 250 mm begrenzt, und es wurde ein Delaminierungsprüfkörper aus dem Brettschichtholz entnommen.

Für die Delaminierungsprüfung wurden 1K-PUR (ohne Primer mit 10 min Offenzeit) und Melaminformaldehyd (30 min Offenzeit) gewählt.

Da beide verwendeten Klebstoffsysteme für tragende Anwendungen zugelassen sind, wurde das für Typ-I-Klebstoffe geeignete Hochtemperaturverfahren angewendet. Jedoch ist bei 1K-PUR ist die Wasserbeständigkeit der Verklebung stark vom Primer abhängig [36]. Die Prozessparameter sind in Tabelle 3 dargestellt.

³ Verklebte Bretter voraus Zugscherproben zugeschnitten werden

Tabelle 3: Verklebungsparameter

Klebstoff	Geschlossene Wartezeit [min]	Presszeit [min]	Pressdruck [N/mm ²]	Auftragsmenge [g/m ²]	Oberflächenvorbereitung	Auftragsmittel
1K PUR	0	75	0.9	125	grob- und fein	Holzspatel
	0	75	0.9	200	grob- und fein	Holzspatel
	0	75	0.9	125	normal gehobelt	Holzspatel
	0	75	0.9	200	normal gehobelt	Holzspatel
MF	0	120	1	250	grob- und fein	Holzspatel
	0	120	1	400	grob- und fein	Holzspatel
	20	120	1	250	normal gehobelt	Holzspatel
	20	120	1	400	normal gehobelt	Holzspatel

3. Ergebnisse und Diskussion

3.1. Rauheit

Die Rauheitsanalyse der strukturierten gehobelten Oberflächen zeigt, dass die Grösse des verwendeten Musters die gemessene Rauheit erheblich beeinflussen kann. **Abbildung 1** zeigt einen Vergleich aller im Rahmen dieser Arbeit verwendeten Bearbeitungsmethoden. Die Grobstruktur weist den höchsten R_a -Wert auf, gefolgt von der Feinstruktur, die im Vergleich eine geringere Rauheit aufweist. Die normal gehobelte Oberfläche weist eine geringere Rauheit auf als die schlecht gehobelte und die geschliffene Oberfläche. Kläusler *et al.* [14] führten ähnliche Untersuchungen an Buchenholz (*Fagus sylvatica* L.) durch und kamen zu den gleichen Ergebnissen. Sie berichteten, dass scharfes Hobeln die glattesten Oberflächen ergibt, gefolgt von feinem Schleifen und stumpfem Hobeln. Bei ihren Untersuchungen verwendeten sie ein viel glatteres Hobeln, da der Vorschub f_z 0,5 mm betrug. Demgegenüber steht der zu 1,4 mm gewählte Vorschub bei der für dieses Projekt verwendeten Dickenhobelmaschine. Die Vierseitenhobelmaschine hatte einen weniger harten Zahnvorschub ($f_z=1,13$ mm) mit weniger tiefen Hobelschlägen, was sicherlich auch zur Glättung der Rauigkeit beigetragen hat. Obwohl die grob strukturierte Serie die raueste Oberfläche aufwies, lieferte sie nicht die besten Ergebnisse im Zugscherversuch. Dies veranschaulicht einmal mehr, warum es nicht so einfach ist, die Verklebungsqualität basierend auf der Rauheit als Oberflächenparameter vollständig vorherzusagen. Die schlecht gehobelte Oberfläche wies eine geringere Dispersion auf und war sogar glatter als das Schleifen mit einer P100-Körnung. Für beide Gruppen (PPGB, BPGB) liegen die Medianwerte recht nahe beieinander, so dass der Unterschied in Bezug auf die Rauheit nicht signifikant zu sein scheint. In der vorgenannten Studie wurde nicht mit P100-Schleifpapier geschliffen. Der mit P100-Schleifpapier erzielte Wert scheint im Vergleich zu dem von Kläusler *et al.* [14] für mit P120 geschliffene Oberflächen ermittelten Wert recht hoch zu sein. Der Unterschied ist wahrscheinlich auf unterschiedliche Schleifparameter zurückzuführen. Hernández und Cool, [37] fanden ein anderes Verhalten bei einem leichteren Hartholz – Birke. Sie berichteten, dass scharfes Hobeln eine grössere Rauheit aufweist als das Schleifen in drei aufeinanderfolgenden Stufen mit den Körnungen 100 – 120 – 150. Die Wahl einer solch feinen Körnung ist nachvollziehbar, da die genannte Studie darauf abzielte, die Holzbeschichtung zu optimieren.

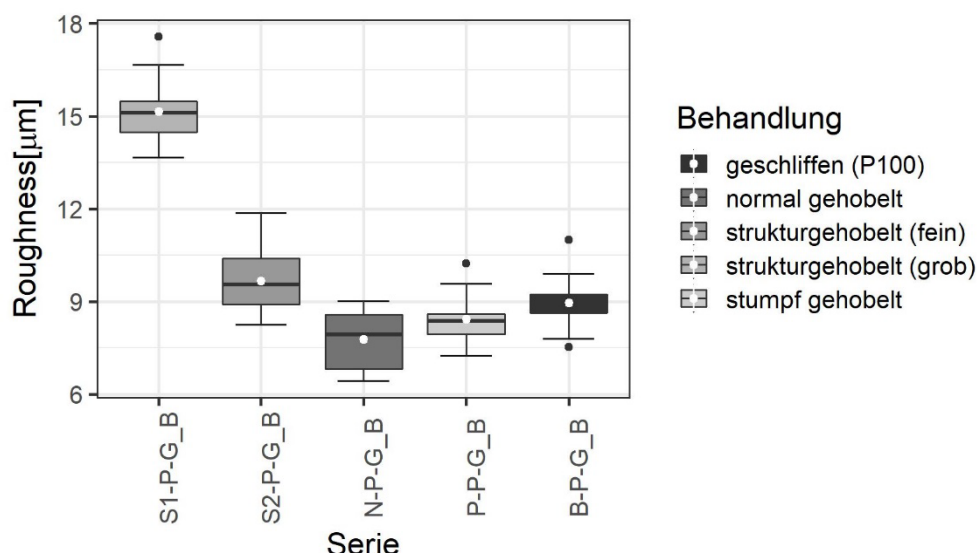


Abbildung 1: Boxplots zeigen Minimal- und Maximalwert, der weisse Punkt zeigt den arithmetischen Mittelwert, die dicke horizontale Linie den Median, die untere Linie des Kastens steht für das erste Quartil und der Obere Linie stellt das dritte Quartil dar. Die Ausreisser werden durch dunkle Punkte dargestellt.

3.2. Zugscherfestigkeit

Im trockenen Zustand schnitten die normal gehobelten Bretter am besten ab. Aber die gemessene Zugscherfestigkeit bezieht sich mehr auf das Holz, da der Holzbruchanteil sehr gross war. Die grob strukturierten Prüfkörper zeigten die zweithöchste Zugscherfestigkeit (rund 15 MPa) und die geringste Streuung (siehe **Abbildung 2**). Diese geringe Streuung ist auf den niedrigen Holzbruchanteil zurückzuführen. An dieser Stelle wurde Klebstoff effektiv geprüft. Beim Schleifen war die Streuung am grössten, obwohl der Mittelwert über der 15-MPa-Linie liegt, was sich durch die hohe Streuung beim Holzausfallprozentsatz (WFP) erklären lässt. Wenn bei einer Trockenprüfung der WFP nahe bei 100 % liegt, entspricht die gemessene Zugscherfestigkeit der Holzfestigkeit. Die niedrigste WFP-Leistung wurde bei den grob strukturierten, gehobelten Proben festgestellt. Da sie recht hohe TSS-Werte aufwiesen, kann man daraus schliessen, dass diese Gruppe in der Trockenphase gut abschneidet. Die grobe Struktur scheint die Last gut auf die Schnittstelle zu verteilen. Die normal gehobelten Bretter übertrafen die anderen Gruppen bei den prozentualen Werten des Holzversagens. Die meisten Proben dieser Gruppe wiesen einen WFP von 100 % auf. Die gemeldeten hohen Widerstandswerte können mit der Holzfestigkeit in Verbindung gebracht werden. Selbst im nassen Zustand wies diese Gruppe einen höheren WFP auf. Alle Proben erfüllten die Anforderungen der Trockenprüfung. Dieses Ergebnis stimmt mit dem überein, was in früheren Forschungsprojekten bereits festgestellt wurde. Es wurde berichtet, dass selbst schlecht gehobelte Bretter in dieser Stufe gut abschnitten [14] [2]. Die Aussagekraft von einem A1 Test (nach EN 302-1 Tabelle 1) ist durch den hohen Holzbruchanteil beeinträchtigt.

Unter nassen Prüfbedingungen sind schlecht gehobelte Proben am schwächsten, da sie einen weit niedrigeren Durchschnittswert und einen dramatisch niedrigen Medianwert zusammen mit der grössten gemeldeten Dispersion aufweisen, wie in **Abbildung 2** dargestellt. Die geschliffenen Exemplare haben den Test knapp bestanden. Die meisten Gruppen haben ein WFP von Null - die Ergebnisse zeigen, dass das prozentuale Versagensverhalten des Holzes bei Einkomponenten-Polyurethan (ohne Primer) nicht zuverlässig durch die Wahl einer bestimmten Oberflächenvorbereitungsmethode beeinflusst werden kann. Diese Beobachtung wurde bereits in einer anderen Studie gemacht, die 1K-PUR untersucht hat [14]. Die geringste Streuung der Zugscherfestigkeit wurde bei grob strukturierten, gehobelten Probekörpern beobachtet. Die hohe Rauheit dieser Gruppe scheint mehr Verankerung für eine bessere Haftung zu bieten. Obwohl alle WFP gleich Null sind, ist die Haftung stabil genug, um das Bestehen der Prüfung zuverlässig zu gewährleisten. Die feinere Struktur zeigt ein anderes Verhalten mit einer recht hohen Dispersion; der zweithöchsten gemessenen Dispersion nach den stumpf gehobelten Proben. Die scharf gehobelte Ober-

fläche weist einen besseren Zugscherfestigkeits-Durchschnittswert auf als die geschliffene. Dieses Ergebnis stimmt mit anderen Untersuchungen überein, die an verschiedenen Holzarten durchgeführt wurden [14][15][26]. Dennoch konnten zerkleinerte Zellen nicht mit Hilfe der Fluoreszenzmikroskopie beobachtet werden, wie es Murmanis *et al.* [26] taten. Dies ist darauf zurückzuführen, dass sie eine sehr grobe Körnung (36) verwendeten. Die relativ aktuelle Studie von Kiliç,[15] zeigte, dass eine übermäßige Rauheit die Scherfestigkeit von PUR- und PVAc-Klebstoffen verringert, wobei die mit einer Kreissäge erzeugte Oberfläche das niedrigste Ergebnis lieferte, während die scharf gehobelte Oberfläche die beste Leistung aufwies.

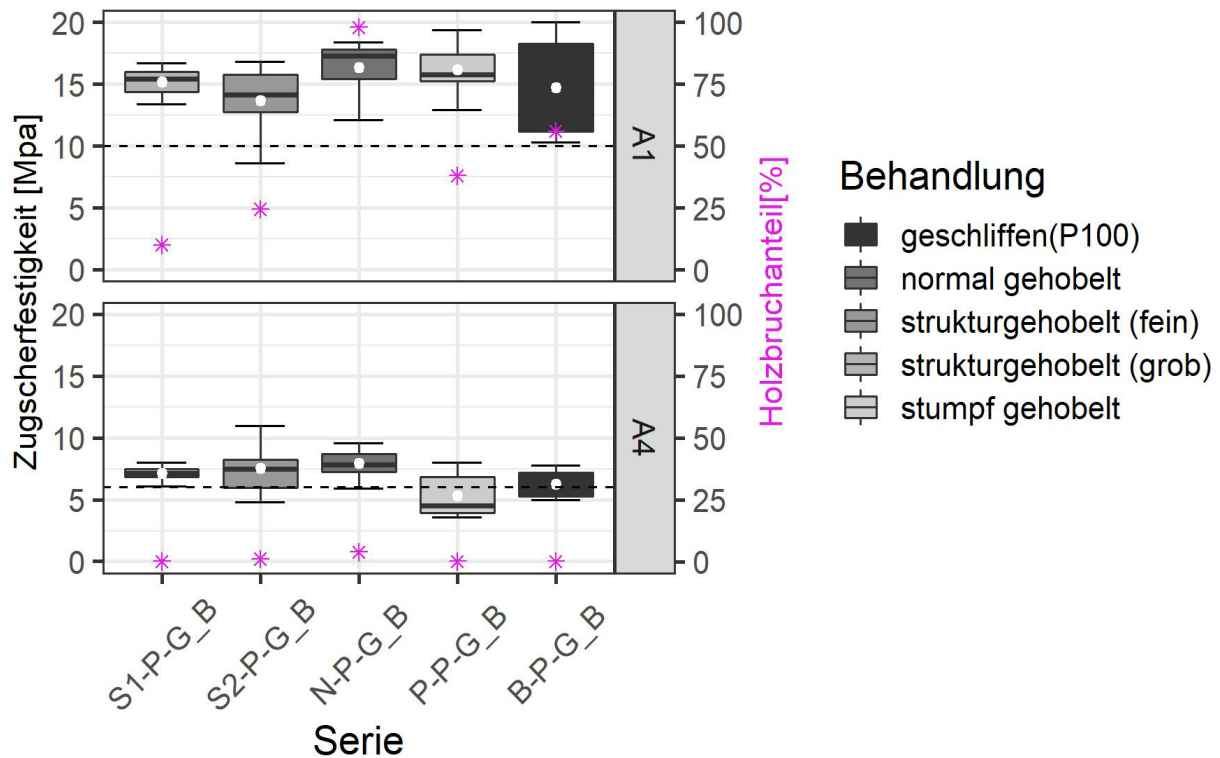


Abbildung 2: Zugscherfestigkeit nach EN 302-1 für die fünf Oberflächenbearbeitungen. Boxplots zeigen Minimal- und Maximalwert, der weiße Punkt zeigt den arithmetischen Mittelwert an, die dicke horizontale Linie stellt den Median dar. Der Holzbruchanteil wird durch einen Stern dargestellt.

3.3. Delaminierungsprüfung

Ergebnisse für 1K PUR

Die Ergebnisse wurden als Durchschnittswerte in Form von Farbbalken in einem Balkendiagramm dargestellt (vgl. Abbildung 3)

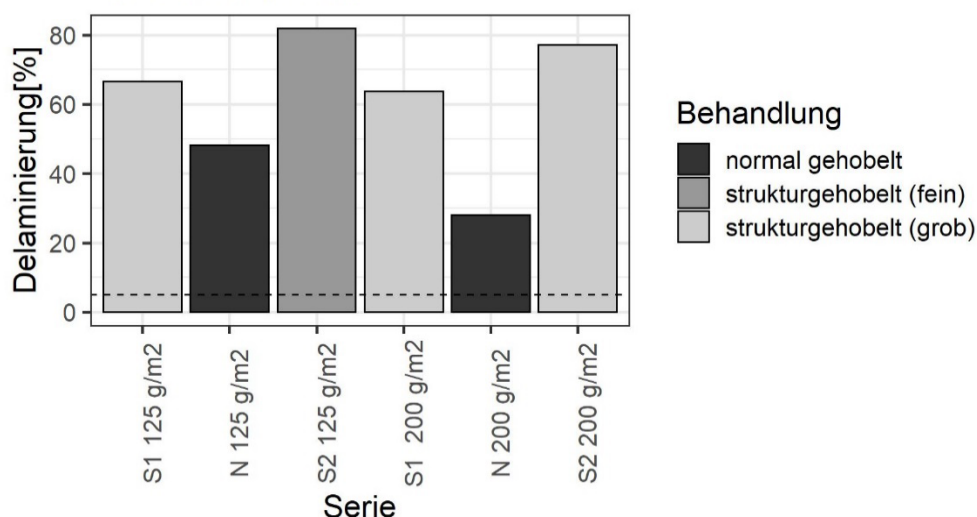


Abbildung 3: Delaminierungsergebnisse nach EN 302-2 für 1K-PUR. die gestrichelte Linie zeigt den nach der verwendeten Norm (SN EN 302-2) zulässigen Höchstwert der Delaminierung.

Keine mit PUR verklebte Probe bestand den Test. Sogar beide Referenzplatten zeigten viel höhere Delaminierungswerte als die zugelassene Delaminierung. Ein positiver Einfluss der Mikrostrukturierung konnte bei diesen Daten nicht festgestellt werden, im Gegensatz zu dem, was in der Literatur gefunden wurde [3]. Eine Primerlösung kann nicht durch das Strukturhobeln ersetzt werden. Wie erwartet, haben die normal gehobelten Oberflächen ohne Primer den Delaminierungstest eindeutig nicht bestanden. In vielen Studien wurde die Bedeutung der chemischen Vorbehandlung von Laubholz etabliert [2][12][38][39]. Dennoch ist noch nicht vollständig geklärt, warum strukturiert gehobelte Brettschichthölzer noch schlechter abschneiden als normal gehobelte Brettschichthölzer. Ein Erklärungsversuch könnte die positive Wirkung der Rauigkeit sein. De Moura und Hernández,[40] berichteten über ein besseres Alterungsverhalten für Oberflächen mit geringerer Rauheit, als sie geschliffene mit gehobelten Oberflächen verglichen. Die Rauigkeit ist auf die Oberfläche beschränkt, aber auch Schäden knapp unter der Holzoberfläche können die Delaminierungsbeständigkeit beeinflussen[11].

Ergebnisse für Melaminformaldehyd

Die Ergebnisse der Delaminierungsprüfung für mit Melaminformaldehyd verklebten Balken ist in **Abbildung 4** zusammengefasst. Beide strukturgehobelten Leimbalken erfüllten die Delaminierungsanforderung nach EN 302-1 für Klebstoffe vom Typ I ohne geschlossene Wartezeit. Dies bestätigt die Ergebnisse von Lehmann und Volkmer, [3]. Das mit 400 g/m² geklebte Referenz-Leimholz (normal gehobelt) mit einer geschlossenen Wartezeit von 20 Minuten hat den Delaminierungsversuch nicht bestanden, da der Delaminierungswert leicht erhöht war, während ein mit nur 250 g/m² geklebtes Brettschichtholz den Test bestanden hat. Ausserdem stimmen die Ergebnisse mit den Erkenntnissen aus den Zug-scherfestigkeitsprüfungen überein, die zeigten, dass fein strukturierte, gehobelte Oberflächen besser abschneiden. Es wurde auch festgestellt, dass die normal gehobelten Prüfkörper ein besseres Klebeverhalten aufweisen, wenn die Auftragsmenge des Klebstoffs abnimmt. Geringere Auftragsmengen auf strukturgehobelten Oberflächen führen zu einer noch schlechteren Delaminierungsbeständigkeit.

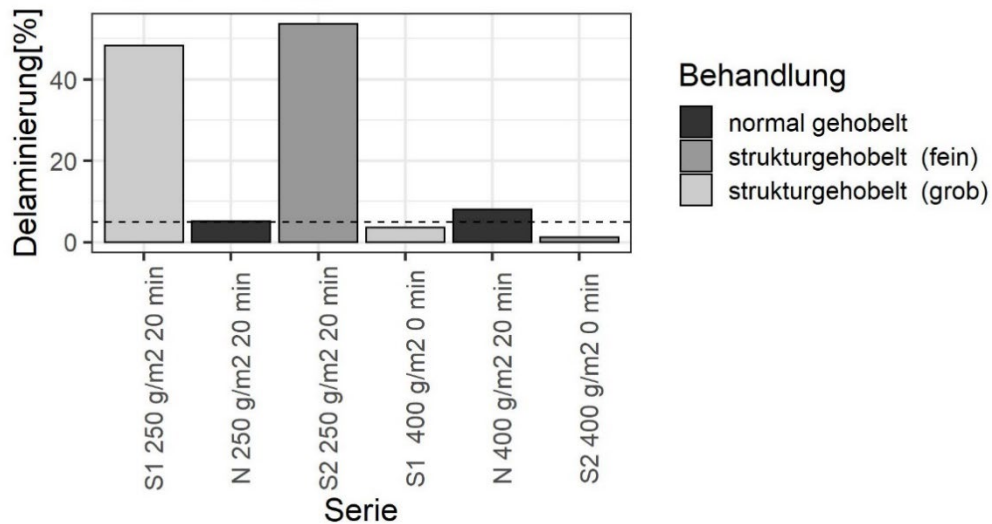


Abbildung 4: Die Balken stellen die arithmetischen Mittelwerte dar; die gestrichelte Linie zeigt den nach der verwendeten Norm (SN EN 302-2) zulässigen Höchstwert der Delaminierung.

Standzeit

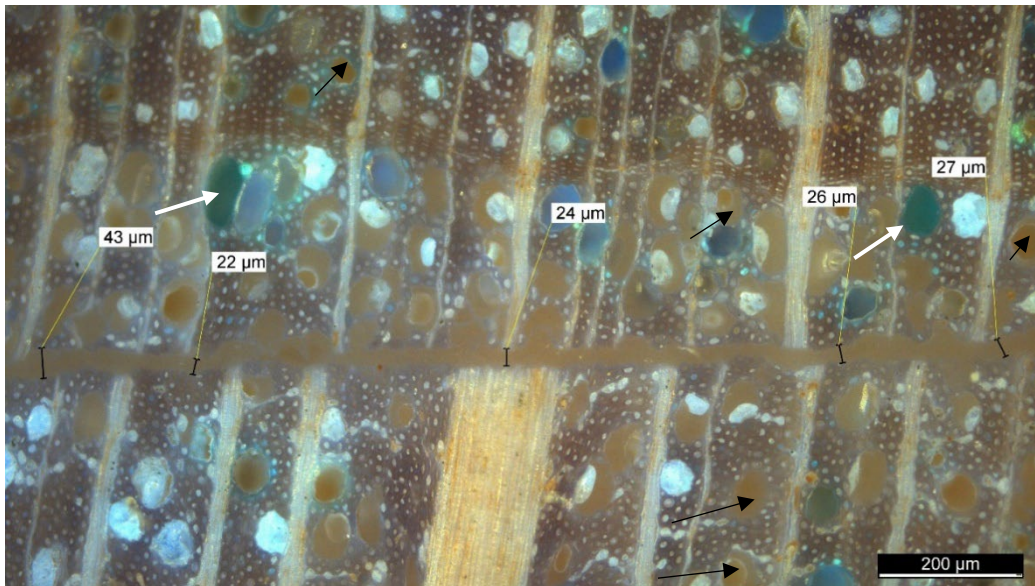


Abbildung 5: SIIMGDx4, vierte Klebefuge des Brettschichtholzes schwarze Pfeile zeigen die Eindringung des Klebstoffs. Weisse Pfeile zeigen das für das Einbetten verwendete Epoxidharz.

Die Häufigkeit, mit der die Messer gewechselt werden müssen, ist für die Industrie sehr entscheidend. Wechsel- und Rüstzeiten können die Gesamtproduktivität der Anlage erheblich beeinträchtigen. Bei diesem Projekt wurden weniger als 300 Laufmeter gehobelt. Die Beobachtung von Verschleissindikatoren bei einem so kurzen Einsatz (geringe Anzahl von gehobelten Proben) stellt eine Herausforderung für eine industrielle Umsetzung (siehe **Abbildung 6**). Die durch die Verkürzung des Verklebungszeit gewonnene Produktivität kann durch die Werkzeugwechselzeiten wieder verloren gehen.

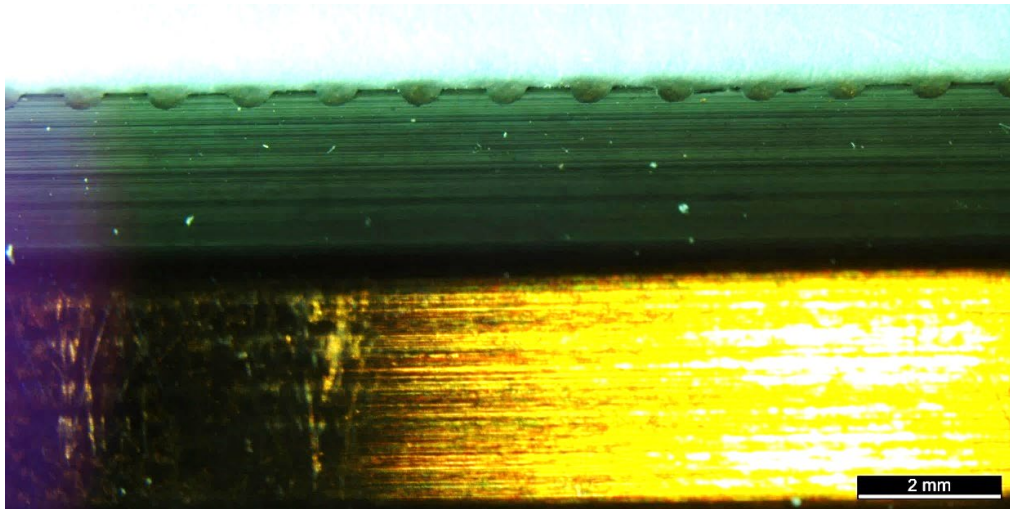


Abbildung 6: grob strukturiertes Messer unter der Lupe betrachtet. Das Vorhandensein von beschädigten Abschnitten in der Messerstruktur ist erkennbar. Die weissen Pfeile zeigen beschädigte Stellen an.

4. Schlussfolgerungen

Ziel der Masterarbeit war es, die Auswirkungen des Strukturhobelns auf Buchenholz (*Fagus Sylvatica* L.) zu bewerten. Auf der Grundlage der Ergebnisse, die bei den verschiedenen Aktivitäten dieses Projekts beobachtet wurden, können die folgenden Schlussfolgerungen gezogen werden:

Die topografische Analyse hat gezeigt, dass das Strukturhobeln die effektive Adhäsionsfläche nicht wesentlich vergrößert. Die grobe Struktur hat eine Vergrößerung von weniger als 3% gezeigt, während die fein strukturierten gehobelten Oberflächen eine vernachlässigbare Flächenvergrößerung aufwiesen. Der Einfluss der Strukturhobelung auf die Zellen knapp unter der Holzoberfläche scheint wichtiger zu sein.

Fein strukturiert gehobelte Oberflächen haben in Kombination mit einer geringen Klebstoffmenge sowohl im trockenen als auch im nassen Zustand eine schlechte Verklebungsqualität. Strukturhobeln erhöht den Prozentsatz des Holzversagens nicht effektiv. In dieser Hinsicht gleicht diese Bearbeitungsmethode den berichteten Verfahren (Schleifen, Hobeln mit scharfen Messern, Hobeln mit stumpfen Schneiden). Der Klebstoff und das Holz scheinen einen grösseren Einfluss zu haben.

Im trockenen Zustand erfüllten alle Proben die Anforderungen an die Scherzugfestigkeit. Bei Melamin-Formaldehyd-Klebstoff ersetzt das Strukturhobeln die Beobachtung der geschlossenen Wartezeit. Die Mechanismen, die zu diesem Verhalten führen, sind noch unbekannt, da die Mikrostrukturierung auf den Klebeverbindungen, die den Delaminierungstest erfolgreich bestanden haben, nicht mehr sichtbar war. So ist beispielsweise noch unklar, warum die Struktur bei einigen Klebefugen mit tiefen Delaminierungsbeständigkeiten nicht zu beobachten ist, während sie bei leistungsfähigen Verklebungen vollständig in die Klebefuge übergeht. Es sollten weitere mikroskopische Analysen durchgeführt werden, um den Untergrund zu untersuchen. Auch die Auswirkungen des Drucks auf die strukturierten, gehobelten Oberflächen sollten untersucht werden.

Das Delaminierungsverhalten von Polyurethan (für ein System mit kurzer offener Zeit) in Verbindung mit Strukturhobeln wurde in der zweiten Runde der Delaminierungsversuche nicht geprüft. Die beobachteten sehr hohen Delaminierungswerte zeigten, dass das Strukturhobeln beim derzeitigen Kenntnisstand eine chemische Vorbehandlung der Laubholzoberfläche zur Verbesserung der Verklebungsqualität nicht ersetzen kann.

Das für die Herstellung der strukturierten Messer verwendete Material neigt dazu, schneller zu brechen und zu verschleissen als herkömmliche Messer. Dies stellt eine Hürde vor der industriellen Umsetzung dieser Technologie. Hochwertige Messer müssen entwickelt werden, um eine zulässige Standzeit zu gewährleisten.

5. Danksagung

Ich bedanke mich für die finanzielle Unterstützung dieses Forschungsprojekts durch die Innosuisse (Bern, Schweiz). Ich danke den Firmen Henkel & Cie. AG (Sempach-Station, Schweiz) und Fagus Suisse SA für die Bereitstellung der benötigten Klebstoffe und ich möchte meinem Betreuer und Zweitgutachter meine aufrichtige Anerkennung aussprechen: Prof. Dr. Frédéric Pichelin und Dr. Ing Martin Lehmann für ihre Unterstützung und Ratschläge. Mein aufrichtiger Dank geht auch an Prof. Dr. Peter Niemz für seinen Einsatz als externer Gutachter. An Prof. Dr. Thomas Volkmer möchte ich mich für seine konstruktiven Gespräche bedanken.

6. Referenzen

- [1] U.-B. Brändli, M. Abegg, and B. Allgaier Leuch, Schweizerisches Landesforstinventar. Ergebnisse der vierten Erhebung 2009–2017. Bern: Eidgenössische Forschungsanstalt für Wald, Schnee und Landschaft WSL, Birmensdorf Bundesamt für Umwelt BAFU, Bern, 2020.
- [2] J. Konnerth, M. Kluge, G. Schweizer, M. Miljković, and W. Gindl-Altmutter, «Survey of selected adhesive bonding properties of nine European softwood and hardwood species», *Eur. J. Wood Wood Prod.*, vol. 74, no. 6, pp. 809–819, 2016, doi: 10.1007/s00107-016-1087-1.
- [3] M. Lehmann and T. Volkmer, «Investigation of the bond quality of hardwoods with micro structured surfaces», *Proc. 68th For. Prod. Soc. Int. Conv.*, 2014.
- [4] M. Lindner et al., «Climate change impacts, adaptive capacity, and vulnerability of European forest ecosystems», *For. Ecol. Manage.*, vol. 259, no. 4, pp. 698–709, 2010, doi: 10.1016/j.foreco.2009.09.023.
- [5] O. Kläusler, P. Hass, C. Amen, S. Schlegel, and P. Niemz, «Improvement of tensile shear strength and wood failure percentage of 1C PUR bonded wooden joints at wet stage by means of DMF priming», *Eur. J. Wood Wood Prod.*, vol. 72, no. 3, pp. 343–354, 2014, doi: 10.1007/s00107-014-0786-8.
- [6] D. J. Gardner, M. Blumentritt, L. Wang, and N. Yildirim, «Adhesion theories in wood adhesive bonding: A critical review», *Rev. Adhes. Adhes.*, vol. 2, no. 2, pp. 127–172, 2014, doi: 10.7569/RAA.2014.097304.
- [7] C. Frihart and R. Rowell, «Wood Adhesion and Adhesives», in *Handbook of Wood Chemistry and Wood Composites*, Second Edition, no. September 2012, 2012, pp. 255–320.
- [8] P. F. Hass, «PENETRATION BEHAVIOR OF ADHESIVES INTO SOLID WOOD AND MICROMECHANICS OF THE BONDLINE», ETH ZÜRICH, 2012.
- [9] M. Trouy-triboulot and D. Masson, «Matériaux dérivés du bois», *Tech. l'ingénieur*, vol. 33, no. 0, 2017.
- [10] C. R. Frihart and C. G. Hunt, «Adhesives with Wood Materials- Bond Formation and Performance», *Wood Handb. Wood as an Eng. Mater.*, no. General Technical Report FPL-GTR-190, Chapter 10, pp. 10.1–10.24, 2010.
- [11] M. Knorz, E. Neuhaeuser, S. Torno, and J. W. Van De Kuilen, «Influence of surface preparation methods on moisture-related performance of structural hardwood-adhesive bonds», *Int. J. Adhes. Adhes.*, vol. 57, pp. 40–48, 2015, doi: 10.1016/j.ijadhadh.2014.10.003.
- [12] J. Luedtke, C. Amen, A. van Ofen, and C. Lehringer, «1C-PUR-bonded hardwoods for engineered wood products: influence of selected processing parameters», *Eur. J. Wood Wood Prod.*, vol. 73, no. 2, pp. 167–178, 2015, doi: 10.1007/s00107-014-0875-8.
- [13] L. MURMANIS, B. RIVER, and H. STEWART, «Surface and subsurface characteristics related to abrasive-planing conditions», *Wood fiber Sci.*, vol. 18, no. 1, pp. 107–117, 1986.
- [14] O. Kläusler, K. Rehm, F. Elstermann, and P. Niemz, «Influence of wood machining on tensile shear strength and wood failure percentage of onecomponent polyurethane bonded wooden joints after wetting», *Int. Wood Prod. J.*, vol. 5, no. 1, pp. 18–26, 2014, doi: 10.1179/2042645313Y.0000000039.
- [15] M. Kiliç, «Effects of machining methods on the surface roughness values of Pinus nigra arnold wood», *BioResources*, vol. 10, no. 3, pp. 5596–5606, 2015, doi: 10.15376/biores.10.3.5596-5606.

- [16] A. P. Singh, C. R. Anderson, J. M. Warnes, and J. Matsumura, «The effect of planing on the microscopic structure of *Pinus radiata* wood cells in relation to penetration of PVA glue», *Holz als Roh – und Werkst.*, vol. 60, no. 5, pp. 333–341, 2002, doi: 10.1007/s00107-002-0321-1.
- [17] L. F. de Moura and R. E. Hernández, «Evaluation of varnish coating performance for two surfacing methods on sugar maple wood», *Wood Fiber Sci.*, vol. 37, no. 2, pp. 355–366, 2005.
- [18] J. Cool and R. E. Hernández, «Evaluation of four surfacing methods on black spruce wood in relation to gluing performance», *J. Wood Sci.*, vol. 59, no. 3, pp. 185–194, 2013, doi: 10.1007/s10086-012-1318-y.
- [19] H. A. Stewart, «Some Surfacing Defects and Problems Related to Wood Moisture-Content», *Wood Fiber*, vol. 12, no. 3, pp. 175–182, 1980.
- [20] C. Gottlöber, «Zerspanung von Holz und Holzwerkstoffen», *Zerspanung von Holz und Holzwerkstoffen*, pp. 1–9, 2014, doi: 10.3139/9783446440036.fm.
- [21] R. Jokerst and H. Stewart, «Knife- Versus Abrasive-Planed Wood: Quality of Adhesive Bonds», *Wood Fiber Sci.*, vol. 8, no. 2, pp. 107–113, 1976.
- [22] D. Bamokina Moanda, M. Lehmann, and P. Niemz, «Investigation of the Impact of Micro-Structuring on the Bonding Performance of Beechwood (*Fagus Sylvatica* L.)», pp. 1–18, 2022.
- [23] L. F. de Moura, J. Cool, and R. E. Hernandez, «Anatomical Evaluation of Wood Surfaces Produced By Oblique Cutting And Face Milling», vol. 64, no. 2, pp. 1225–1228, 2010.
- [24] C. Bustos A, C. Moya L, J. Lisperguer M, and E. Viveros M, «Effect of knife wear on the gluability of planed surfaces of radiata pine», *Wood Fiber Sci.*, vol. 42, no. 2, pp. 185–191, 2010.
- [25] J. Sandak and M. Negri, «Wood surface roughness – what is it?», *BOKU Univ. Nat. Sources Appl. Life Sci.*, no. January, pp. 1–10, 2005.
- [26] L. Murmanis, B. H. River, and H. Stewart, «Microscopy of abrasive-planed and knife-planed surfaces in wood-adhesive bonds», *Wood Fiber Sci.*, vol. 15, no. 2, pp. 102–115, 1983, [Online]. Available: <http://wfs.swst.org/index.php/wfs/article/view/1181>.
- [27] M. Schmidt, P. Glos, and G. Wegener, «Verklebung von Buchenholz für tragende Holzbau-teile», *Eur. J. Wood Wood Prod.*, vol. 68, no. 1, pp. 43–57, 2010, doi: 10.1007/s00107-009-0382-5.
- [28] Kipfer H. U., «Neue Entwicklungen beschichteter Holzoberflächen im Aussenbereich», vol. 42, Weinfelden, 2010, pp. 179–183.
- [29] D. Ohnesorge, K. Richter, and G. Becker, «Influence of wood properties and bonding parameters on bond durability of European Beech (*Fagus sylvatica* L.) glulams», *Ann. For. Sci.*, vol. 67, no. 6, 2010, doi: 10.1051/forest/2010016.
- [30] J. Follrich, A. Teischinger, W. Gindl, and U. Müller, «Tensile strength of softwood butt end joints. Part 1: Effect of grain angle on adhesive bond strength», *Wood Mater. Sci. Eng.*, vol. 2, no. 2, pp. 83–89, 2007, doi: 10.1080/17480270701841043.
- [31] P. Hass, C. Müller, S. Clauss, and P. Niemz, «Influence of growth ring angle, adhesive system and viscosity on the shear strength of adhesive bonds», *Wood Mater. Sci. Eng.*, vol. 4, no. 3–4, pp. 140–146, 2009, doi: 10.1080/17480270903421529.
- [32] SN EN 302-1:2013, «Klebstoffe für tragende Holzbauteile – Prüfverfahren – Teil 1: Bestimmung der Längszugscherfestigkeit», SCHWEIZERISCHE NORMEN-VEREINIGUNG NORME, 2013.
- [33] SN EN 205:2016, «Klebstoffe – Holzklebstoffe für nicht tragende Anwendungen – Bestimmung der Klebfestigkeit von Längsklebung im Zugversuch Adhésifs – Colles pour bois à usages non structuraux – Détermination de la résistance au cisaillement en traction des joints à reco», Schweizerische Normen-Vereinigung (SNV), 2016.
- [34] DIN EN ISO 4287:2010, «Geometrical Product Specifications (GPS) - Surface texture: Profile method - Terms, definitions and surface texture parameters», Dtsch. Inst. für Normung, 2010.
- [35] SN EN 302-2:2018, «Adhésifs pour structures portantes en bois – Méthodes d'essais – Partie 2 : Détermination de la résistance à la délamination Klebstoffe für tragende Holzbauteile – Prüfverfahren – Teil 2 : Bestimmung der Delaminierungsbeständigkeit Adh», Schweizerische Normen-Vereinigung (SNV), 2018.)

- [36] C. Lehringer and J. Gabriel, «Review of Recent Research Activities on One-Component PUR-Adhesives for Engineered Wood Products’, in *Materials and Joints in Timber Structures*, vol. 9, Dordrecht: Springer, 2014, pp. 405–420.
- [37] R. E. Hernández and J. Cool, «Einfluss von Fräsparametern auf die Oberflächenqualität von Papierbirke, die mit Zwei Fräsverfahren Quer zur Faser Bearbeitet Wurde’, *Holz als Roh- und Werkst.*, vol. 66, no. 2, pp. 147–154, 2008, doi: 10.1007/s00107-007-0222-4.
- [38] P. Hass, O. Kläusler, S. Schlegel, and P. Niemz, «Effects of mechanical and chemical surface preparation on adhesively bonded wooden joints’, *Int. J. Adhes. Adhes.*, vol. 51, pp. 95–102, 2014, doi: 10.1016/j.ijadhadh.2014.02.014.
- [39] G. Clerc et al., «Improvement of ash (*Fraxinus excelsior* L.) bonding quality with one-component polyurethane adhesive and hydrophilic primer for load-bearing application’, *Int. J. Adhes. Adhes.*, vol. 85, no. June, pp. 303–307, 2018, doi: 10.1016/j.ijadhadh.2018.06.017.
- [40] L. F. De Moura and R. E. Hernández, «Evaluation of varnish coating performance for three surfacing methods on sugar maple wood’, *For. Prod. J.*, vol. 56, no. 11–12, pp. 130–136, 2006.

Investigation of Fleural Properties of Glued Laminated Timber Composed of Oil Palm Wood

Martin Hackel
Technische Hochschule Ostwestfalen-Lippe
Lemgo, Deutschland



Investigation of Flexural Properties of Glued Laminated Timber Composed of Oil Palm Wood

1. Introduction

As global population increases, raw material consumption rises. The main drivers of this development are the food industry, energy sector, chemical and pharmaceutical industry as well as the construction sector. Oil palms (*Elaeis guineensis* JACQ.) supply all these industries with raw material. The increased material consumption has led to an expansion of oil palm cultivation areas, especially in Southeast Asia. Between 1995 and 2020, the cultivation area increased by 350 % to 28.7 million hectares [1]. The economic lifespan of oil palms is limited to approximately 25 – 30 years [2]. The clearing of plantation areas after the economic lifespan results in about 100 million m³ usable oil palm wood per year [2]. The accumulated material is only used to a limited extent. The material has the potential for substituting tropical timbers, for example, as raw material for building products in its areas of cultivation.

The development of building products based on wood or other lignified plants (palms, bamboo) is an economically costly process. Use cases, production and properties of building products are specified in the European Union and worldwide by corresponding standards (Glulam: DIN EN 408:2012-10 [3], DIN EN 14080:2013-09 [4]). To show compliance, respective tests need to be carried out. These tests are associated with a significant economic effort.

Digitalisation and improvements in computer science offer opportunities to reduce the economic effort of developing building products. In this context, the finite element method (FEM) is a common tool. Using FEM, larger test series can be performed by varying the input data of a predefined model and time and material consumption can be reduced. The application quality of the FEM depends on the quality of the material and experiment parameters used for modelling. In the literature, necessary material characteristics for oil palm wood are limited. As a result, no modelling of products made of oil palm wood has been carried out to date.

The objective of this work is to examine the suitability of the FEM for modelling the flexural behaviour of glulam beams made of oil palm wood. Based on the examination of literature on the modelling of layered materials and elastic constants of oil palm wood, methods for modelling oil palm glulam beams are developed. The methods are implemented and the results compared with laboratory tests. Local and global bending modulus of elasticity (MOE) and correlations between MOE and density of the specimens are determined. Influences of model parameters are to be examined. Representation dimension (two- / three-dimensional), underlying material model (isotropic linear elastic / orthotropic linear elastic), riders in the support situation, material properties (destructive / non-destructive material testing) and element size are the focussed parameters. The significance of the influencing factors is investigated. The suitability of the software RFEM 6.02 (Dlubal Software GmbH) for the given task is evaluated.

2. State of the Art

The following sections provide an overview of the state of knowledge in the fields of oil palm wood with its anatomical, physical and mechanical characteristics relevant for modelling and the application of the FEM for layer-based wooden and composite materials.

2.1. Anatomical features of oil palm wood

Oil palms (*Elaeis guineensis* JACQ.) are monocotyledons. Their anatomical structure differs from conifers and deciduous trees (dicotyledons). Oil palms lack various features typical for

dicotyledons, for example annual rings, wood rays, a differentiation between heartwood and sapwood, knots, fibre deviations and other inhomogeneities. The tissue is considered anisotropic. Differences between radial and tangential direction do not occur [5, 6].

On a macroscopic level, the tissue of the oil palm (oil palm wood) consists of two structural features, low-density parenchymatic ground tissue and high-density vascular bundles. The vascular bundles run mostly parallel to the surface of the trunk. Killmann and Lim [5] report helically running vascular bundles in the upper part of the trunk. The distribution of vascular bundles within the trunk influences the properties of the oil palm wood. Starting from the trunk periphery, the stem is characterised by a 15 - 26 mm thick layer of parenchymatous ground tissue with irregular fibre strands and undirected vascular bundles, referred to as the cortex. This structure differs from the internal zones of the trunks [5]. Lim and Khoo [2] define three zones. The outer zone occupies approximately 20 % of the stem cross section. It is characterised by a low proportion of parenchymatous tissue and a high vascular bundles content [5]. The inner zone occupies about 40 % of the stem cross section and is characterised by scattered larger vascular bundles. The central zone represents a transitional area between peripheral and inner zone. It occupies 40% of the stem cross section [7]. Fathi [8] confirms this relationship and describes a decrease of vascular bundles towards the inner zone. Lim and Khoo [2] report a correlation between stem height and the proportion of vascular bundles per unit area. Fathi [8] confirms the results of Lim and Khoo [6].

The density is crucial for the elastic properties of oil palm wood. The density of oil palm wood varies significantly depending on its position in the trunk. Lim and Khoo [6] indicate a density range of 170 - 700 kg/m³ and report a correlation between proportion of vascular bundles and density. Within the horizontal plane the density increases with increasing distance from the stem centre. Density decreases with increasing stem height [5, 6, 8]. Kölli [7] describes the variation of the density along the stem axis and in the horizontal direction using exponential functions.

2.2. Elastic constants of oil palm wood

The material behaviour of oil palm wood in the linear elastic range can be described using nine elastic constants. The constants are the Young's moduli (E) along the three anatomical axes, three shear moduli in the symmetry planes (G) and three Poisson's ratios (μ). Fruehwald-Koenig [9] uses ultrasonic measurements to determine the dynamic MOE in the direction of the vascular bundles. The results exceed the results of static bending tests and show linear correlation with the density ($R^2 = 0.81$). Fruehwald-Koenig and Heister [10] determine a Young's modulus in tension parallel to the vascular bundles of 488 - 13102 MPa and report an exponential relationship between density and tensile Young's modulus ($R^2 = 0.53$).

Kölli [11] determines shear moduli G_{TL} and G_{RL} in static tests and shows linear ($R^2 = 0.39$) or exponential relationships ($R^2 = 0.43$) between density and shear modulus. Fruehwald-Koenig and Faust [12] determine the shear modulus in all three planes using dynamic ultrasonic measurements. The results of G_{LR} and G_{TL} show a correlation ($R^2 = 0.87$) to the density, whereas for G_{RT} the correlation is weaker ($R^2 = 0.56$).

Poisson's ratios are determined by Fruehwald-Koenig and Faust [12] using ultrasonic measurements ($\mu_{LR} = 0.389$, $\mu_{RL} = 0.026$, $\mu_{LT} = 0.911$, $\mu_{TL} = 0.044$, $\mu_{RT} = 0.647$ and $\mu_{TR} = 0.707$). Hackel [13] determines Poisson's ratios in compression tests, using digital image correlation. Radial and tangential direction are not differentiated. The ratios $\mu_{LR/T} = 0.379 - 0.523$ are obtained. There are no correlations between density and Poisson's ratio ($R^2 = 0.0024$). In a separate evaluation on the test specimen, a ratio of $\mu_{RT} = 0.117$ is obtained.

2.3. FEM for layered wooden materials

The use of the FEM is an established technique for modelling the flexural behaviour of glulam beams and other layered wooden materials. One of the first applications of FEM to predict the load-bearing capacity of spruce glulam beams is presented by Ehlbeck *et al.* [14]. In a two-step process, the structure of the beams with varying material properties and inhomogeneities is generated and then the load-bearing capacity is calculated using the FEM. Linear-elastic material behaviour is assigned to the elements in the tension zone

and ideal plastic behaviour to the compression zone. If the tensile strength within an element is reached, a failure of the element is assumed. If the compressive strength is exceeded, the properties of the elements are changed so that no further forces can be absorbed [14]. An improvement of the approach of Ehlbeck *et al.* [14] («Karlsruhe calculation model») and transfer to beech wood is carried out by Blaß *et al.* [15, pp. 58-61]. The model is formed analogous to Ehlbeck *et al.* [14]. In the first stage, the production of glulam lamellas with stochastically distributed properties is simulated. The modelling of a four-point bending test (DIN EN 408:2004-08) using FEM to determine the MOE and the bending strength forms the second stage [15, 16]. The possibility of applying the described method to other wood species is discussed by Gao *et al.* [17], using the wood species Cathay Poplar. Compared to real tests on corresponding glulam beams, the MOE is overestimated with FEM, but the bending strength is underestimated [17].

Further, FEM can be used to model the flexural behaviour of hybrid glulam beams. Ferrier *et al.* [18] use FEM to investigate glulam beams made of wood, concrete and carbon fibre reinforced plastic. The individual zones of the model (wood, concrete, plastics) are assigned to material parameters corresponding to the material behaviour. The connection between the materials is assumed to be a perfect bond. The model is compared with laboratory tests. Load-displacement diagrams of modelling and laboratory tests show good agreement.

3. Material

The test specimen modelled in this work are layered beams produced and physically tested by Heister [19]. The properties of the lamellae used to set up the beams vary over the height of the beam. The dimensions of the beams are 2200 mm x 50 mm x 102 mm (length x width x height). The beams consist of six 17 mm thick lamellae. The properties of the lamellae are selected so that the beams achieve strength class C 14 (DIN EN 338:2016-07 [20]) and the extrapolated strength class C 10 defined by Heister [19]. Densities and other material properties are assigned to the three zones of the beam (tension, shear, compression). The density range for tension lamellae is set to 335 – 363 kg/m³ (C 10) and > 427 kg/m³ (C 14). The compression zone density ranges are 289 – 335 kg/m³ (C 10) and 363 – 427 kg/m³ (C 14). In the shear zone lamellae show densities < 289 kg/m³ (C 10, C 14). Two types of lamellas were used to build up the GLT beams: Specimens with the identification N (natural) are composed of inhomogeneous lamellae showing natural property gradients. Specimens with the identification A (assembled) are formed of lamellae manufactured from narrow stripes of homogeneous density showing reduced property gradients.

3.1. Determination of the material parameters

The Young's moduli and shear moduli are calculated with regression functions between density and the corresponding material constants. Fruehwald-Koenig and Faust [12] provide relationships shown in equation (1) – (3) for Young's moduli along the anatomical axes and in equation (4) – (6) for the shear moduli in the symmetry planes (all determined from ultrasonic testing).

$$E_L(\rho) = 22.345 \rho + 204.89 \quad (1) \quad G_{RT}(\rho) = 0.6917 \rho - 16.657 \quad (4)$$

$$E_R(\rho) = 0.318 \rho + 223.38 \quad (2) \quad G_{TL}(\rho) = 1.3857 \rho - 91.621 \quad (5)$$

$$E_T(\rho) = 1.37 \rho - 42.164 \quad (3) \quad G_{LR}(\rho) = 1.0738 \rho - 37.963 \quad (6)$$

$$E_{L,R,T} = \text{Young's moduli along the anatomical axes [MPa]}, G_{RT,TL,LR} = \text{shear moduli in the symmetry planes [MPa]}, \rho = \text{density} \left[\frac{\text{kg}}{\text{m}^3} \right]$$

Fruehwald-Koenig and Heister [10] determine the relationship between density and Young's modulus parallel to the vascular bundles shown in equation (7) using static tensile tests. Respectively, equation (8) shows the relationship between density and shear modulus in the TL plane longitudinal direction determined by Kölli [11] in a two-plate shear test.

$$E_{t,0}(\rho) = 0.0021 \rho^{2.41} \quad (7) \quad G_{TL,stat}(\rho) = 0.2812 \rho - 1.7586 \quad (8)$$

$$E_{t,0} = \text{Young's modulus parallel to the vascular bundles [MPa]}, G_{TL,stat} = \text{static shear modulus TL plane [MPa]}, \rho = \text{density} \left[\frac{\text{kg}}{\text{m}^3} \right]$$

Comparing Young's modulus and shear modulus, calculated for the average lamella density (379 kg/m³) using dynamic and static relationships, shows overestimations of 152 % (Young's modulus) and 314 % (shear modulus) by the dynamic relationship. Missing static properties are derived from the dynamic properties by appropriate reduction. Poisson's ratios are not density dependent, the values $\mu_{LT} = 0.497$, $\mu_{LR} = 0.497$ and $\mu_{RT} = 0.117$ are used [13].

4. Methods

The following sections present the methods used in this work. The determination of the elastic flexural properties, the selection of modelling parameters and corresponding experiments are illustrated. The implementation of the experiments into the software package RFEM 6.02 is presented.

4.1. Determination of the elastic flexural properties according to DIN EN 408:2012-10

The elastic flexural properties are determined according to DIN EN 408:2012-10 [3] in a four-point bending test. The support points are spaced 1836 mm apart, corresponding 18 times the height of the beam (h). The beam length (l) of 2200 mm (21.5 x h) fulfils the requirements given in DIN EN 408:2012-10 [3] ($l \geq 19 \times h$). Figure 1 shows the corresponding test setup.

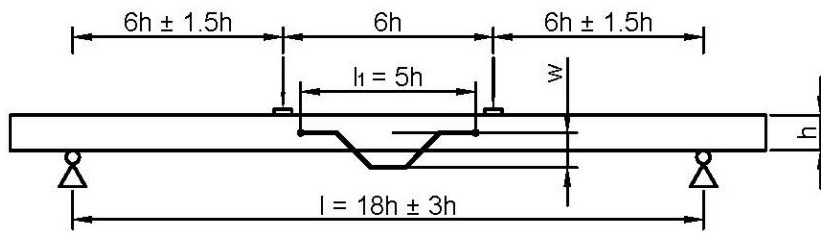


Figure 1: Test setup to determine the flexural properties in a 4-point-bending-test according to DIN EN 408:2012-10 [3]

The distance of the load points equals 6 h (612 mm). In the investigations by Heister [19], these values deviate from the standard with distances of 646 mm, 612 mm and 595 mm. The shortest distance between support and load points is set to $6 \pm 1.5 h$ (459 – 765 mm); distances of 595 mm, 612 mm and 620.5 mm selected by Heister [19] correspond to the specification. Riders may be inserted at the load points to minimise local deformations. Heister [19] uses plywood (beech, birch), pine and oil palm wood riders at load and support points. The applied force must not exceed 0.4 times the estimated maximum force ($F_{max,est}$). Heister [19] assumes $0.4 * F_{max,est} = 1200 \text{ N}$. DIN EN 408:2012-10 [3] distinguishes between local and global MOE. The MOEs correspond to the proportionality constants of the load-deformation curves of the tested beams. The MOEs are determined in the range of 10 % to 40 % of the estimated maximum force. The local MOE is determined using equation (9), the global MOE using equation (10). Due to insufficient data, Heister [19] sets the value for the shear modulus equal to infinity.

$$E_{m,l} = \frac{al_1^2(F_2 - F_1)}{16I(w_2 - w_1)} \quad (9)$$

$$E_{m,g} = \frac{3al^2 - 4a^3}{2bh^3 \left(2 \frac{w_2 - w_1}{F_2 - F_1} - \frac{6a}{5Gb} \right)} \quad (10)$$

$E_{m,l}$ = local MOE [MPa], $E_{m,g}$ = global MOE [MPa], a = smallest distance support to load point [mm], l = distance between supports [mm], l_1 = measuring distance local MOE [mm], I = moment of inertia [mm⁴], b = beam width [mm], h = beam height [mm], $F_2 - F_1$ = load difference load states [N], $w_2 - w_1$ = deflection difference states [mm], G = shear modulus [mm]

4.2. Determination of modelling parameters and experiments

The effects of five parameters and their influence on the results of the experiments are investigated. The parameters are the geometry (2D or 3D representation), riders, the material model (isotropic, orthotropic), the material constants determination (non-destructive (nd), destructive (d)) and the element size (8.5 mm, 5.66 mm). Geometry, riders, material model and element size are evaluated to determine parameter settings for further experiments. The investigation of the parameter material properties serves as a starting point for optimisation of the modelling results. Between each experiment one parameter is changed. This makes it possible to observe the parameter effect. The experiments are carried out using 23 beams. The total number of experiments is 138.

4.3. Experiment implementation in RFEM 6.02

The experiments are implemented in RFEM 6.02. Geometric modelling, implementation of the support situation, load application and meshing structure are considered. The beams are represented in the form of two- or three-dimensional models. Planes or volume bodies represent the lamellae. A perfect bond is assumed between the lamellae. Modelling of the adhesive joints is omitted in this work, as no failure is reported by Heister [19].

Isotropic and orthotropic linear elastic material models are used to describe the material behaviour of the lamellae. In the isotropic case, one Young's modulus, one shear modulus and one Poisson's ratio are required. For the Young's modulus, the Young's modulus parallel to the vascular bundles is used. The shear modulus is defined by the mean value of the three material specific shear moduli. Young's and shear modulus are assigned according to the lamella density. The Poisson's ratio is set to $\mu = 0.497$. In the orthotropic case, nine elastic constants are necessary. The Young's and shear moduli are assigned according to the lamella density using the equations (1) – (6) and the Poisson's ratios $\mu_{LT} = 0.497$, $\mu_{LR} = 0.497$ and $\mu_{RT} = 0.117$ are used.

The supports are defined as nodal or line supports. No displacement is possible along the Y and Z-axes. The bearings in the X-direction are described by a spring with a spring constant of 0.1 kN/m (see Figure 2) and allow displacements along this axis.

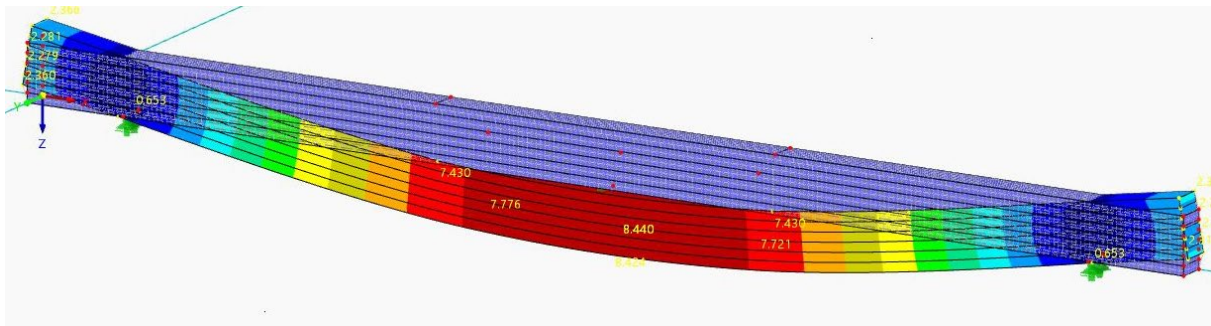


Figure 2: Visual representation of the deformation of specimen A2 (C10)

Four nodal supports are defined to determine the deflection. The supports comply with the specifications in DIN EN 408:2012-10 [3]. Loads are applied in the form of nodal or line loads. The loads act along the Z-axis. Each load point is subjected to half of the total load. The lamellae are modelled out of rectangular plate elements (2D) or cube-shaped volume elements (3D). The default element size is set to 8.5 mm or 5.66 mm. The element sizes correspond to two, respectively three, elements over the lamella thickness. Riders (experiments 5 and 6) are additional volume bodies in the areas of the support and load points. The riders vary in size, material and material parameters according to Heister [19]. Movement between beam and rider is restricted. The models consist of 3108 elements with 3380 nodes (experiment 1) up to 366019 elements with 110802 nodes (experiment 6).

Deformation and further results, such as equivalent stresses, are calculated using the solver of RFEM 6.02. The results are portrayed as graphical representations (see Figure 2) and nodal displacements in table form.

4.4. Determination of the influence of the homogenisation of the lamellae

Natural property gradients are only representable to a limited extend by modelling. The assignment of one density and corresponding material properties to the respective lamella leads to an artificial homogenisation of this lamella. The homogenisation of wood leads to a reduction in the variance of the material properties [21, pp. 681-682]. It can be assumed that the artificial lamella homogenisation shows reduced coefficients of variation (COV). To take effects acting on both specimen groups A and N into account, the quotient of their COVs is calculated (coefficient of comparison (CC)). Changes can be examined by comparing the CCs of the experiments with the CC of Heister [19]. Reduction of the COV of group N with COV of group A leads to an increased value of CC. The CC is calculated according to equation (11).

$$CC = \frac{COV_A}{COV_N} \quad (111)$$

$CC = \text{comparison Coefficient, } COV_{A,N} = \text{COV specimen groups A and N } [\%]$

5. Results and Discussion

The results of this work are shown and discussed in the following sections. Local and global bending MOE are considered separately and compared afterwards. The influence of shear lamellae density on local and global MOE is investigated. The influence of artificial homogenisation on the specimen collective N is considered. Subsequently, the methods applied and the modelling software used are discussed.

5.1. Local MOE

Table 1 shows the statistical variation parameters of the experiments. The local MOE differs between the experiments. The maximum values range from 5603 MPa to 11078 MPa, surrounding the maximum value determined by Heister [19] of 7128 MPa. The minimum values range from 2746 MPa to 8238 MPa and include the minimum of 3151 MPa recorded by Heister [19]. The mean values show the same behaviour as the maximum and minimum values. The highest mean value of 9625 MPa is achieved in experiment 2. The lowest mean value of 4050 MPa is recorded in experiment 6. The mean values of experiments 1 - 3 are about 5350 MPa higher than the mean values of experiments 4 - 6. With 5422 MPa, the mean value of Heister [19] lies in between these two experiment groups. The standard deviations vary between 815 MPa and 864 MPa. The standard deviation of Heister [19] is 1055 MPa and exceeds this range of about 200 MPa. The COVs of experiments 1 - 3 (mean 8.79 %) are 11.66 % below the COVs of experiments 4 - 6 (mean 20.45 %). Heister [19] determines a COV of 19.46 %.

Table 1: Statistical parameters of the local MOE

	Exp. 1	Exp. 2	Exp. 3	Exp. 4	Exp. 5	Exp. 6	Heister [18]
Parameters	2D, iso, nr nd, 8.5	3D, iso, nr, nd, 8.5	3D, ortho, nr, nd, 8.5	3D, ortho, nr, d, 8.5	3D, ortho, r, d, 8.5	3D, ortho, r, d, 5.66	
MIN [MPa]	7934	8238	7961	2759	2756	2746	3151
MAX [MPa]	10848	11078	10701	5768	5613	5603	7128
AVG [MPa]	9347	9625	9313	4155	4051	4050	5422
SD [MPa]	838	832	815	864	820	823	1055
COV [%]	8.97	8.64	8.75	20.78	20.23	20.32	19.46

Performing a one-factor ANOVA with repeated measurements provides a p-value of $< 2e-16$. Tested against a significance level $\alpha = 0.05$, the null hypothesis (H_0 : mean values local MOE are equal) must be rejected. A posterior pairwise t-test with alpha error correction according to Bonferroni provides the results discussed as follows. P values of 1 result in acceptance of the null hypothesis (H_0 : mean values are equal). There are no significant differences between experiments 1 and 2, 1 and 3, 2 and 3, 4 and 5, 4 and 6, and 5 and 6. Based on the p-values of $< 2e-16$, respectively $4e-5$, $6.4e-6$ and $6.2e-6$, the null hypothesis must be rejected for the remaining pairings. Significant differences between the results of Heister [19] and all experiments can be assumed.

Figure 3 on the left shows the relationships between density and local MOEs. Positive linear correlations are given in all experiments. The coefficient of determination R^2 of the correlations is between 0.5155 and 0.5492. The slopes of the linear relationships vary between 25.3 and 26.78. The slopes of the experiments differ from the slope of 33.451 given by Heister [19]. Differences between the linear correlations are limited to the ordinate intercept. Due to a deviating slope, the ordinate intercept shows limited comparability with the data from Heister [19].

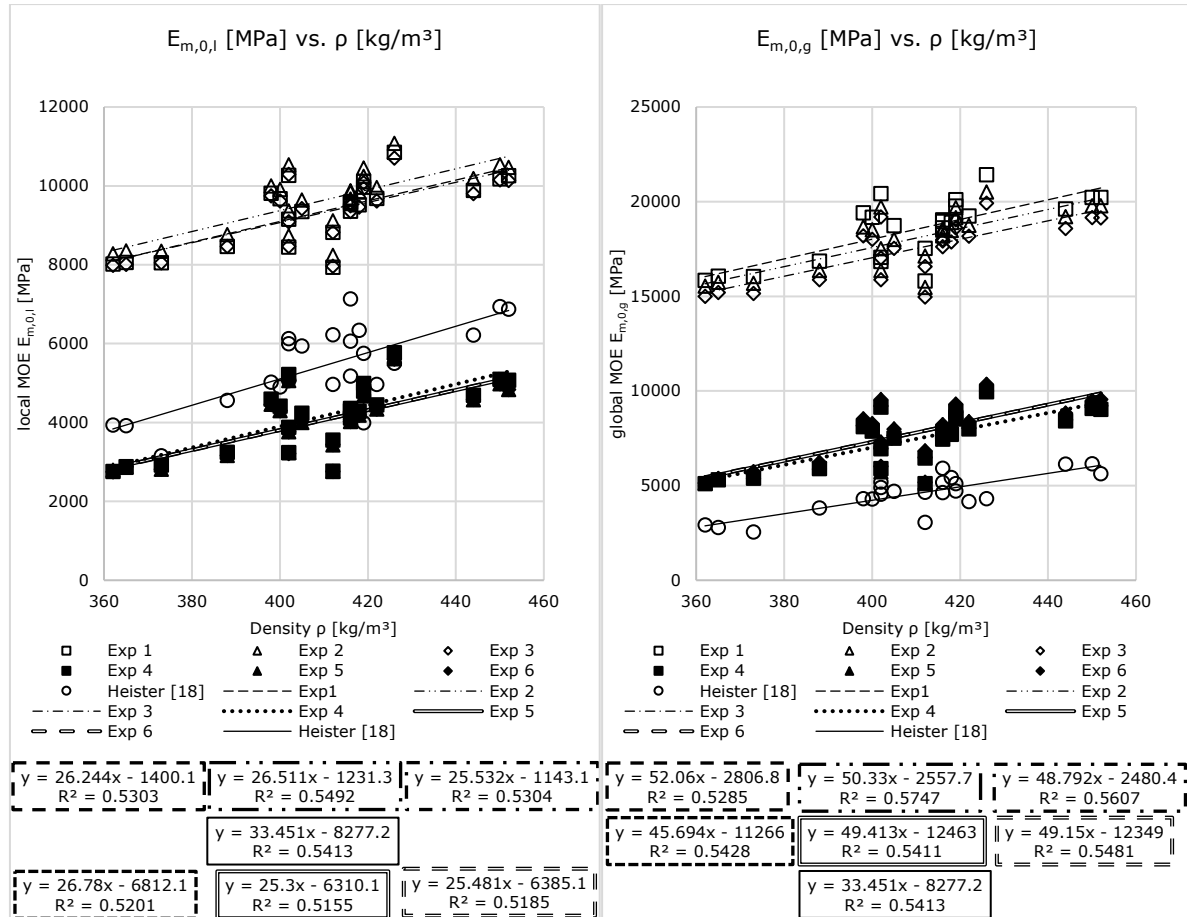


Figure 3: Relationship between density and local MOE (left) respectively global MOE (right) for the six experiments

5.2. Global MOE

Table 2 shows the statistical variation parameters of the experiments. The global MOE varies between the experiments. The maximum values range from 9953 MPa to 21414 MPa. The range lies above the maximum value 6142 MPa of Heister [19]. The minimum value 2541 MPa of Heister [19] lies below the range of the experiments from 5092 MPa to 15806 MPa. The mean values show the same behaviour as maximum and minimum values and range from 7447 MPa to 18513 MPa exceeding the mean value 4562 MPa of Heister [19]. The mean values of experiments 1 – 3 are about 10400 MPa higher than of the experiments 4 – 6. The mean values of all experiments exceed the value of Heister [19] by 2885 MPa to 13951 MPa. The standard deviations of the experiments vary between 1442 MPa and 1666 MPa and surpass the standard deviation (1022 MPa) of Heister [19]. The mean COV of experiments 1 – 3 (8.74 %) is 11.03 % lower than the mean COV of experiments 4 – 6 (19.77 %). The COV for Heister [19] is 22.41 % and about 3 % higher than the mean COV of experiments 4 – 6.

Table 2: Statistical parameters of the global MOE

	Exp. 1	Exp. 2	Exp. 3	Exp. 4	Exp. 5	Exp. 6	Heister [18]
MIN [MPa]	15806	15475	14955	5092	5128	5128	2541
MAX [MPa]	21414	20500	19911	9953	10350	10335	6142
AVG [MPa]	18513	18053	17501	7447	7773	7779	4562
SD [MPa]	1666	1544	1515	1442	1562	1544	1022
COV [%]	9.00	8.55	8.66	19.37	20.10	19.85	22.41

The one-factor ANOVA with repeated measures yields a p-value of $< 2e-16$. When tested against a significance level $\alpha = 0.05$, the null hypothesis (H_0 : mean values global MOE are equal) must be rejected. Significant differences between the mean values of the experiments can be assumed. A posterior pairwise t-test with alpha error correction according to Bonferroni delivers a p-value of 0.46 and 1 for the experiment pairings 1 and 2, 1 and 3, 4 and 5, 4 and 6 and 5 and 6. When tested against a significance level $\alpha = 0.05$ the null hypothesis (H_0 : mean values are equal) needs to be accepted for these pairings. All experiments show significant differences to the results of Heister [19]. Due to p-values < 0.05 , the null hypothesis is to be rejected for the remaining pairings. Figure 3 on the right shows the relationships between density and global MOEs. A positive linear relationship between density and global MOE is given in all experiments. The coefficient of determination R^2 lies between 0.5285 and 0.5747. The $R^2 = 0.6537$ in the study by Heister [19] is higher. The slopes of the linear correlations vary between 45.694 and 52.06, whereas the slope of Heister [19] with 35.545 is lower. Differences between the linear correlations are mainly limited to the ordinate intercept. Comparison of the ordinate intercepts is only possible to a limited extent due to the deviating slopes.

5.3. Discussion of the differences between the experiments for local and global MOE

Differences between the experiments can be attributed to varying factors. The difference between experiments 1 and 2 is the representation dimension (2D, 3D). Limited effects occur based on homogeneous material structure across the beam width. Small differences in the results between experiment 2 and 3 can be attributed to stress distribution in a four-point bending test. The beams are subject to stresses in fibre direction. Ehlbeck *et al.* [14] point out that the Young's modulus in fibre direction is an influencing factor for bending properties of beams. In experiments 1, 2 and 3 the Young's modulus along fibre direction is equal. The results vary insignificantly. Riders in experiments 5 and 6 shows no significant effect. This can be attributed to modelling in the elastic range (no plastic deformations). Riders only distribute the load. Minimising the element size shows no significant effect. Glišović *et al.* [22] and Vida *et al.* [23] confirm the sufficient discretisation by two or three elements over the lamella thickness. Significant differences between experiment groups 1 – 3 and 4 – 6 can be attributed to the material parameters. The mean reduction of the Young's modulus in the fibre direction of 55.4 % corresponds to the mean reduction of the results of the local and global MOE with 56.7 % and 57.5 %.

5.4. Comparison local vs. global MOE

The global MOE shows higher values than the local MOE in all experiments. Heister [19] reports an opposite relationship. Smaller global than local MOE is confirmed for spruce by Boström [24]. This relationship is not reported for small global MOEs. Boström [24] describes a transition for the relationship at 10000 MPa (local MOE $<$ global MOE). Nocetti *et al.* [25] confirm a transition for spruce at 8300 MPa. Boström [24] attributes the differences between local and global MOE to shear deformations and the influence of timber defects. The effects described are consistent with the results of experiments 4 – 6. Transferability of the results is limited due to the different materials investigated. The results of Heister [19] and experiments 1 – 3 cannot be explained by the effects described. The ratio of the mean values of local to global MOE in this investigation ranges from 0.505 to 0.558. The data from Heister [19] provide a ratio of 1.189. Boström [24] reports a ratio of 0.99 for spruce. The values determined by the modelling are below the literature values.

The relationships determined by modelling show high coefficients of determination $R^2 = 0.9783 - 0.9981$. The slopes of the regression lines of the experiments range differ from the slopes of the regression line of Heister [19] and DIN EN 384:2022-08 [26]. The relationship described in DIN EN 384:2022-08 [26] cannot be transferred to oil palm wood based on the present test results.

5.5. Influence of the shear lamellae density on the local and global MOE

Deviations of the calculated shear lamellae density from the density ranges provided by Heister [19] justify the investigation of the influence of the shear lamellae density on the local and global MOE. The investigation is carried out using one representative specimen and the modelling approach of experiment 4. Shear lamellae density is varied between 250 kg/m^3 and 452 kg/m^3 . The material constants are varied correspondingly. For both MOEs, a linear relationship between shear lamellae density and the corresponding MOE can be noted. The coefficient of determination of the relationships is $R^2 = 0.9987$ (global MOE) and $R^2 = 0.9952$ (local MOE). An increase in shear lamellae density by 202 kg/m^3 corresponds to an increase in the global MOE of 598 MPa (7.7 %) and an increase in the local MOE of 212 MPa (4.7 %). The influence of shear lamella density described here can explain part of the differences between the results of the global MOE of the experiments and Heister [19]. For a more precise determination of the effects, the number of experiments should be increased.

5.6. Influence of the homogenisation of the lamellae

Using equation (11), the coefficients of comparison are determined. A CC of 0.6 is recorded for the global MOE in Heister [19]. The CCs of the experiments show values from 0.85 to 0.96. An average increase of 0.31 in the CCs is noted. The comparison of the COVs of specimen groups A with the corresponding value of 14.77 % in Heister [19] shows mean deviations from -6.88 % to 3.45 %. Specimen group N shows deviations from -15.45 % to -3.95 % from the comparative COV of 24.46 %. The observation of increasing CCs and decreasing COVs compared to Heister [19] suggests an influence of artificial homogenisation of the lamellae on the modelling results of specimen group N. For the local MOE, due to the small deviations of the CCs of maximum 4.7 % in connection with small deviations of the COV, an effect of artificial homogenisation cannot be proven.

5.7. Discussion of methods and modelling software

The software RFEM 6.02 can be considered suitable for modelling the flexural behaviour of oil palm glulam. The modelling results differ from comparative laboratory tests. The differences are attributed to the material constants used. An optimization of the results is possible by adjusting the material constants. The material constants and the methods for material constant adjustment show limited applicability. The use of dynamically determined material constants leads to significant overestimations of local and global MOE, the use of corrected elastic properties leads to significant differences from the comparative tests. The parameter settings of the experiments are suitable for representing the tests carried out by Heister [19]. The depiction of the support and load represent reality with sufficient accuracy. The results show no significant difference between two and three-dimensional geometry models. Two-dimensional geometry models can be used to reduce computational effort. Changing the material model from isotropic to orthotropic shows no significant effect on the test results. Riders do not show influences on the experiments. The element sizes used show no significant influence on the modelling results. The reduction of the element size leads to a significant increase of the calculation time. The use of two elements over the lamella thickness is recommended.

The release date of RFEM 6.02 is recent at the time of writing. Inconveniences using RFEM can be noted. It is not possible to add user defined materials to the material library. Materials need to be created anew for each model. Importing material data from external sources (e.g. Excel files) is restricted. It is possible to control RFEM using programming languages, for example Python. This interface does not allow for the creation and saving of user-defined materials. Geometric models can be created via a graphical user interface or table input. Both variants are suitable for creating easy geometric models. The import

of CAD data can be realised to a limited extent. More exact modelling of property gradients in oil palm wood cannot be implemented in RFEM. The assignment of separate material properties to individual elements cannot be implemented. An adjustment of the mesh structure is possible to a limited extent. Finally, it can be stated that RFEM 6.02 is suitable for the modelling in the context of this work.

6. Conclusion and Outlook

The results of the experiments confirm the applicability of FEM for modelling oil palm wood-based glulam. The geometric models, volume and plane models based on individual layers with varying material properties, are suitable to represent the comparative tests. The investigation of the factors model dimension, material model, riders, material parameter determination and element size show no significant influence on the modelling results, the material parameter determination. The results of this work show significant deviations from laboratory tests, which can be attributed to the elastic constants used. Further investigations need to be carried out to guarantee reliable input parameters. The correlations between density and local and global MOE shown in this work are comparable to laboratory tests. Adjustments of the material parameters can be used to optimize the results. The comparison of the local and global MOE shows deviating behaviour from literature for common wood species. The global MOE exceeds the local MOE in all experiments. Further investigations on the global MOE of oil palm glulam are necessary and can use the findings of this work. The shear lamella density shows influences on the local and global MOE. Further experiments are needed to consolidate this influence. An influence of artificial homogenisation of lamellae on the results of the global MOE can be demonstrated (specimens N). RFEM 6.02 is suitable for the modelling carried out in the context of this work. Negative aspects include difficult input of user defined materials and limited usability of software interfaces. RFEM 6.02 can be used and recommended to a limited extent for modelling of complex structures and material inhomogeneity. The results of this work offer starting points for further modelling investigations. Considerations of the bending strength of glulam, realistic representation of inhomogeneous material structures and optimisation of results themselves and of investigated products are field of further investigations.

7. Acknowledgements

The investigation was financed by the German Federal Ministry of Education and Research through the «Bioökonomie International 2017» project «Oilpalmsugar (031B0767A)».

8. References

- [1] Food and Agriculture Organization of the United Nations. «Crops and livestock products.» <https://www.fao.org/faostat/en/#data/QCL> (accessed Jun. 3, 2022).
- [2] A. Fruehwald and K. Fruehwald-Koenig, «The Use of Oil Palm Trunks for Wood Products,» in *By-Products of Palm Trees and Their Applications*, 2019, pp. 69–80, doi: 10.21741/9781644900178-3.
- [3] DIN Deutsches Institut für Normung e. V., *DIN EN 408:2012-10 Holzbauwerke – Bauholz für tragende Zwecke und Brettschichtholz – Bestimmung einiger physikalischer und mechanischer Eigenschaften; Deutsche Fassung EN 408:2010+A1:2012.*
- [4] DIN Deutsches Institut für Normung e. V., *DIN EN 14080:2013-09 Holzbauwerke – Brettschichtholz und Balkenschichtholz – Anforderungen; Deutsche Fassung EN 14080:2013.*
- [5] W. Killmann and S. C. Lim, «Anatomy and properties of oil palm stem,» in *Proceedings NATIONAL SYMPOSIUM OF OIL PALM BY-PRODUCTS*, Kuala Lumpur, Forest Research Institute Malaysia (FRIM), Ed., vol. 87, 1985, pp. 1–25.
- [6] S. C. Lim and K. C. Khoo, «Characteristics of oil palm trunk and its potential utilization,» *Malaysian Forest*, vol. 49, pp. 3–22, 1986.
- [7] N. Kölli, «Density and Moisture Distribution in Oil Palm Trunks from Peninsular Malaysia,» Bachelor-Thesis, University of Hamburg, Hamburg, 2016a.
- [8] L. Fathi, «Structural and mechanical properties of the wood from coconut palms, oil palms and date palms,» Doctoral Thesis, University of Hamburg, Hamburg, 2014.

- [9] K. Fruehwald-Koenig, «Properties and Grading of Oil Palm Lumber,» in *Proceedings: 21st International Nondestructive Testing and Evaluation of Wood Symposium.*, Freiburg, X. Wang, U. H. Sauter, and R. J. Ross, Eds., 2019, pp. 204–212.
- [10] K. Fruehwald-Koenig and L. Heister, «Macromechanical and Micromechanical Behavior of Oil Palm Wood (*Elaeis guineensis* JACQ.) – Part 1: Tensile, Compression and Bending Properties,» *Publication in preparation*, 2022.
- [11] N. Kölli, «Relation shear modulus and densitiy for oil palm wood (*Elaeis guineensis* JACQ.),» *Personal communication*, 2022b.
- [12] K. Fruehwald-Koenig and B. Faust, «Evaluation of Elastic Constants of Oil Palm Wood using Ultrasonic Measurement,» in *Proceedings: 22st International Nondestructive Testing and Evaluation of Wood Symposium.*, Quebec City, Canada, X. Wang and R. J. Ross, Eds., 2022, pp. 29–39.
- [13] M. Hackel, «Bestimmung der Querdehnungszahlen von Ölpalmenholz (*Elaeis guineensis* Jacq.) im Druckversuch parallel zur Faser an Probekörpern in Gebrauchsabmessungen,» Scientific Internship, Ostwestfalen-Lippe University of Applied Sciences and Arts, Lemgo, 2022.
- [14] J. Ehlbeck, F. Colling, and R. Görlacher, «Einfluß keilgezinkter Lamellen auf die Biegefestigkeit von Brettschichtholzträgern,» *Holz als Roh-und Werkstoff*, vol. 43, no. 8, pp. 333–337, 1985, doi: 10.1007/BF02607817.
- [15] H. J. Blaß, J. Denzler, M. Frese, P. Glos, and P. Linsemann, *Biegefestigkeit von Brettschichtholz aus Buche* (Karlsruher Berichte zum Ingenieurholzbau 1). Universitätsverlag Karlsruhe, 2005.
- [16] M. Frese and H. J. Blaß, «Characteristic bending strength of beech glulam,» *Mater Struct*, vol. 40, no. 1, pp. 3–13, 2007, doi: 10.1617/s11527-006-9117-9.
- [17] Y. Gao, Y. Wu, X. Zhu, L. Zhu, Z. Yu, and Y. Wu, «Numerical Analysis of the Bending Properties of Cathay Poplar Glulam,» *Materials (Basel, Switzerland)*, early access. doi: 10.3390/ma8105362.
- [18] E. Ferrier, P. Labossière, and K. W. Neale, «Modelling the bending behaviour of a new hybrid glulam beam reinforced with FRP and ultra-high-performance concrete,» *Applied Mathematical Modelling*, vol. 36, no. 8, pp. 3883–3902, 2012, doi: 10.1016/j.apm.2011.11.062.
- [19] L. Heister, «Untersuchung des Einflusses der Rohdichte auf die Biegeeigenschaften von Ölpalme (*Elaeis guineensis* Jacq.),» Master-Thesis, Ostwestfalen-Lippe University of Applied Sciences and Arts, Lemgo, 2020.
- [20] DIN Deutsches Institut für Normung e. V., *DIN EN 338:2016-07 Bauholz für tragende Zwecke – Festigkeitsklassen; Deutsche Fassung EN 338:2016*.
- [21] F. Kollmann, *Technologie des Holzes und der Holzwerkstoffe: Anatomie und Pathologie, Chemie, Physik, Elastizität und Festigkeit*, 2nd ed. Springer Berlin Heidelberg, 1951.
- [22] I. Glišović, M. Pavlović, B. Stevanović, and M. Todorović, «Numerical analysis of glulam beams reinforced with CFRP plates,» *Journal of Civil Engineering and Management*, vol. 23, no. 7, pp. 868–879, 2017, doi: 10.3846/13923730.2017.1341953.
- [23] C. Vida, M. Lukacevic, J. Eberhardsteiner, and J. Füssl, «Modeling approach to estimate the bending strength and failure mechanisms of glued laminated timber beams,» *Engineering Structures*, vol. 255, p. 113862, 2022, doi: 10.1016/j.engstruct.2022.113862.
- [24] L. Boström, «Determination of the modulus of elasticity in bending of structural timber - comparison of two methods,» *Holz als Roh-und Werkstoff*, vol. 57, no. 2, pp. 145–149, 1999, doi: 10.1007/s001070050030.
- [25] M. Nocetti, L. Brancheriau, M. Bacher, M. Brunetti, and A. Crivellaro, «Relationship between local and global modulus of elasticity in bending and its consequence on structural timber grading,» *Holz als Roh-und Werkstoff*, vol. 71, no. 3, pp. 297–308, 2013, doi: 10.1007/s00107-013-0682-7.
- [26] DIN Deutsches Institut für Normung e. V., *DIN EN 384:2022-08 Bauholz für tragende Zwecke – Bestimmung charakteristischer Werte für mechanische Eigenschaften und Rohdichte; Deutsche Fassung EN 384:2016+A2:2022*.

Real-time digital collaboration interphases for timber structure analysis and calculation

Matias Penroz
Institut für digitale Bau- und Holzwirtschaft IdBH
Bern University of Applied Sciences
Biel/Bienne, Switzerland



Real-time digital collaboration interphases for timber structure analysis and calculation

1. Introduction

Timber buildings have been planned in a digital and industrialized fashion over the past decades, developing structured interphases for model-based communication even before Building Information Modeling (BIM) was introduced. Moreover, BIM has become the standard methodology to strengthen the digital model-based collaboration within the Architecture, Engineering and Construction (AEC) industry.

However, load-bearing structural planning for timber buildings using BIM requires iterative modelling exchanges (iteration loops) between detailed and non-detailed digital models (multi-scale models) from different disciplines, i. e. architecture and structural engineering. These iteration loops tend to overinform models, making the data analysis process within a model-based collaboration a complex task to perform, especially for industrialized timber construction where a high level of coordination in the early stages of buildings is required. Among model-based interphases, parametric modelling techniques perform well in reducing iteration loops, especially for complex multi-scale model systems. Additionally, real-time model-based interphases could be ideal for enhancing digital communication between architecture and structural engineering.

2. Real-time collaboration

Real-time collaboration is a term used for software or technologies that allow multiple users to work together on a project in real-time or simultaneously [1]. Applied to modern digital construction processes, real-time collaboration must cover at least three main aspects:

Multiple users working together (1) on the same project (2), and simultaneously (3).

To enable multi-user collaboration in construction projects, the AEC industry needed to develop a common language or structure to handle data exchange from one software to another without losing any data in the process. However, the technical aspects of simultaneously collaborating with several digital models are not yet fully developed due to each software utilize a different file format unreadable for other software interphases (Fig. 1). Furthermore, model-based communication tends to recur to non-standardized software maneuvering to overcome computational problems when exchanging or including new attributes from one model to another.

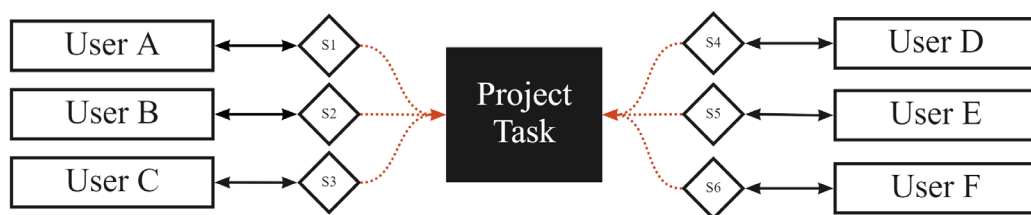


Figure 1: System expansion towards multi-user interphases. Each user is enabled to work on their Software ($S_1, S_2, S_3, \dots, S_n$).

2.1. BIM exchange protocols and IFC schema

BuildingSMART international regulates the BIM methodology and data exchange protocols, describing it as object-oriented and parametric [3]. Objects representing building elements have dynamic relations with other ones – for example, if a wall is relocated, so do the associated components. The core definition of BIM states that the parametric aspect of objects shall also cover the spatial relation between them, defining rules to define interconnected data layers. However, geometry instantiation in different software is not the same, even though objects sharing the same class will not explicitly mean sharing the

same geometry type. Real-time collaboration is one of the most significant barriers to the BIM methodology. The single model paradigm is based on a closed BIM environment where all trades operate from one centralized model containing all live project information. OpenBIM, on the contrary, is based on different trade models being continuously exchanged throughout the planning process of built assets, thus a neutral and flexible collaborative process (Fig. 2).

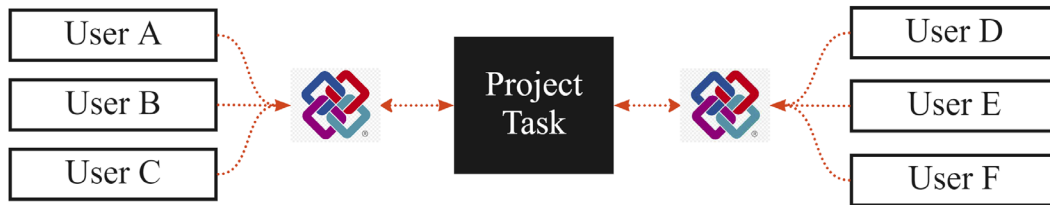


Figure 2: openBIM proposal for a collaborative multi-user workflow environment, different users sharing a common language, regardless of their native software.

OpenBIM collaboration is supported by the Industry Foundation Classes (IFC) standard, defined as a data structure or specification, therefore a schema rather than an exchange format [3]. IFC defines construction objects within a built asset by their attributes and parameters (BIM-Objects), thus an object-oriented specification.

2.2 Parametric methods for interoperability

Parametric design methods demonstrate a reliable manner of transferring, controlling and analyzing geometry between models based on functions and logical operations. Thus, requiring computer programming knowledge and applied mathematics to manage abstract geometrical operations between entities. One of the most common interfaces within this field is the Rhinoceros 3D/Grasshopper, based on visual design programming (VDP) to define and control geometry with the help of algorithms. These methods allow users to intuitively program and perform a series of controlled geometric actions to work out a particular design proposal.

The term algorithm refers to «a procedure or set of rules used in calculation and problem-solving» (OED Dictionary). Applied to VDP is the action of interconnecting a series of pre-defined parameters, processes, and functions to build up a specific «recipe» to solve a particular problem or design task (Fig. 3).

$$\text{Algorithm} = \underbrace{(\text{Semantic})}_{\text{IFC schema}} + \underbrace{(\text{Geometry})}_{\text{Geometrical constraints Dimensional constraints}} + \underbrace{(\text{Topology})}_{\text{Spatial relations}}$$

Figure 3: Proposed method to define the content and relation of objects with algorithmic design.

Architectural and structural engineering software combines such methods with native BIM object libraries to enhance interoperability and diminish user error when analyzing complex models containing significant amounts of variable and undefined entities with interdependent requirements from different disciplines. However, further development of exchange protocols to systematically manage parametric IFC entities throughout the construction planning process for load-bearing timber structures has not been addressed.

3. Model-based quality gates

The BIM methodology is based on a series of exchange phases where models are generally exchanged from one coordination phase to another specific level of development (LOD) correlating to five key stages of a project from 100 to 500 [4]. Consequently, several instances to allocate attributes of construction entities occur within one development phase, resulting in a condensed collection of data merged into heavy coordination models for each phase (Fig. 4).

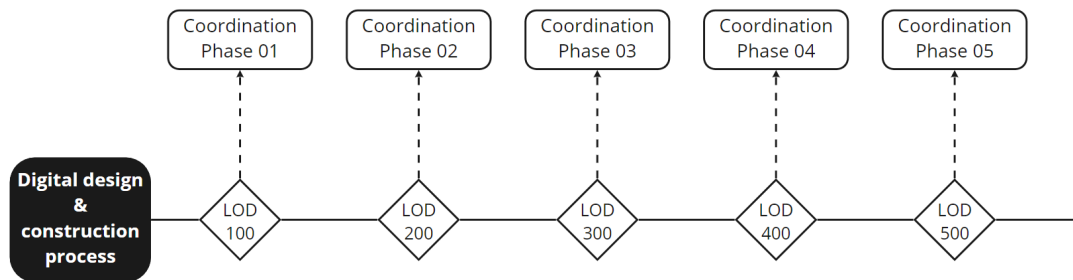


Figure 4: Linear description of the development and coordination process within a BIM workflow

Such a planning process is not compatible with timber buildings since assemblies are not planned by linear processes in which data enrichment is only validated by a specific LOD [5]. Iterative exchanges of digital models (iteration loops) must enable a flexible yet systematic construction of interconnected layers with different LOD demanding early recognition of anchoring geometry to allocate requirements (placeholders).

3.1 Data-Vessels

A suitable technique to simplify and reduce layer combinations is splitting construction components into three main layers creating a layering system [5].

The proposed methodology uses generic bounding boxes (data vessels) to transform complex layering systems into simplified geometric entities, avoiding the exchange of condensed data over phases. In addition, data vessels carry the minimum geometric and alphanumeric information to perform analysis and adjustments between phases and models. A core layer represents the load-bearing system, whereas the sublayers either a facade or an interior layer regarding the component spatial position within the built asset. After defining the scope of data vessels and the layering system, models exchange protocols need to be implemented.

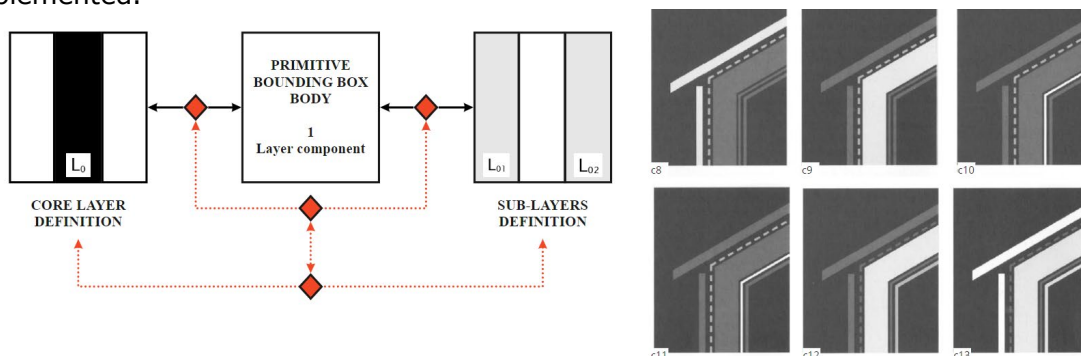


Figure 5: Schematic representation for multi-layer development of complex building components.

For such purposes, a two-steps approach will cover the modelling iteration loops and the structure of coordination models, redefining in this manner how data is created and thoroughly parametrized to accomplish project goals:

- Coordination phases must be correlated with target project milestones instead of project LOD, defining and constraining modelling purposes, requirements, and the scope of the data use, and
- Data vessels are defined by placeholders, merging multi-layer components into simplified geometry.

By this, data vessels cover the possibility that any incoming data can be created within a particular milestone regardless of their LOD and subdividing them into operative layers based on spatial position (Fig. 5).

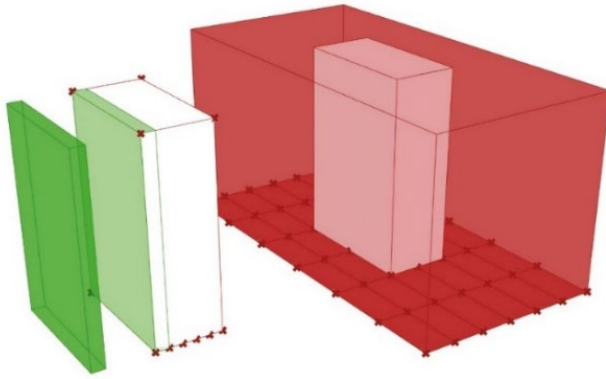


Figure 6: Data vessels in the form of simplified bounding boxes representing IFC entities when transferring data, vertical core element with a related division wall component.

For timber construction, layers represent and allocate the different requirements of disciplines involved in the planning sequence. Thus, not all data is necessarily allocated into one single layer but into sublayers which dependence can be parametrized by data vessels. The layering system represents a simplification of the possible layer combination within a data vessel, where different layer arrangements can describe timber assemblies. By this, layers are categorized according to their function and location within a building asset (Fig. 6). As a result, attributes are attached to single-layer data vessels and consequently to the sub-layers based on their functionality, defining spatial relations, and enabling data vessels to inherit requirements or attributes from parent classes (Fig. 7).

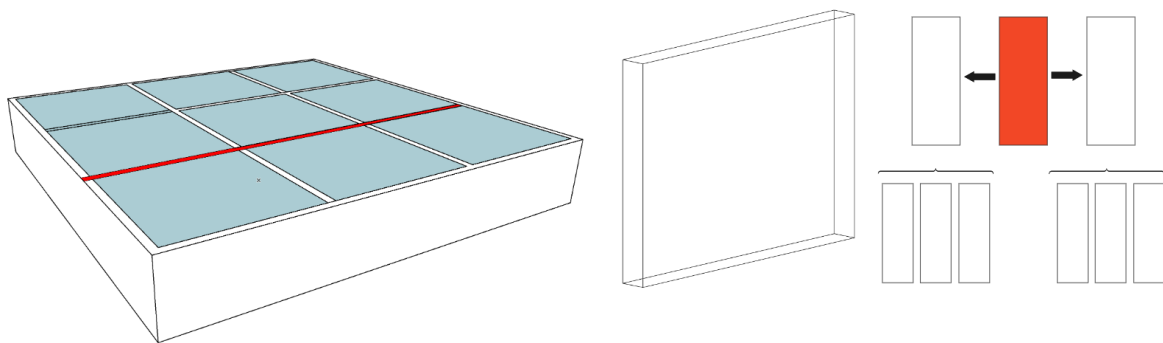


Figure 7: Volumetric process of a single IfcWall entity derived from the adjacent room configuration. Sub-layers are created from the parent entity, inheriting the requirements according to the sublayers functionality

Furthermore, if coupled with parametric design methods, designers could develop specific algorithms for each development phase and deploy model-based quality gates for coordination purposes, averting overinformed models transferring all gathered data from one phase to another. Model exchange instances within development phases are reduced, and interconnected parametrized data vessels throughout the planning process are structured (Fig. 8). The advantage of this process is that planning teams are encouraged to define early input-output constraints for data vessels based on project milestones instead of non-regulated LOD, shifting the design process from a push to pull methodology [6]. The creation of data is only to fulfil the requirements of a specific milestone, and instead of larger models for multiple purposes, simplified models for target milestones are created.

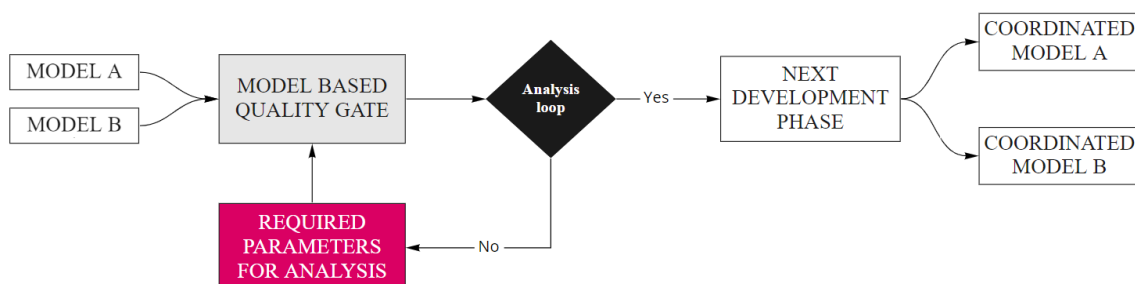


Figure 8: Generic process definition for model-based quality gates implementation.

For interoperability purposes, project milestones will derive the model-based quality gates with correspondingly parametrized barriers to retain data and test models against each other to examine whether the predefined data-vessels requirements fulfil the project milestone or not (Fig. 9).

The system's definition is in this regard based on three main components:

- Construction classes correlated with an IFC entity represented by a spatial bounding-box structured into data vessels,
- Parametrized data vessels describing the entity's attributes or state and
- Parametrized quality gates defined by project milestones and input-output requirements criteria, extracted by the milestone definition.

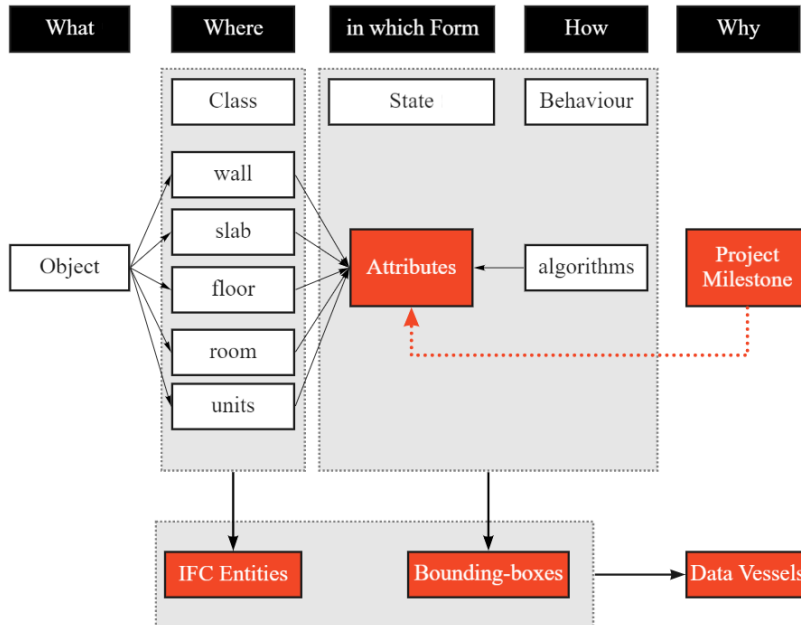


Figure 9: Extension of object classes categorization diagram includes project milestones and their influences on defining boundary conditions for data-vessels.

After structuring the content and instantiation of data vessels, topological relationships between them shall indicate how individual entities spatially relate to each other [7]. These spatial relations are of utmost relevance for designers since attributes can be inherited from one entity to another or be a calculated result based on spatial relations between them, even across non-corresponding classes, i.e. room attributes to wall or slab elements (Fig. 10).

Furthermore, superordinate spatial dependencies among entities allow a more precise definition of spaces, mainly if changes in earlier phases must be executed when specific project requirements do not comply with the intended design.

Requirements

$$\text{Room.A} + \text{Room.B} = \text{ConstructionComponent}$$

LayerConstruction

$$\text{ConstructionComponent} = 1\text{LayerConstructionComponent}$$

$$1\text{LayerConstructionComponent} = L1+L2+L3+... Ln$$

Figure 10: Spatial construction and allocation of the requirements for individual construction components

Combining topology with semantic models creates a systematic and robust manner to preserve intrinsic spatial conditions over project milestones. Without establishing topological relations between entities, designers cannot thoroughly define spaces in the sense of spatial continuity from one entity to another (Fig. 11).

Thus, models from early development phases could not be tested or analyzed against later ones due to non-existing spatial relationships. By this, zones and rooms may define spatial reference elements such as points, edges and surfaces, where walls, columns, or beams can be instantiated in further reference models, defining relationships between classes over primitive geometrical elements. Hence, closing the loop between spatially interconnected entities coexisting at the same location but in different development phases.

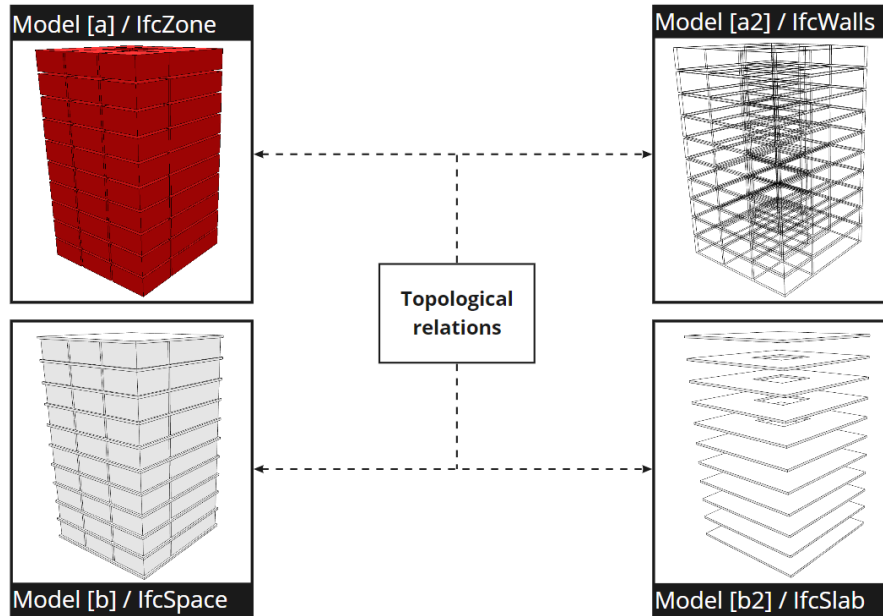


Figure 11: Topology and semantic relations

3.2 Interphase implementation

Project objectives and requirements define how BIM models interact throughout the planning process by defining roles and exchange phases. Typically, such data is stored within a BIM execution plan (BEP), transferred to the information delivery manual (IDM) and organized into use cases which will structure data into model view definitions (MVD), finally utilizing the IFC specification schema to relate entities into semantic construction objects [8].

From these methods, a sequence of exchange phases and project coordination gates are defined and agreed upon from the very beginning (Fig. 8). As previously proposed, defining project milestones contribute to the early identification of valuable criteria for the model-based quality gates describing the minimum input-output requirements for real-time interphases between disciplines. The proposed setup methodology expands the linear delivery process from the BIM methodology towards structured iteration loops supporting variable LOD data consolidation towards real-time collaboration interphases.

To accurately switch from a push to a pull process, the triggering of any activity related to data creation is covered by the predefined milestones. Therefore, buffering of data waiting to be analyzed is avoided by acting only over specific tasks and the exchange of models is replaced by real-time collaboration interphases to coordinate data towards the target milestone.

The generic process architecture (Fig. 11) represents the proposed pull data stream to define and create models systematically. Starting from a specified milestone, defining the requirements to construct the model-based quality gates will determine the parameters over which different disciplines can build models.

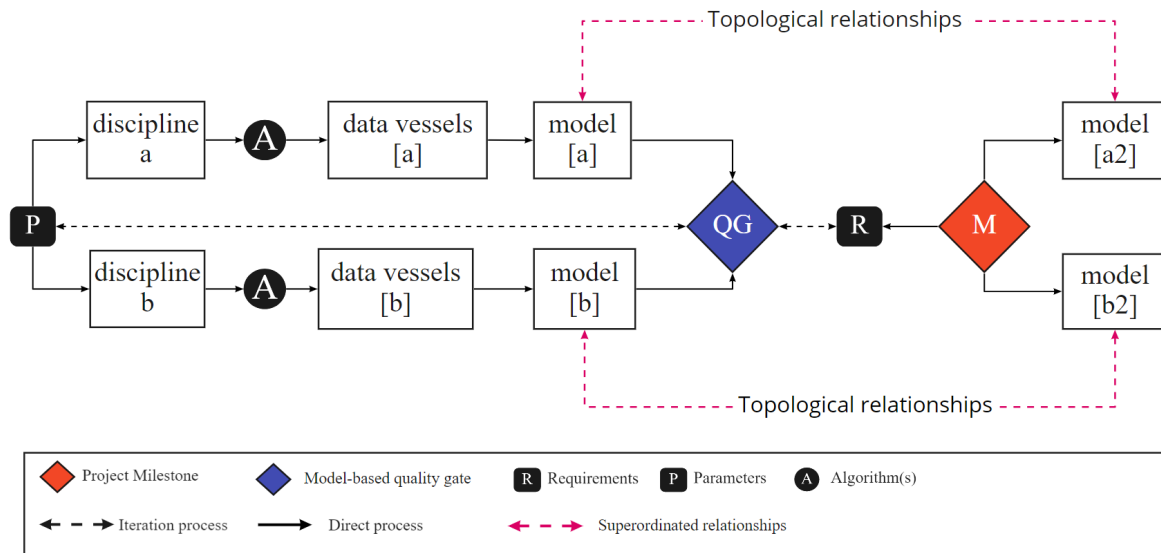


Figure 11: Detailed process architecture of pull planning methods to validate the structure and content of different discipline models and their resulting data vessels.

Even though project milestones define the alignment of modelling purposes, spatial relations within models act as a superordinated definition to link data vessels between non-corresponding classes without losing the primitive parent topology. This means that by preserving a clear description of models topology, traceability of changes or inheriting attributes from one class to another can be assessed by user-defined algorithms.

It is to be also tested that models from earlier phases can influence models in later ones because the system is proven to work with minor buffering of data.

Following the pull planning principle:

→ Fewer exchange phases → fewer data to be created → fewer communicational issues.

For load-bearing structures in timber buildings, the following milestones are proposed to manage the iterative loops to develop layering systems systematically. Each milestone is controlled by a model-based quality gate and described by a use case (Table 1).

Table 1: Milestones system for the layer development and coordination in timber structures

	Milestone	Model-based quality gate	Use Case
M1	Global Structural Analysis	Core and shell model analysis	Reference System Model
M2	Prefabrication level Analysis (scope/def)	Single-layer range model analysis	Breakthrough Coordination model
M3	Construction System Analysis	Three-layer range model analysis	Raw construction model

3.3 Reference models

To practically test and illustrate the systematic development of model-based quality gates, a generic case study building is selected and defined by following attributes (Fig. 12):

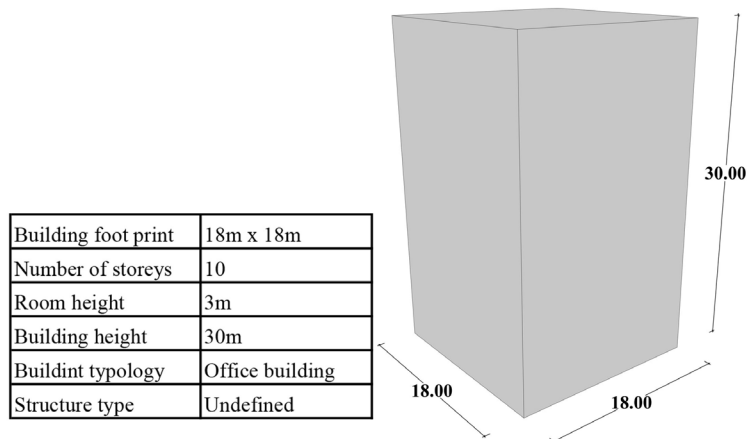


Figure 12: Definition of the case study building to test the proposed methodologies. Boundary conditions are defined according to the left-sided table and right-sided figure

Secondly, the project milestone defines the boundary conditions of how disciplines shall interact (Fig. 13). For these research purposes, the test setup involves two disciplines; Structural Engineering and Architecture, where the milestone requirements restrict both domains, thus the scope of data generation is reduced by only «modelling» what is requested by the model-based quality gate definition.

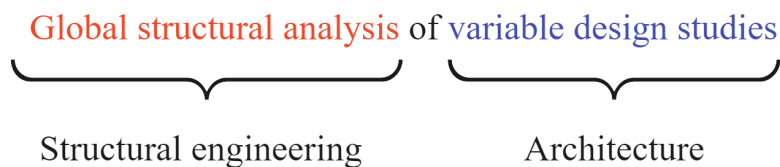


Figure 13: Definition of the project milestone and the identification of the two interacting disciplines for the real-time collaboration instance.

With this, two relevant steps are accomplished before sorting the individual parameters for the model-based quality gate:

- The project milestone definition covers two different disciplines: structural engineering and architecture
- Input-output requirements can be tested on a model-based quality gate, and simultaneously the necessary parameters to define and structure the data vessels content are defined.

On the one hand, data vessels represent an idealized version of the geometrical properties of a built asset. On the other hand, IFC entities correspond to the semantic description of the physical material version of components such as walls, slabs or beams. To systematically reach the proposed milestone, interconnected models are parametrically constructed and linked within each other. The proposed models are defined as follow:

1. Raw geometry model
2. Mass model
3. Room model
4. Core and shell model
5. Analytical model
6. Single-layer components model

These reference models are developed by defining raw geometry in Rhino/Grasshopper, including semantic information from Archicad and performing the structural analysis to estimate the core layer dimension in RFEM by iterative loops (Fig. 14).

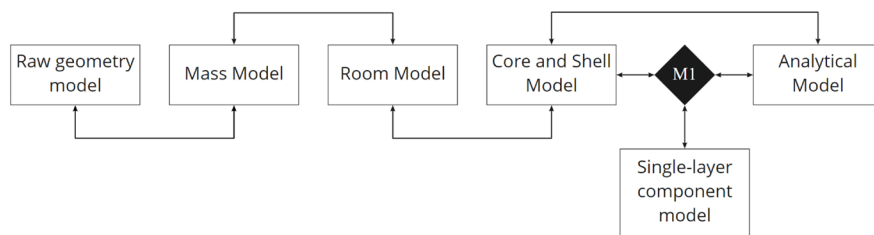


Figure 14: Process Architecture for the interaction between models in an iterative digital workflow environment

4. Model-based quality gates

Additionally, the spatial relations within all reference models algorithms are defined using the Topologic toolkit for Grasshopper developed by TopologicApp. The latter allows controlled user-defined modifications in real-time when facing the model-based quality gates without losing spatial continuity between coexisting entities. These techniques allow for recursive analysis by using abstract topological components such as faces, edges or vertices, to act as «supports» when defining BIM Queries for IFC entities. Topological queries are used to evaluate further design steps, i.e., searching and listing all adjacent data-vessels of a particular one or identifying all data-vessels with shared edges [9]. Furthermore, by utilizing VDP, the interoperability between models is executed by parametrized interphases. Different data types may be allocated among models without losing the continuity from one model to another while defining the needed reference elements. (Fig. 15).

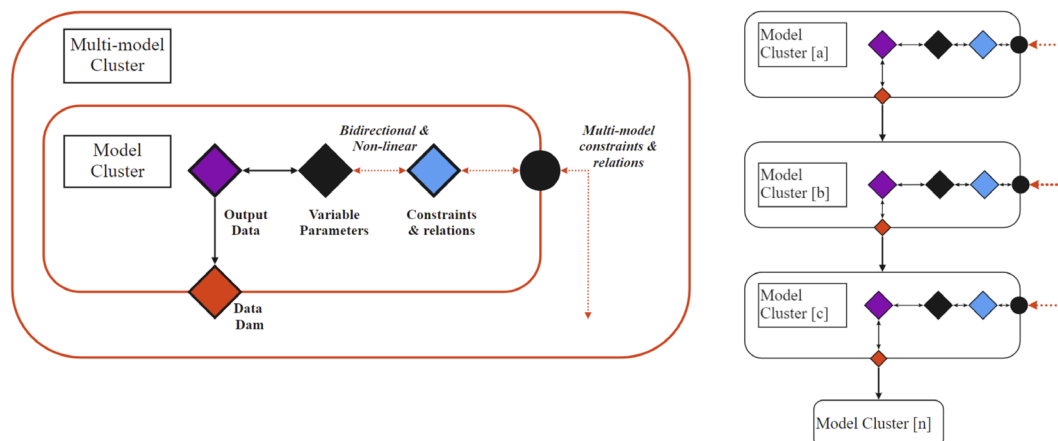


Figure 15: System definition for interconnected parametric models. Interoperability setup between clusters. Black dots as an open gate towards requirements based on constraints and relations between data.

4.1 Modelling iteration loops

The parametric script is ruled by a set of separated definitions linked to each other (model cluster) containing four main aspects:

- target-specific parameter sets,
- variable parameters,
- output data and a final
- data dam as final instance of the interphase to «retain» data before transferring it to the following reference model.

Each reference model is intended to exhibit a common data structure to allocate variable data vessel typologies and several model clusters comprise a multi-model cluster system. The proposed process architecture, defining in this manner the algorithmic interphase to link data among them (Fig. 16).

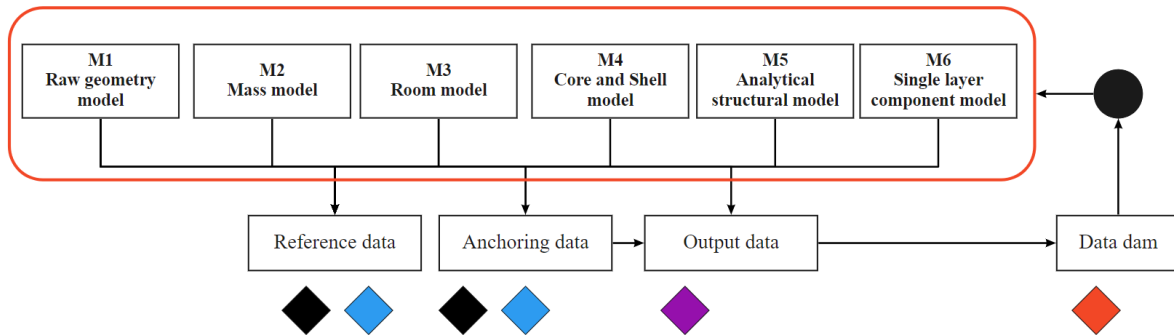


Figure 16: Process architecture for the multi-model cluster interphases

The multi-model cluster reduced the typologies of generated data by simplifying reference geometry throughout all models. In addition, topological relations contributed to managing overlapping geometry by enabling different geometry objects to share primitive geometry without duplicating them into the model (Fig. 17).

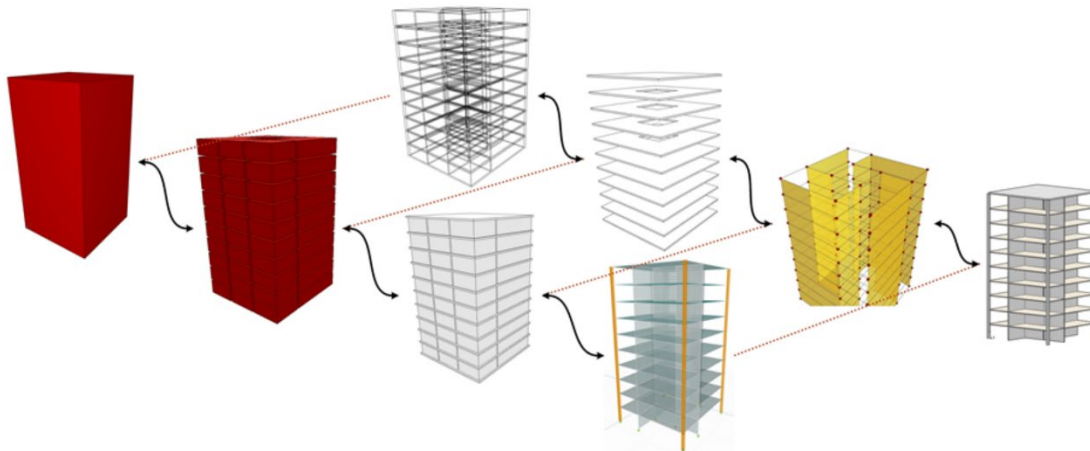


Figure 17: Summary of reference models acting as a conglomerate in an interconnected cascade effect.

However, data resulting from iterative development loops of multi-layer assemblies can neither be related nor indexed due to the lack of interconnected topological multi-scale models on a conceptual level. The proposed algorithmic interphases are programmed to ensure multi-scale operative interphases over planning phases by linking reference models based on topology, therefore reducing data creation. Moreover, by defining topological models, anchoring elements for further new spatial relations ensures that iteration loops automatically update the complete system interphase. In addition, model-based quality gates create, control and specify the layering system of topologically defined data vessels. In this regard, not only the coexistence and linkage of different entities can occur at the same location, but also the possibility of different LOD simultaneously occurring within entities can also be possible (Fig. 18).

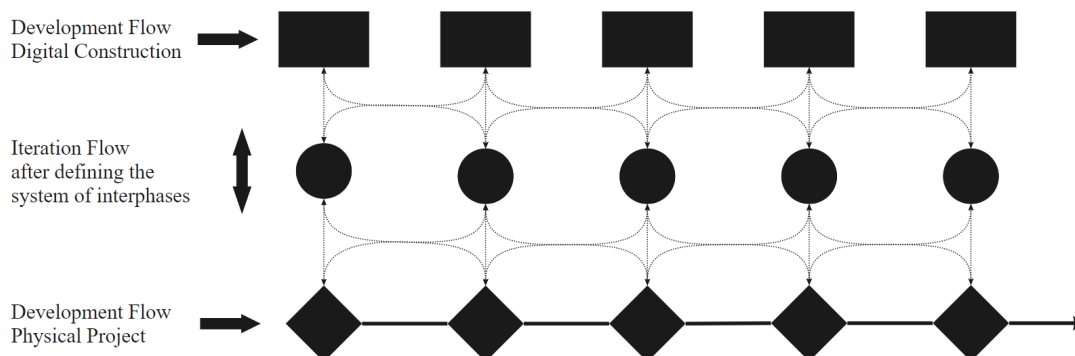


Figure 18: Iteration flow with incorporated algorithmic interphases

Planning aspects from industrialized timber construction demonstrate that modelling iteration loops benefit from defined and undefined categories for instantiating interconnected layering systems. For instance, a timber frame wall belonging to a core layer may not need to contain all individual studs to coordinate connection details between structural engineering and architecture but rather be represented by single-layer data vessels with anchoring elements. As an example, a node with all corresponding sublayers and the corresponding adjacent single-layer data vessels (Fig. 19).

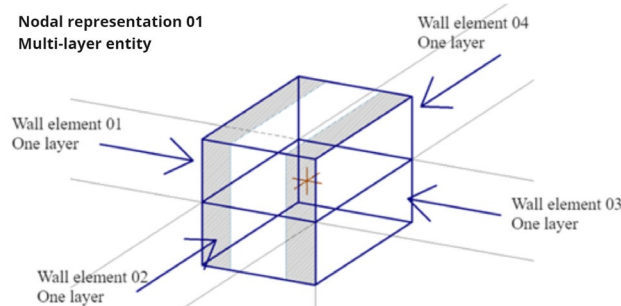


Figure 19: Graphic representation for multi-scale modelled objects; Four wall types represented by single layer entities and a structural joint represented by a multi-layer entity with the corresponding anchoring reference node.

4.2 Influences of DfMA in timber structures

Design for manufacturing and assembly has shown to be an effective planning methodology in the early phases of timber structures, mainly for two critical aspects:

- Offsite prefabrication of components requires an early estimation of needed raw material for manufacturing purposes.
- Timber structures commonly comprise complex assemblies with multi-layer systems distributed in various construction systems for vertical and horizontal load distribution.

Production know-how can be pulled into early design stages, improving assembly sequences, a better quality of final components, and project-specific detail catalogues for parametric joints can be thoroughly defined. In this regard, DfMA aspects can be adapted towards design for prefabricated timber construction (DfPTC) [10] by not just focusing on assembly and manufacturing aspects but also on the layer-oriented development of timber construction processes.

4.3 Layer development in timber construction

The introduced layering system method to isolate load-bearing from the non-load bearing layers determined that interphases to develop the core-layer match well with the model-based quality gates and real-time collaboration instances by showing models without any geometrical errors between the used software among analysis loops (Fig. 20)

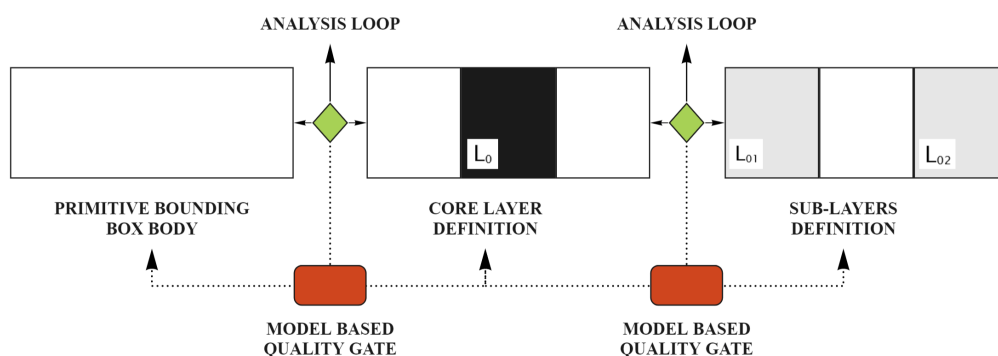


Figure 201: Layer-oriented development process coupled with multi-scale model-based quality gates.

Before implementing the layering system for the model-based quality gates, non-regulated relations between complex entities comprised unsorted data from different IFC entities. Thus, sublayer categorization cannot be correctly allocated into target data vessels due to the non-existing filtering parameter sets (Fig. 21)

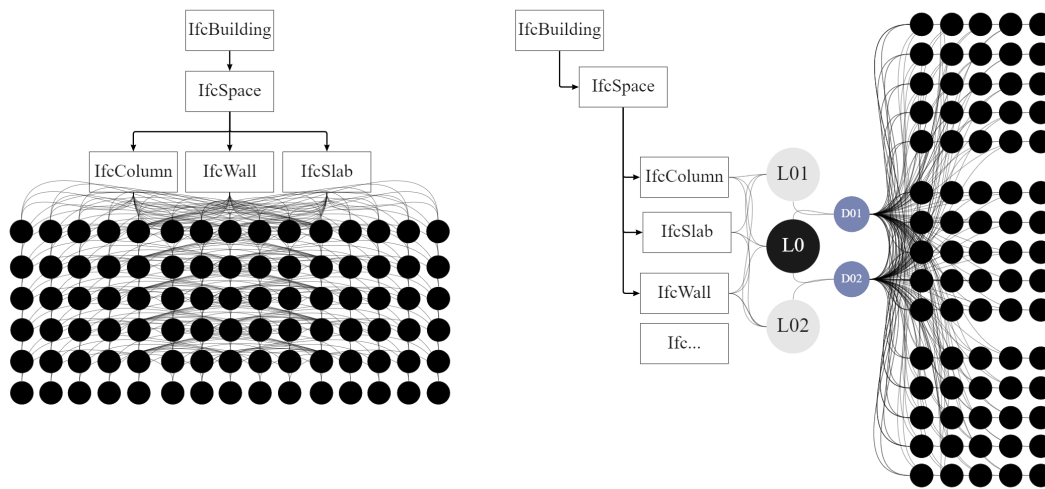


Figure 21: Abstract visualization of a non-regulated (left) and regulated (right) system for complex layering systems and varying layer combinations between non-corresponding IFC entities.

According to multi-scale models from the digital simulations (reference models 2,3,4,5, and 6), implementing up to three-layers data vessels resulted in topologically related non-corresponding classes from the IFC schema (Fig. 21).

Moreover, for the core load-bearing layer, the obtained results are:

- Simplified models with fewer data vessels
- Reduced amount of IFC entities to transmit semantic information
- Linked data between all reference models

5. Conclusions

The real-time collaboration interphases were demonstrated to simplify the model-based collaboration for planning load-bearing timber structures, averting the exchange of reference models and generating accurate geometry and semantic information of the evaluated construction components. With the systematic implementation of the layering system, a reduced amount of reference axis systems are needed to develop further subsequent layers in complex timber assemblies.

With an accurate development of multi-scale modelling techniques and defining spatially related multi-layer components, the effects of varying requirements for systems, components and assemblies can be assessed without geometric and alphanumeric information loss throughout all the planning phases of a built asset.

However, managing model-based quality gates by parametric modelling techniques towards real-time interphases cannot be organized with current BIM methodologies or data management standards. The IFC schema does not support a flexible development of spaces before construction components, leading to unrelated systems from the very beginning.

6. Acknowledgement

The author acknowledge the contribution of the BIMwood research project team.

7. References

- [1] Techopedia, (2008). Retrieved from Techopedia.com: real-time-collaboration
- [2] Jinfeng Lou, W. L. (2020). A review of BIM data exchange method in BIM collaboration.
- [3] Baldwin, M. (2019). The BIM Manager – A practical Guide for BIM Project Management.
- [4] Hausknecht, K. (2016). BIM-Kompodium – Building Information Modeling als neue Planungsmethode: IRB Verlag.
- [5] Kolb, J. (2008). Systems in Timber Engineering. Basel, Boston, Berlin: Birkhäuser.
- [6] Nicholas, J. (2011). Lean production for competitive advantage. New York: Productivity Press Taylor & Francis Group.
- [7] G. Arun Francis, S. M. (2018). A perspective approach to set topological definitions. International of Pure and Applied Mathematics, 118(20), 485-490.
- [8] A. Borrmann, A. K. (2015). Building Information Modeling – Technologische Grundlagen und industrielle Praxis. Wiesbaden: Springer.
- [9] R. Aish, A. P. (2012). Spatial Information Modeling of Buildings Using Non-Manifold Topology with ASM and Design Script. Advances in Architectural Geometry, 25-36.
- [10] BIMwood (2022); <https://sites.hslu.ch/architektur/bimwood/>

Analysis and evaluation of mass data for production planning and system configuration

Niki Karatza
TH Rosenheim/holzbau.tech
Rosenheim, Deutschland



Analysis and evaluation of mass data for production planning and system configuration

1. Introduction

The increasing rates of approved residential and non-residential buildings in timber construction in Germany reflect today's demand for timber buildings [1]. With the growing market, the field of application of timber construction is also expanding. Buildings are being planned and constructed with ever-increasing size and complexity.

The rising number of ever-larger timber construction projects lead to company expansions. Growth is particularly evident in companies with 20 or more employees. Both the number of companies of this size and the number of employees in these companies have increased by about 10% in 2021 [1].

To make work along the process chain as efficient as possible despite any changes, the development and optimization of production concepts and products are becoming more and more relevant for timber construction companies. The main goal here is to gain capacity by eliminating waste or by expanding resources.

In this context, the start-up holzbau.tech has been working on individual production planning and system configuration for timber construction companies. Data analysis plays a major role in this because it makes it possible to create customized concepts for specific requirements.

In this paper, the approach to production planning and the use of data for this purpose is presented. The focus is placed on the motivations and the benefits. The required programming process is only described superficially here.

2. Motivations for production planning and system configurations

More than 95% of timber construction companies in Germany have fewer than 20 employees. This illustrates that the timber construction industry is predominantly characterized by craftsmanship [1].

However, one major obstacle to capacity increase is the ongoing shortage of skilled workers. Business surveys conducted by Holzbau Deutschland have shown for years that the difficulty of finding workers is one of the top 5 obstacles to success for timber construction companies [1]. Therefore, to make companies sustainable and to be able to expand independently of personnel expansions, automation solutions should be implemented.

When converting to automated production, it is important to ensure that the upstream and downstream processes are also designed accordingly. This means, for example, that product designs that are too complex may not be efficiently manufactured by automation. If a company's products are too complex, they should be partially standardized so that they can be produced automatically by the technology used. This requires specific product development as well as system configuration.

As the level of automation increases, so does the relevance of end-to-end digitization. Data from construction planning must be created in such a way that it can be processed by machines and the materials and building elements can be produced automatically. The level of detail required here is higher than in manual productions.

Thus, if you follow the changes in the wood construction market and want to adapt your company and production to them, many necessary courses of action quickly arise. To always be future-oriented, a continuous improvement process should be introduced, and existing systems should be regularly questioned. This applies both to the processes of planning and production as well as to the technologies and systems used.

3. Today's common way of production planning and system configuration

Since every company usually differs from other companies in terms of products or processes, production planning should be carried out as individually as possible. First, the current state of the respective area of a company is analyzed to determine what needs to be optimized. In order to make effective changes, the goals should be clearly defined beforehand. But here is where the difficulty often arises. In many cases, the targets are defined by assumptions. For instance, production planning is usually based on information from a few reference elements. These are normally determined from an average. However, the problem is that these reference products can be outdated and often do not reflect the whole reality. More complex designs, for example, are often overlooked.

Another approach is to assume the worst case for production planning. A case in point is that the prefabricated walls in timber construction are usually a maximum of 13m long. With the thought of being able to cover all element lengths, planning is often done according to this maximum length without questioning whether this is really necessary and profitable (Figure 1). This unnecessarily takes up a lot of space in the production hall that could be used for other activities.



Figure 1: Negative example of producing mainly shorter elements on 13m-long tables

Thus, both approaches in planning do not meet the actual demand. It must be taken into account that both these approaches include exceptions. If these exceptions occur only very rarely, however, the concepts may be a hindrance to the actual demand.

4. Approach for realistic planning: data analysis

For a better reflection of reality in production planning and to focus on the truly relevant requirements, attention should be paid to data. The Economist called data «The world's most valuable resource» on its cover of the May 2017 issue. By analyzing data, well-founded conclusions can be drawn about previous projects. Data evaluation provides information about the actual consumption of resources, such as the processing times required, or the materials used. Calculated costs can be compared with actual costs.

In addition to conclusions that data analyses reveal retroactively, inferences for the future can also be recognized. Products of past projects can be examined, whereby it can be recognized, for example, whether designs are error-prone or ineffectively manufactured with the current production methods. E.g., If there are a lot of production stops because of a certain product design or because of some construction details, an optimization would be reasonable. Another example is the configuration of a new machine. The requirements can be identified based on the data analysis of the previously produced parts and thus a precise system configuration can be developed. Among other things, this means that machines are not unnecessarily oversized and are equipped with all the capabilities that are really needed.



Figure 2: Example optimized table length based on product analysis through data

4.1. Today's impediments for timber construction companies

While the benefits of data analytics for production planning are clear, experience shows that the approach is hardly practiced in the timber construction industry. What is stopping timber construction companies from collecting and analyzing the data they create?

A common response from companies is that they simply have no data to analyze. However, this is not correct. They just lack the understanding of what useful data is and what

it can reveal when analyzed. Therefore, the first step to using data analytics is to recognize what data is needed, generated, and used already.

Every company has data and information in the form of invoices, purchase orders or self-created charts. These can, for example, provide information about how much raw material was procured.

Beyond that, a large amount of data is generated in the planning department of timber construction companies. After all, of all the construction methods, timber construction is the one with the highest proportion of self-planning by an executing company. This is due to the prefabrication of building elements for which the manufacturing companies need their own workshop planning. Thus, they have been producing their own 3D models for decades [2].

So while data is generated in any case in timber construction, it is not used further beyond production. To change this and enable the analysis of numerous data sets, the first prerequisite is their accumulation and storage instead of leaving them unused.

4.2. What to do to enable data analysis

As described above, the first step towards data analysis is to gain an understanding of the data itself. To do this, it is best to catalog them first (Figure 3). This means getting an overview of where data is generated and needed, both on computers and on machines. Once an overview of the data has been obtained, it must be backed up first, if it has not already been done, in order to avoid data loss. Depending on the digitization of the company, this can work in conjunction with an existing ERP (Enterprise Resource Planning) system, cloud systems or similar platforms.

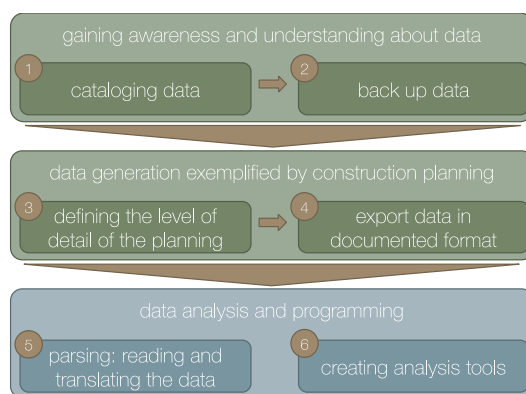


Figure 3: Simplified process for data analysis

Having established the awareness of the value that created data brings, attention should be paid to the quality of its creation. The most important area here is the construction planning. The plans provide the most information about the products and production. Depending on the degree of prefabrication and automation of the company, plans are already drawn up in greater or lesser detail. In principle, the more information that is created about an element, the more insight the data and its analysis will provide in retrospect. It is therefore important to define the level of detail of the plans and to maintain it consistently. The fact that the plans should also be created as

error-free as possible is just as important for the data analysis as for the production itself. After the data has been created in the form of manufacturing plans, it must be exported in a format that can be further processed by data analysts. It is referred to as a documented format. This means that a defined interface description exists for the output information, which describes the meaning of the individual data. An example is the universal data format BTL. It is not only supported by timber construction CAD and machine software, but a wide range of software solutions can also read and write the format [3]. But even a simple export as an Excel spreadsheet can be used for evaluation.

Paying attention to the quality of the data and its output format is essential for smooth data analysis. «Data science is the easy part. Getting the right data, and getting the data ready for analysis, is much more difficult» [4]. The 2016 Data Science Report found that 60% of Data Scientists' work time is spent «cleaning and organizing data» [5]. To minimize the effort here, the quality, level of detail and file format should be as constant as possible.

Countless data can then be fed into a software, which begins parsing and translating the previously somewhat abstract data in an intelligible way. From the translated data, innumerable evaluations and analyses can be created with a wide variety of considerations and objectives.

5. Examples from practice

For profitable solutions and concepts that are elaborated on the basis of data analyses, clear objectives should be defined. In this way, the analyses, evaluations, and simulations are designed precisely to meet the need. The following are some practical examples of how holzbau.tech has used data analytics in the context of production planning.

5.1. Simulation automated blowing of loose insulation

In this example, numerous walls of a company were analyzed using their data. Predefined parameters were used to specify which compartments could be insulated automatically and which could not. The result can be seen as an example in Figure 4. The analysis revealed a proportion of the structural compartments that the intended technology would not be able to process. With this knowledge, planned systems can be optimally redesigned so that the automated processes become possible. Alternatively, as it also makes sense here, the construction design can be changed so that non-automatable areas are avoided and thus machine stops do not occur because of this.

If only individual reference walls were considered instead of a mass data analysis, this would most likely result in a different proportion and sources of error would remain undetected.

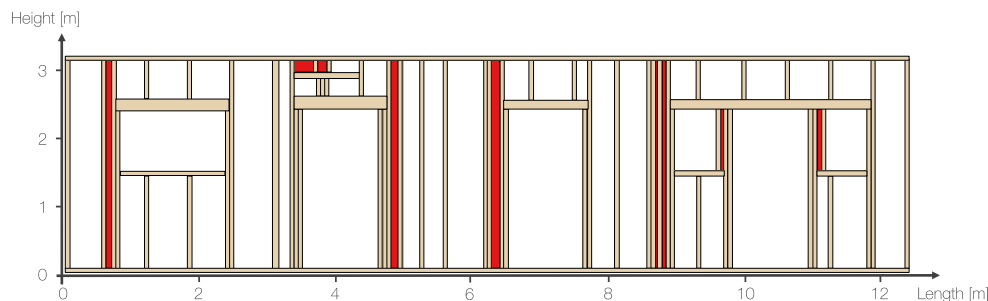


Figure 4: Example element: analysis by holzbau.tech, which spaces cannot be insulated automatically (red)

5.2. Waste analysis when machining 13m timber

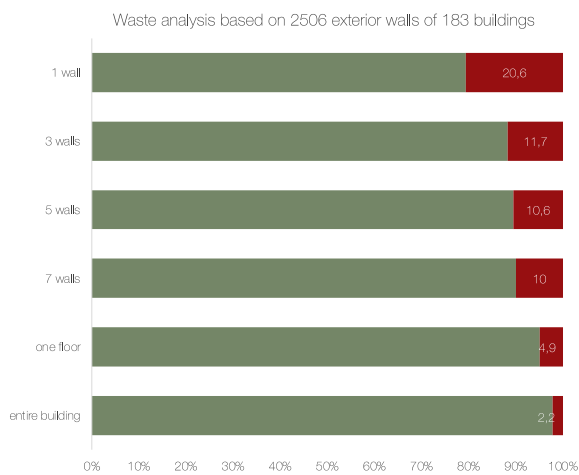


Figure 5: Waste analysis when machining 13m timber

Most timber construction companies process 13m long raw timber for the individual components of the elements. In order to generate as little waste as possible, the parts for one element are usually not cut individually, but combined in batches of several elements. In this way, the different timber parts are distributed more optimally among the long raw timbers and the timber is better utilized. The analysis carried out here (Figure 5) shows the effects of the batch size on the waste. It can be seen that the more parts are combined in one batch, the less waste is generated.

With this knowledge, productions can adjust their wood cutting accordingly. For the downstream process, this means sorting the parts of a batch after it has been machined for their particular element, so that the assembly process for the elements gets the right parts at the right time. In process development, therefore, it is not only the cutting process that has to be considered, but also the downstream sorting process and the respective effort involved.

5.3. Analysis of the wall dimensions

Figure 6 shows the analysis of well over 2000 walls and displays the distribution of the dimensions. Usually, one quickly focuses only on the average. However, if one wants to create a production layout with new workstations, for example, the big picture should be considered. To return to the above example of the 13m-long tables, we look in particular at the rear part of the evaluation. We can see that the distribution of dimensions decreases significantly after 9m length. Consequently, when planning new tables, it becomes evident that they do not necessarily have to be 13m long. Most walls can be made on shorter tables. One possible course of action would therefore be to design the production layout for predominantly smaller walls. The few walls that are longer can then be produced on a custom processing table. In this way, significant space can be saved and used more sensibly.

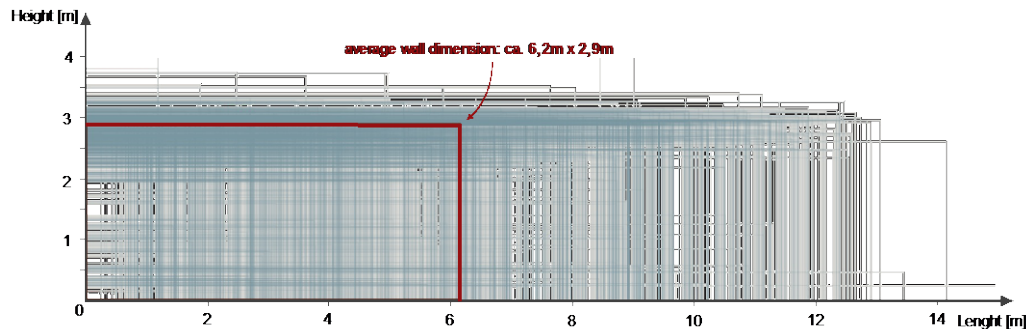


Figure 6: Analysis of the wall dimensions

5.4. Software tools to enable professionals to analyze data

The examples described above were made by IT experts on the basis of previously clearly defined objectives. However, the IT partners often lack the necessary expertise to recognize or understand errors or inconsistencies in the evaluations. This often results in long consultations and revisions. To avoid this waste in the processes, the approach of creating software tools for experts makes sense. This can be, for example, an online tool that is programmed specifically for a customer and addresses the specific issues. The data required for evaluation is implemented there and can be analyzed in a user-friendly manner. Optimally, the deciding experts can then use this tool and set parameters as desired to identify different effects. For instance, if a potential sales price has an impact on the overall profitability of a project, different values can be entered and different results can be compared (Figure 7).

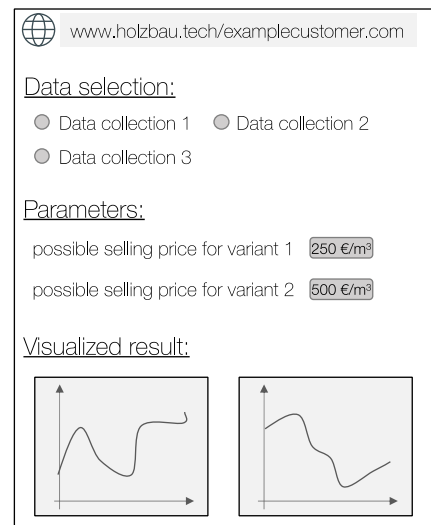


Figure 7: Example of a software tool

6. Conclusion

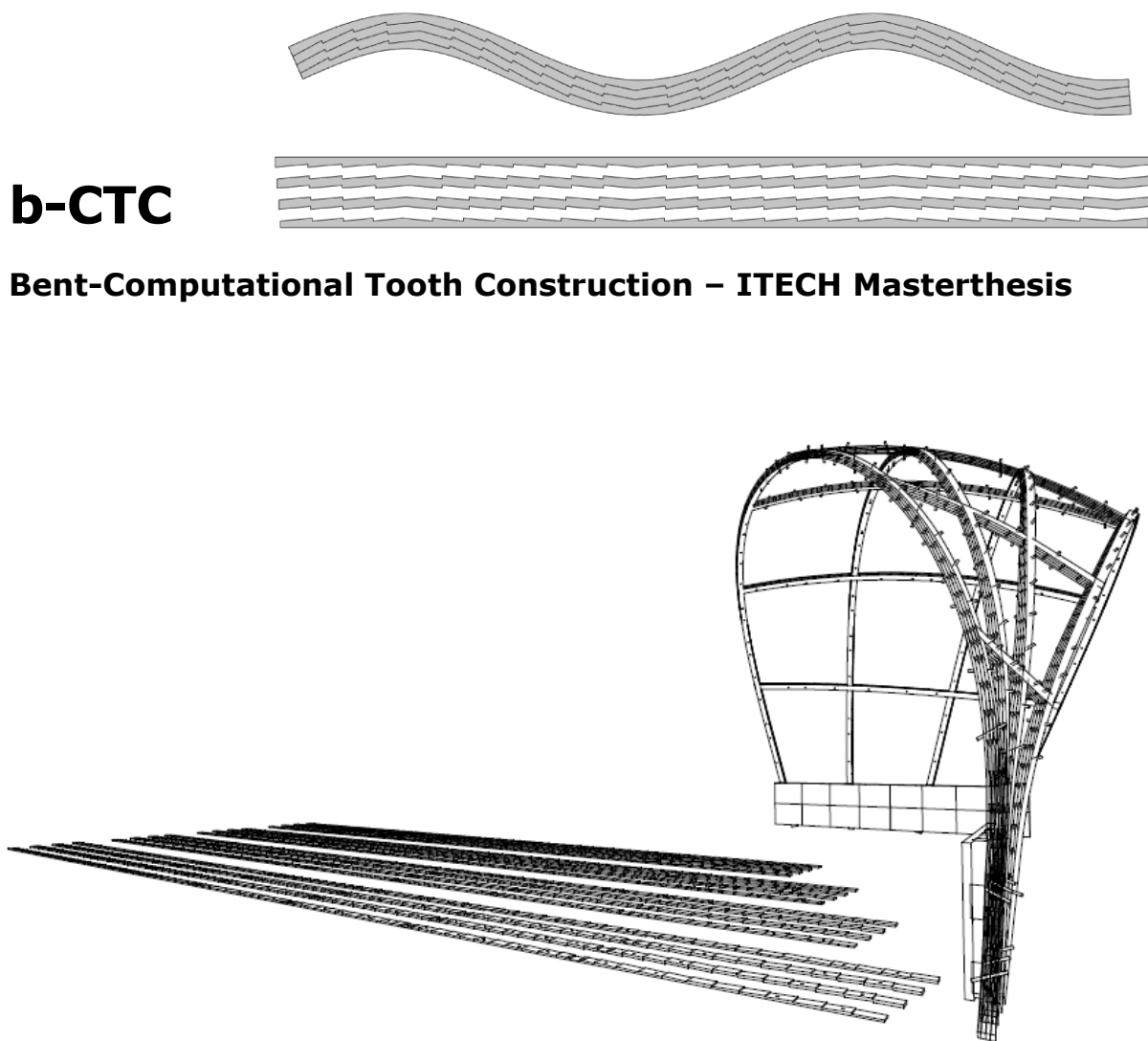
In conclusion, the use of data holds huge potential for the timber construction industry. It is important that the understanding for data analysis is created and that timber construction companies realize that they have these possibilities and how they can take advantage of them.

7. Sources

- [1] Kabelitz-Ciré, Rainer (2022): *LAGEBERICHT 2022*, Holzbau Deutschland Bund Deutscher Zimmermeister, Holzbau Deutschland – Bund Deutscher Zimmermeister im Zentralverband des Deutschen Baugewerbes e.V., [online] https://www.holzbau-deutschland.de/fileadmin/user_upload/eingebundene_Downloads/Lagebericht_2022.pdf [abgerufen am 24.10.2022].
- [2] Prause, Gerd (n.d.): BIM im Holzbau, Baunetz Wissen, [online] <https://www.baunetzwissen.de/holz/fachwissen/planungsprozesse/warum-braucht-der-holzbau-einen-anderen-planungsprozess-6969531> [abgerufen am 27.10.2022].
- [3] dach+holzbau (2014): Einfacher BTL-Import, in: *Dach+Holzbau*, no. 06/2014.
- [4] McKinsey Analytics (2018): *Analytics comes of age*, McKinsey & Company, [PDF] <https://www.mckinsey.com/~media/mckinsey/business%20functions/mckinsey%20analytics/our%20insights/analytics%20comes%20of%20age/analytics-comes-of-age.pdf>.
- [5] *Data Science Report 2016* (2016): CrowdFlower, [online] https://visit.figure-eight.com/rs/416-ZBE-142/images/CrowdFlower_DataScienceReport_2016.pdf [abgerufen am 28.10.2022].

b-CTC

Bent-Computational Tooth Construction – ITECH Masterthesis



Miro Bannwart
IDBH, BFH/AHB
Biel, Schweiz



Bent-Computational Tooth Construction

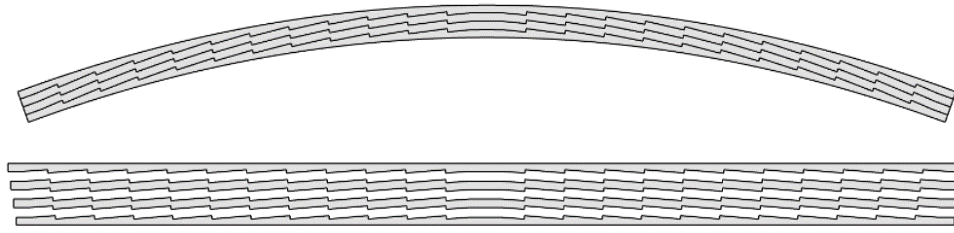


Figure 3: Teeth beam principle, defined curvature through longitudinal teeth patterns

1. Introduction

Bent-Computational Tooth Construction (B-CTC) was developed as an architecture master thesis, aiming to build and design free form structures using bent and interlocked solid timber tooth beams. The timber tooth beam technique, developed by master carpenter Hans Ulrich Grubenmann in the 18th century, allows interlocking bent solid wood beams at a defined curvature. The resulting geometry is determined by a carved tooth pattern on the long side of straight manufactured beam components. The technique has rarely been used since the development of glulam beams, which at the time were cheaper to fabricate than interlocked tooth beams. With contemporary fabrication methods such as CNC machinery and robotic fabrication, however, tooth beams can be fabricated far more efficient than at the time of their invention. Applying integrated digital design to fabrication workflows, the thesis aimed not only to reconsider single tooth beams, but to develop the tooth beam technique further towards its integration into complex architectural and potentially doubly curved shapes. Therefore, the development of beam overcrossings as well as the development of assembly methods constitute important parts of this thesis. Fabricating tooth beam components as flat elements can reduce fabrication complexity significantly and additionally allows efficient transportation. Furthermore, this thesis, with its purely geometrical approach, aimed to use neither glue or glued wood products nor screws. This makes it possible to disassemble a built structure and potentially reuse the wood. Therefore, B-CTC can be allocated within the field of sustainable and ecological architecture.

2. Relevance

2.1. Ecology

A large majority of today's scientists consider man-made climate warming as a fact [J. Cook 2010]. While climate-change processes have been known for several decades, public attention to them is rapidly increasing only nowadays. It may be viewed as a task of contemporary architecture to respond to this tendency in society and therefore develop more ecological building solutions. Owing to the fact that wood binds CO₂, building with wood has a positive impact on climate warming. Therefore, every novel wood building system has the potential to lower the effect of climate warming.

2.2. Economy through a short production chain

To produce conventional complex freeform glulam beams, firstly trees get cut, then the trees are cut into thin lamellas, these lamellas are then glued together again to finally mill the desired shape. B-CTC, a freeform approach as well, has a significantly shorter production chain: The trees are cut, then lamellas get cut, which then directly can be processed into tooth beam components by subtractive milling processes. While the final shape of current freeform glulam beams mostly is milled at curved glued and prefabricated wooden workpieces, fabricating tooth beam components as flat elements reduces the fabrication complexity significantly, and additionally allows more efficient storage and transportation. Further, it must be considered that glued wood cannot be recycled and reused as effectively as solid wood. Glued wood products are, compared to tooth beams, not detachable and cannot be disposed ecologically. To burn glued wood, special permissions and emissions filters are needed.

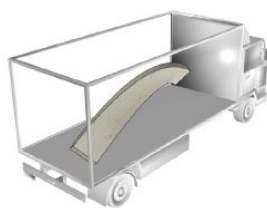


Figure 4:
Transport of a prefabricated freeform glulam beam



Figure 5:
Transport of multiple prefabricated tooth beam lamellas

2.3. Flat fabrication and transportation

Whereas the final shape of current freeform glulam beams is mostly milled from curved glued and prefabricated wooden workpieces, fabricating tooth beam components as flat elements reduces the fabrication complexity significantly and additionally allows for efficient storage and transportation.

2.4. Complex wood design

B-CTC can be applied, similar to well-developed glulam freeform approaches, in complex freeform shapes. As opposed to glulam approaches, b-CTC relies on solid wood exclusively. Therefore b-CTC does not aim to replace existing glulam approaches but rather to complement these as a valid solid-wood-only design and construction alternative.

2.5. In contemporary carpentry

Further, b-CTC is an opportunity for contemporary carpentries and local sustainable economies. CNC-Machines have become, even for smaller carpentries, more and more affordable. Carpenters in need of a curved beam will, with b-CTC, be able to cut their own tooth beam components inhouse, preferably with local wood, instead of ordering a glulam beam from a specialized company far away.

3. Scope: From design towards fabrication and assembly

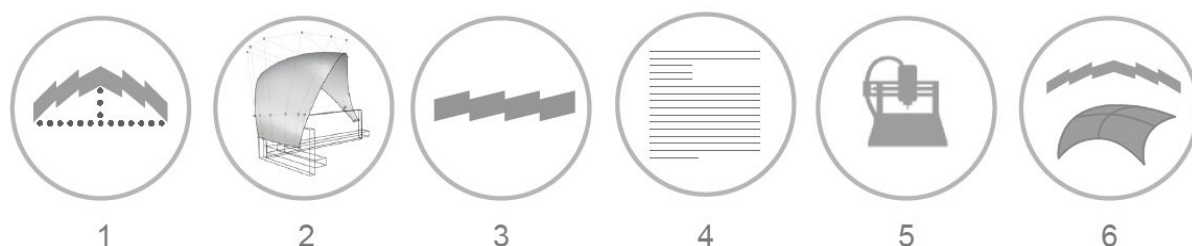


Figure 6: Graphic Scope

In order to integrate the traditional tooth beam technique into contemporary complex wood designs, the scope of b-CTC comprises multiple digital and physical steps: Maximal bending tests (1), digital architectural design methods (2), digital algorithms to calculate tooth geometry (3), CNC-code generation methods (4), fabrication (5) and assembly processes (6). These steps have been investigated and developed in order to fabricate and assemble a 1:1 proof of concept prototype pavilion structure. In this project, b-CTC focused on the loadbearing structural wood construction only and did not investigate any covering façade systems, which would make a tooth beam structure watertight. Further, it was decided to exclude any structural analysis from this research and focus on a purely geometrical approach only.

4. Context and State of the Art Projects

4.1. Between preformed and post-formed wood constructions

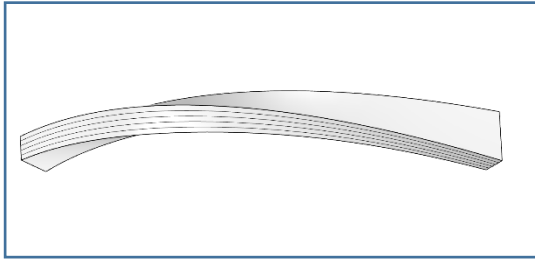


Figure 7: Twisted conventional layered glulam beam

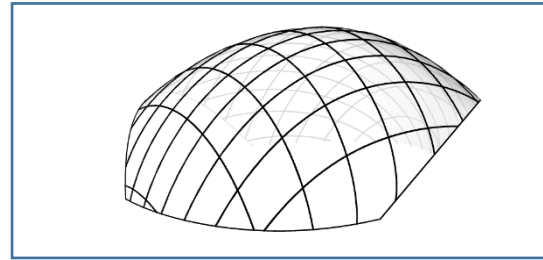


Figure 8: Conventional bent gridshell structure

In today's freeform wood construction, the most common approach to fabricate complex building components is to glue complex shapes from multiple thin layers and further carve them into shape with elaborated and complex CNC-milling processes. Such preformed components can be prefabricated with high accuracy in CNC-equipped companies, and then be assembled relatively easy on site. A typical post-formed construction approach is the grid shell construction system. Multiple layers of solid wood are laid out in a flat grid on site to then be pulled into shape by a crane in a force-consuming process (e.g. Multihalle Mannheim by Frei Otto, 1975). B-CTC, also assembled through an on-site bending process, but from prefabricated lamellas with shape defining tooth patterns, can therefore be allocated between preformed and post-formed construction approaches.

4.2. Historical inspiration



Figure 9: Wintersey bridge



Figure 10: Tooth-beam at the Wintersey-bridge

The technique to define the shape of an arc by bending multiple layers of heavy beams together and interlocking them by a tooth pattern has previously been applied in multiple bridges in Switzerland, by the master carpenter Hans Ullrich Grubenmann (1709 – 1783). The Wintersey bridge, constructed in 1839, (fig. XX) located between the municipalities Hasle and Rüegsau close to Bern in Switzerland, spans 60 meters without pillars [Meyer-Usteri, 2004]. Built with tooth beams as primary structural elements, this bridge is stabilized additionally by a combination of trusses and different wood-joinery methods. At the two sides of the bridge, the bent tooth-beam components form arc-shaped beams, similar as it would be done today with glulam beams. Therefore, both this bridge and the tooth beam method can be considered as having been ahead of their time.

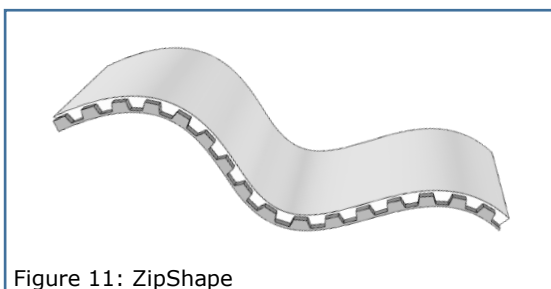


Figure 11: ZipShape

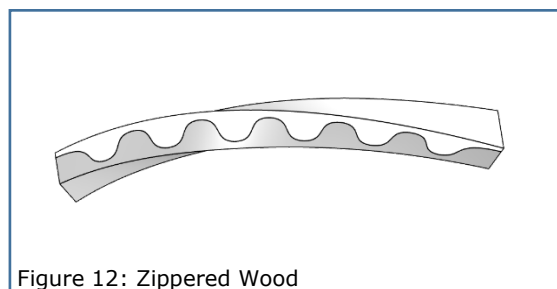


Figure 12: Zippered Wood

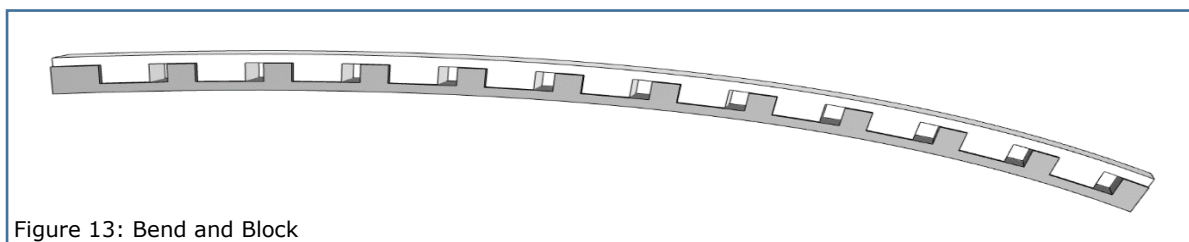


Figure 13: Bend and Block

4.3. ZipShape, a contemporary approach in furniture

Since 2007, Christoph Schindler has been developing the ZipShape as a universal approach to fabricate single curve panels from any plane material without molds [Schindler et. al., 2011]. Like in heavier tooth beams, as used in bridges, interlocked geometry defines the curvature of the product. Unlike the traditional tooth beams, however, the main part of the cross section consists of interlocked teeth, whereas the remaining part of the cross section is very thin in order to achieve a high curvature.

4.4. Zippered Wood

This project, a collaboration of the University of British Columbia's HiLo Lab, the University of Colorado, Denver's LoDo Lab, and HouMinn Practice [Shapiro, 2020], demonstrates the currently increasing fascination of this topic across the globe, as it was developed in parallel with the present work. Zippered Wood is a system development which allows to fabricate curved and twisted wooden beams. The Zippered Wood approach can realize a maximum of possible curvatures due to its geometrical zipp-pattern setup with minimal effective lamella thickness. Yet, this in turn also drastically reduces the effective load bearing capacity because almost all fiber-layers in the wood lamellas are cut. Therefore, Zippered Wood structurally relies on the glue which is used to connect the carved lamellas.

4.5. Bend and Block, A self-shaping dynamic approach

At the University of Applied Arts Vienna, Austria, Efilena Baseta developed a novel approach named «Novel bending-active system with controllable curvature-stiffness relation». Instead of locking beams at a defined curvature as seen in the Ramseyebrücke, by which the beam components are prevented from bending back into their flat state, this approach defines the maximum bending range of beams by preventing further bending by increasing the systems stiffness. This is achieved by blocking them, using rectangular teeth patterns [E. Baseta]. The blocking position and range of possible bending is defined by the size of gaps between the teeth.

5. Method

5.1. Development through digital and physical control loops

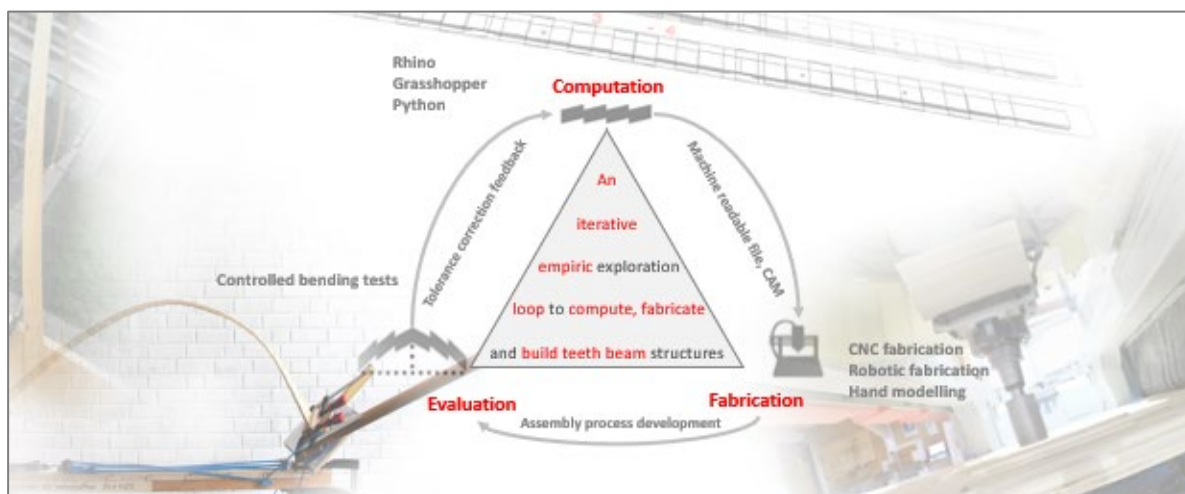


Figure 14: Computation, fabrication, and evaluation principle



Figure 15: First physical tests for evaluation and approximation of a predefined target curvature

To develop a digital workflow within the ecosystem of the Rhino and Grasshopper design and fabrication CAD environment, multiple custom grasshopper codes have been developed. To constantly improve this developed computational model, which is capable of transforming a design input into a fabricable geometry output, the cycle of physical testing, digital development, fabrication and evaluation of the built result was repeated multiple times on different levels. Firstly, the developed codes were mainly applied on single teeth beams to physically approximate digitally defined shapes. To achieve that, it was firstly tested physically how much raw single lamellas of a defined thickness could be bent, then a corresponding digital teeth beam model was set up in order to CNC-fabricate a physical model, which could be compared to the digital one in terms of accuracy and deviation. The result of such deviation evaluations could then be integrated into the computational model to constantly improve the accuracy of the overall workflow.

6. Results

6.1. Forces and geometrical setup of single beams

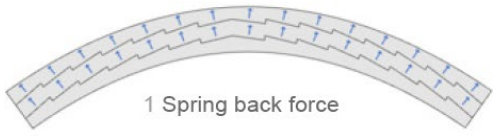
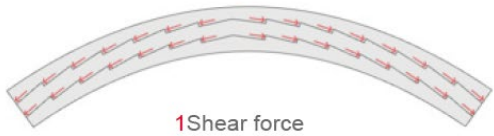






	 1 Spring back force	 1 Shear force
Conventional teeth beam	 Screws	 Teeth
Glulam beam	 Glue	 Glue
b-CTC	 Dowels	 Teeth

Figure 16: Forces

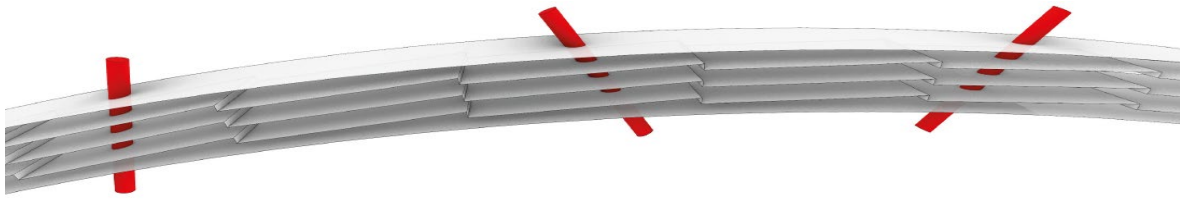


Figure 17: Inclined b-CTC dowels

Tooth beams consist of components which are fabricated in their straight stage and afterwards bent and locked together. Therefore, two main forces occur in a tooth beam: A spring-back force and a shear force. In a conventional tooth beam, the spring-back force is compensated by an iron screw, whereas the shear force is compensated by the tooth-pattern, which is always deployed in the correct direction against the shear force. Aiming to use solid timber only, and neither glued wood products nor screws, inclined wooden dowels are used in b-CTC tooth beams to replace the screws that hold back the snap-back force in conventional tooth beams.

6.2. B-CTC system limitations

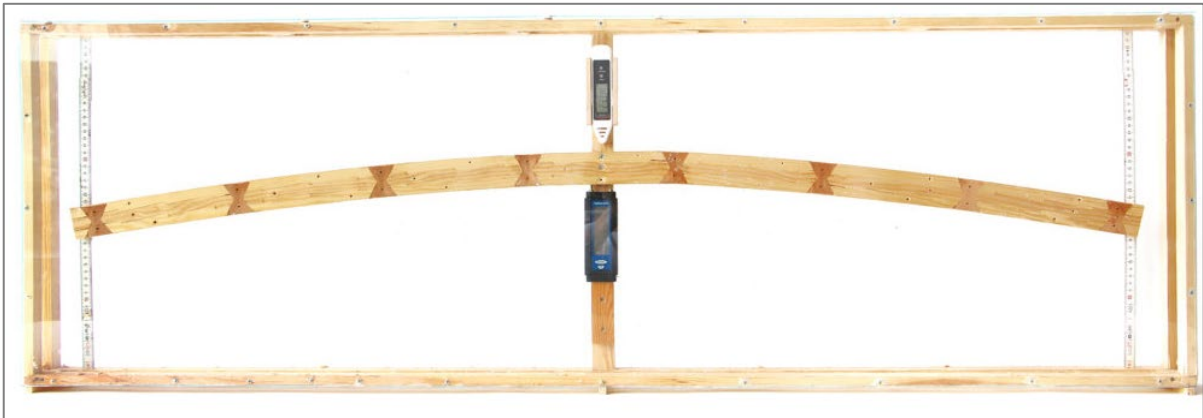


Figure 18: «HygroSim» testing set-up, a plexiglas box to observe beams under humid conditions



Figure 19: «BendMax-TwistoMat» testing set-up, to simultaneously bend and twist tooth beam lamellas

To explore the limitations of the maximum possible simultaneously twisting and bending of tooth-lamellas (see 7.3 Integration of tooth-beams in doubly curved designs), a custom testing setup was created. 100 degrees of twist at a 2-meter-long lamella of a cross-section of 60 to 12 mm with 3 mm teeth depth, bent simultaneously to a depth gauge of 500 mm, could be confirmed. Thinner lamellas were not tested because they need to be at least 8 mm to fix them on the CNC-table by screwing. The maximal possible simultaneous bending and twisting constraint is important especially in complex doubly curved

overall designs with multiple overcrossing teeth beams, since the overcrossing node situation can potentially request additional twisting of the lamellas to align with the overcrossing neighbor beam (see 7.3 Integration of tooth beams in doubly curved designs). Further, a tooth beam test model was observed in a plexiglass box under constant relative air humidity of 90% or more for 17 days. Due to the fact that wood deforms by changing its humidity content, which occurs significantly more in radial and tangential than in longitudinal direction (along which the teeth of a tooth beam lamella are aligned), the change in curvature of a 140 cm long test-tooth beam remained low as expected. Changes were below those that would be of significance for the aimed project at the pavilion scale. In addition, b-CTC beams that are integrated as loadbearing structural elements in built architecture can be completely covered and would therefore not be impacted by moisture.

6.3. Integration of tooth beams in doubly curved designs

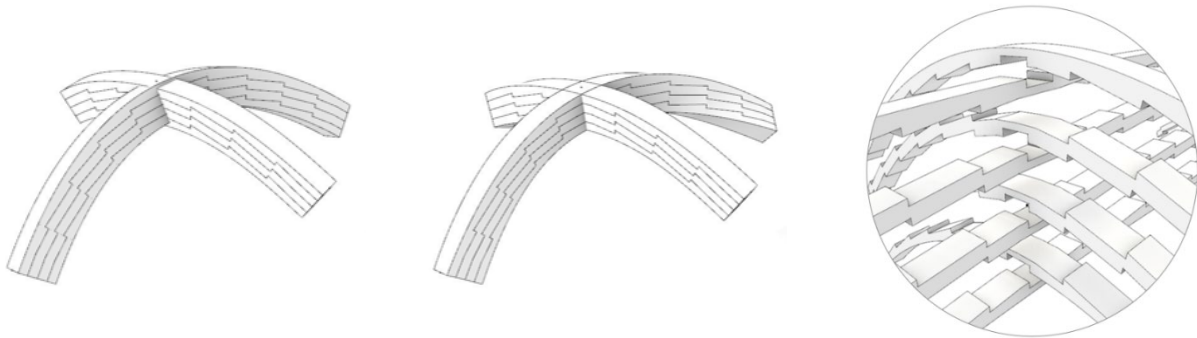


Figure 20: Single curved node

Figure 21: Curved and twisted node

Figure 22: Half-half out cuts

Aiming to develop a lightweight but stable construction system, which is capable of being applied in complex doubly curved designs, it was decided to order the teeth beams in diagrid patterns. To reduce the moment forces at the nodes of the diagrid pattern, the single tooth-beam lamellas cross each other without being cut into shorter elements. To maintain the structural height of the structure, the overcrossing lamellas are interlocked with half-half out-cuts to over cross themselves in their cross-section. This geometrical node setup would be impossible to fabricate with traditional single curved tooth-beams applied in a diagrid pattern on a doubly curved complex shape because the node intersections would be extremely complex and not efficiently fabricable. The solution was to twist the tooth beams additionally to the single curved bending.

6.4. Straight tooth geometry computation – curved and twisted

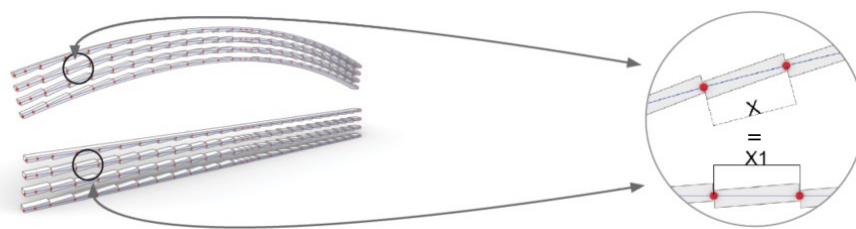


Figure 23: Computation from curved to straight

The core of this research was to develop a computational method that can calculate a straight geometrical representation of a bent target tooth beam component geometry. This was achieved with the following method: The straight stage of a beam was reconstructed depending on those parameters of the beam, which do not change during the bending process: the tooth beam lamellas middle lines and their thicknesses. While the middle line and the beam thickness do not deform, the upsides of the lamellas experience an elongation and the lower sides a compression. To compute the straight geometry is a relatively simple process. Yet, complexity increases as soon as multiple tooth-beams of a whole structure, overcrossing and intersecting each other, have to be calculated. The calculation of the straight representation of bent and additionally twisted beams can be done

with the same method as single curved beams due to the fact that the crucial parameter of the beams' non-deforming middle line is not affected and transformed by additional twisting. To approximate the target curvature and to overcome production inaccuracies as well, a tolerance system was integrated into the computation, which allowed to create minor gaps between the teeth contact surfaces by an input parameter.

6.5. CNC – Fabrication

To CNC-fabricate the final prototype, the highly accurate 5-Axis Reichenbacher Vision 3 model 4105 CNC machine of the Treppenbau.ch AG could be used. The CNC-readable file was generated with the AlphaCam software based on the digital geometry that was created with multiple custom codes. With a milling tool of a diameter of 5 cm, all tooth-beam lamellas could be milled efficiently. To rotate the lamellas on the CNC-table 180 degree around their longitudinal axis to mill tooth patterns on their top as well as on their lower side, the lamellas had been fixed not only by screws, but additionally by positioning dowels, which allowed an accurate flipped repositioning. Over one month, this setup was developed and tested repetitively. The effective milling of the prototype pavilion lamellas took approximately three days with 9 hours of CNC-machining.

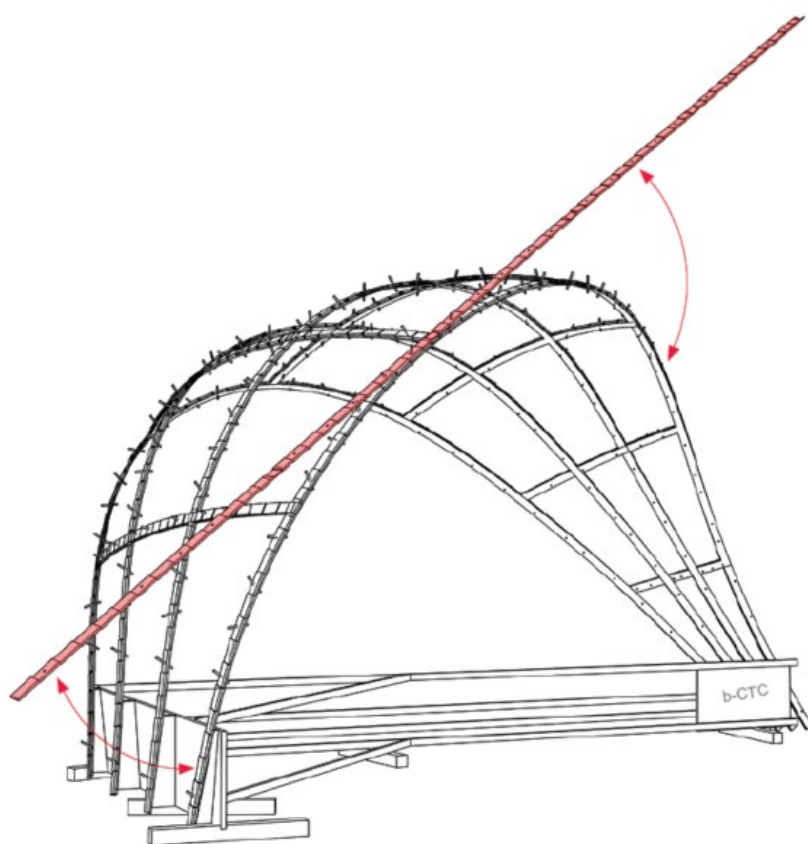


Figure 24: Layer-by-layer assembly process

6.6. Assembly

Having multiple overlaying tooth beam lamellas at the tooth-beam structure nodes, the only possible way to assemble was a layer-by-layer assembly process: By completely assembling every layer, including the overcrossing components, it could be avoided that components cover each other, and therefore overcrossing elements could not be inserted anymore. To assemble a tooth-beam structure as an only wood system without any screws, and relying as conceived on inclined wooden dowels, the following was tested at the prototype pavilion:

In areas of lower curvature, the developed wood-only dowel-connection was shown to work. In areas of higher curvature, several screws were necessary to prevent the lamellas from bending and snapping back.

6.7. Evaluation of the prototype pavilion

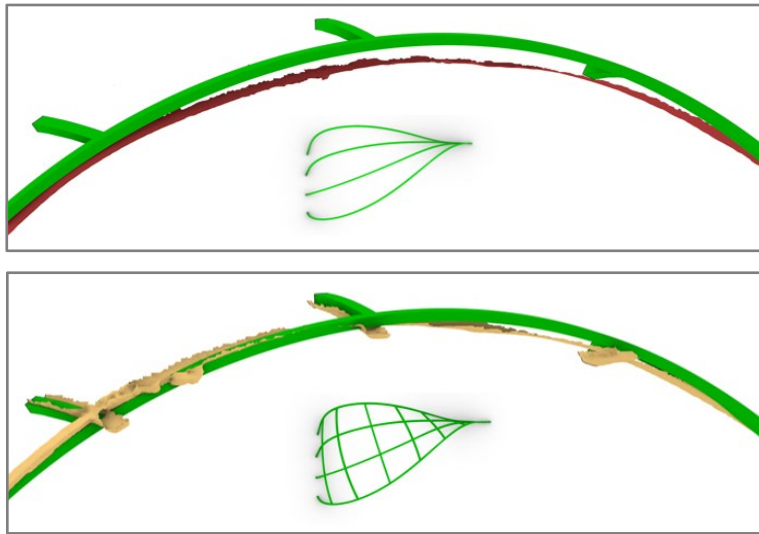


Figure 26: Scan 2, after the complete assembly of all lay-

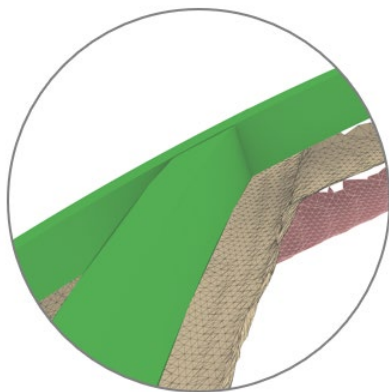


Figure 27: Overlay
scan 1 and scan 2

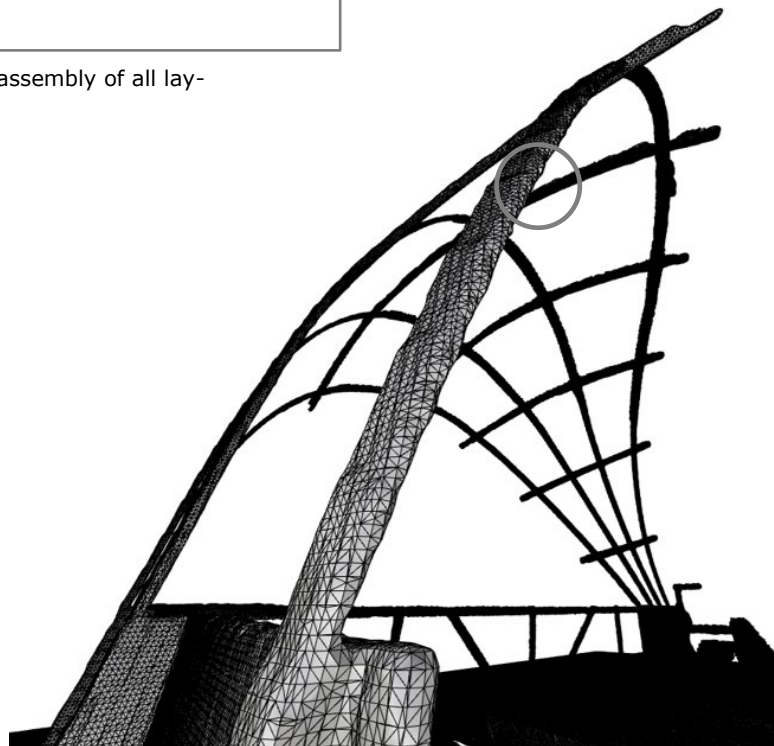


Figure 28: Complete mesh, scan 2

To further improve the developed integrated design towards fabrication workflow, the built prototype pavilion was accurately scanned using a laser scanner. Scanning was performed first during construction after having completed the first layer, and then after the complete assembly. The deviation of the first scan (red, layer 1, with no teeth impact) showed a high deviation of maximally 14 cm compared to the digital twin geometry (green). Scanned after the complete assembly (yellow), the maximal deviation was reduced to maximally 5 cm. In current wood construction, this is still a relatively large deviation, nevertheless it was considered a general success that the structure, with maximal bending close to twisting limits, could successfully be assembled and installed at the planned location, the Zeughaus in Teufen, Switzerland. The measured deviation might derive firstly from the extreme lightweight construction geometrical setup (overall weight of the structure below approx. 62 kg) and secondly from a relatively large digitally implemented security tolerance between the teeth contact surfaces of 1 mm. Therefore, the Autor is confident that accuracy issues can be handled conveniently in future projects.



Figure 29: The finished prototype pavilion at Zeughaus Teufen in Switzerland, spring 2020

7. Discussion and outlook

The conducted research was consolidated into a design, fabrication and assembly workflow for complex contemporary tooth-beam structures. The completed prototype pavilion proves the functionality of the developed systems for small-scale architectural projects. This inherently raises the question whether the developed systems could be used to accomplish large-scale architectural projects as well. Different scenarios in building construction below the achieved complexity are conceivable. Any construction that is commonly built with glulam beams can potentially be constructed using tooth-beams. This range of application covers complex doubly-curved designs as well as less complex single-curved or flat designs with or without beam overcrossings. By being constructed without glue and without glued products, the proposed approach consisting of solid wood only can additionally be interesting for architectural designs following the philosophy of building with pure and low-processed natural materials.

To be applied in such scenarios, the developed systems would need further refinements. With large scale beams, systems would have to be tested concerning accuracy and load bearing capacity. Given this, any contemporary carpentry with a CNC machine at its disposal would be capable of fabricating tooth-beam components and would therefore be capable of accomplishing simple as well as complex designs without being dependent on external specialized glulam beam production companies. Therefore, with b-CTC, possible future production chains could be significantly shorter, less energy consuming, and therefore more ecological than today's building-construction-production chains that rely on common glulam beams.



Figure 30: The prototype pavilion at Zeughaus Teufen in Switzerland, winter 2020



Figure 31: The prototype pavilion at Zeughaus Teufen in Switzerland, winter 2020

8. Acknowledgements

Thanks a lot, to:

Ulrich Vogt, the curator of the Zeughaus Teufen wood construction museum for enabling the prototype pavilion in front of the Zeughaus Teufen

Adrian Scherrer from Treppenbau.ch AG for enabling the collaboration with Treppenbau.ch AG

Everybody from Treppenbau.CH AG for helping to make the final prototype pavilion possible

Pirmin Fischbacher from the **Innoholz AG** for providing high quality swiss solid wood

The **ITECH M.Sc. class 2019** for assisting through many discussions

Hans Jakob Wagner, research associate at the Institute for Computational Design and Construction **ICD** at the University Stuttgart, for tutoring this thesis

Simon Bechert, research associate at the Institute of Building Structures and Structural Design **ITKE**, for tutoring this thesis

Katja Rinderspacher, research associate at the Institute for Computational Design and Construction **ICD** at the University Stuttgart for organising many ITECH thesis issues

Professors **Achim Menges**, Director of the, Institute for Computational Design and Construction **ICD** at the University Stuttgart, for supervising this thesis

Professor **Jan Knippers**, Director of the Institute of Building Structures and Structural Design **ITKE**, for supervising this thesis

The b-CTC research was realized as a master thesis in the framework of the Integrative Technologies and Architectural Design Research M.Sc. Program (ITECH) at the University of Stuttgart, led by the Institute of Computational Design and Construction (ICD) and the Institute of Building Structures and Structural Design (itke).

The work was partially supported by the German Research Foundation under Germany's Excellence Strategy – EXC 2120/1 - 390831618.

To consolidate the b-CTC thesis to this publication as a part of the Forum Holzbau 2021 was supported by the Autor's current affiliation Berner Fachhochschule Architektur Holz und Bau.

9. References

- [1] Cook J., 2010, Gibt es wirklich einen Klimawandel?, Cook J., viewed 25.10.2020, 15:35h <https://www.klimafakten.de/behauptungen/behauptung-es-gibt-noch-keinen-wissenschaftlichen-konsens-zum-klimawandel>
- [2] Shapiro G.F., 2020, Ward: Zippered Wood Twists the Standard 2x4 to Craft New Forms, viewed 25.10.2020, 15:35h https://www.architectmagazine.com/awards/r-d-awards/award-zippered-wood-twists-the-standard-2x4-to-craft-new-forms_o
- [3] Meyer-Usteri, K., 2004, Holzbrücken im Emmental und bernischen Oberargau, Burgdorf, Egger Kommunikation, p. 3
- [4] Schindler C. Salmerón M.E, 2011, Zipshape Mouldless Bending 2 – A shift from Geometry to Experience, Ljubljana, Proceedings of eCaaDe Conference 29, p. 1
- [5] E.Baseta, 2019, Novel bending-active System with controllable curvature-stiffness relation, e-journal archidoc, Vienna, Vol 16, p.4,

Degrees of Parametrization: Rewiring design-to-construction for prefab modular products

Alejandro Arruñada
Technische Hochschule Rosenheim
Rosenheim, Deutschland



Degrees of Parameterization

1. Introduction

The wood construction industry is going through a pivotal moment. The use of innovative materials and practices are awarding this segment of the construction industry with worldwide recognition, financial interest, and the opportunity to rethink the design-to-construction process. We can now see that utilizing wood as a primary structural element complemented with secondary modular and/or prefabricated components – also made from wood – can make a lot of sense. At the same time, breakthroughs in cloud-based platforms, generative design, VR, AR, robotic fabrication, machine learning, and AI – to name a few – allow us to reimagine the future of construction.

However, for small and medium enterprises (in the following referred to as SME's), investing in these solutions may simply be cost and know-how prohibitive. From an SME's point of view, dissecting the extent of digital solutions with good fit and discerning their overlapping functionalities and compatibilities, is tough enough. More complicated still are the challenges faced in the planning stages of a project. Which are intensified in the wood construction industry by the lack of standards, inconsistent building norms, and a misunderstanding of construction and manufacturing constraints by many customers. This master thesis focused on the sequence of events occurring in the planning stages of a project from the perspective of a small specialty subcontractor. Considering the first interactions in sales to the delivery of fabrication data. The study acknowledges that owners, architects, and general contractors should be able to quickly, and reliably, compare alternatives for cost control and expediting schedules. But it also recognizes the challenges a subcontractor providing design-to-construction products encounters while designing, engineering, coordinating, and fabricating their scope of work. And how these create complicated and sometimes overwhelming conditions that only well-balanced enterprises can handle. The proof of concept was meant to provide aspiring subcontractors in this space with a product development strategy that can easily translate schematic proposals into production-ready BIM models.

2. Integrative Design

«While the information-based world is now moving exponentially, our organizational structures are still very linear (1).»

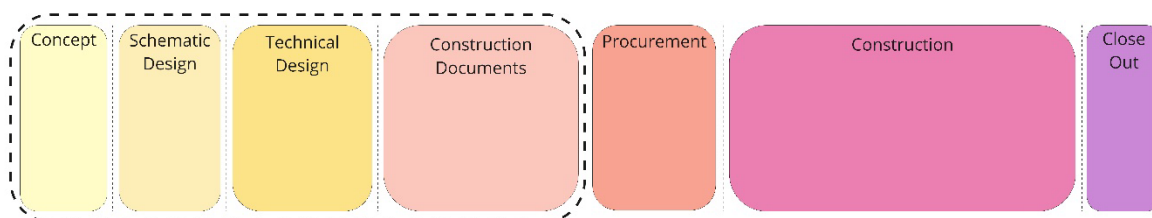


Figure 2.0.1: Universal Construction Stages. (Diagram by Author)

According to the book *Architecture Design Data* by Phillip G. Bernstein, the construction process around the world is fairly universal and has mostly remained intact for decades (2). Figure 2.0.1 is a representation of the seven typical stages of a construction process and highlights those dedicated to planning. Changing scales, specialty subcontractors providing Engineered to Order (in the following referred to as ETO) services also follow a sequential pattern. One that flows from general to specific as information is gathered and integrated into the working model. Figure 2.0.2 shows a generic version of a product creation process (in the following referred to as «PCP») for an ETO architectural product.

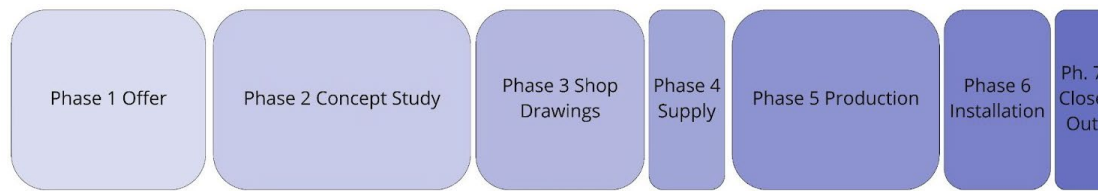


Figure 2.0.2: Product Creation Process. (Diagram by Author)

This thesis recognizes that architectural designs are multi-variant, dependent on an intricate interplay of factors ranging from aesthetic to technical to economic. That a product is selected by balancing questions of appearance, performance, availability, and cost (3). Because most construction projects are unique, adaptations to ETO products are prevalent. In construction, there are different trends and pressures in the market creating an expectation that individualized design and sublime craftsmanship can or should happen faster and cheaper than ever before. (4)

On the other hand, just-in-time (in the following referred to as «JIT») supply chains and manufacturing methods have spread throughout the construction process. These sequential schedules, although effective, also require a high degree of communication and clear transitions among the different stakeholders at every stage. «But construction is a dynamic process that relies heavily on an understanding of sequence, assembly logic as well as complex orchestration of labor, materials, and delivery – not to mention cash flow (5).»

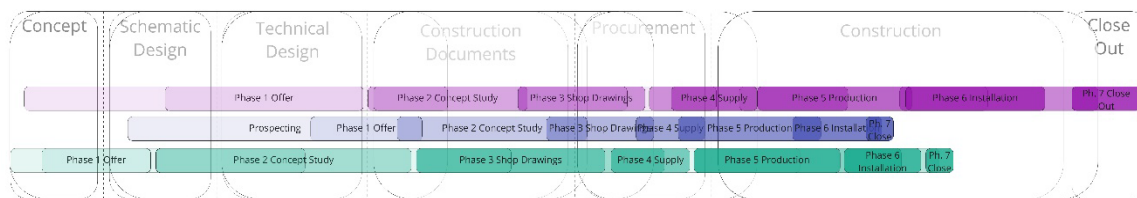


Figure 2.0.3: Different PCP's across the Universal Construction Stages. (Diagram by Author)

Figure 2.0.3 overlays a few Product Creation Processes over the Universal Construction Stages of a construction project. This diagram is meant to help visualize the simultaneous progression of several ETO products (micro) across the different stages of a construction project (macro). This figure also shows the «waterfall effect» occurring within each subcontractor's PCP. The overlapping areas represent setbacks in the product's progression. For example, activities or work packages began in one phase are carried to subsequent phases until completed. These delays can occur for many reasons. Among them is the unreliable precision and timing of the exchanges of information among stakeholders (6). In essence, we don't get what we need when we need it. And when we do, it's wrong, off, or missing key details. But why? An argument made is that modifications are mainly carried out by manually adjusting a model via typing commands, clicking, picking, and dragging in a 2D and 3D environment. Meaning, that they take time and are prone to human-error.

In 2020, a study in Chile analyzed the behavior and performance of a design and engineering team working on a 2-story building. In short, the experiment tracked each participant's log data. And examined the relevance of commands used, and their effect on the progression of the project

Table 2. Total number of commands executed by each designer.

Designer	Total	Contributory Commands			Non-Contributory Commands			Contributory Vs Backwards
		G	NG	C	N	U	B	
Architectural	9430	1770	169	372	3291	3228	657	2150
Structural	6433	1353	203	228	2470	920	1296	1425
Mechanical	5555	1032	121	141	2496	726	1039	1052
Electrical	6523	1296	165	184	2918	994	966	1401
Plumbing	7360	1190	366	165	3101	776	1762	1309

G: Geometrical modeling; NG: Non-geometrical modeling; C: Collaborative; N: Necessary; U: Unnecessary; B: Backwards.

Table 2.0.4: Total number of commands executed by each designer. [Table 2.](#)

(Image courtesy of Forcael & et al., 2020)

Table 2.0.4 is an excerpt from the study and summarizes the findings. The number of times the designers typed in the wrong command, hit back, exit, or undo, makeup about one-third of all commands. (7). This finding aligned with the author's experience perfectly and became the focal point for the proof of concept (in the following referred to as «POC»). In short, it triggered the following question. How can we get to zero non-contributory commands?

The same study in Chile recommended improvements in the precise timing of information delivery to improve activity flows and streamline the work packages. But JIT logistics align material orders from suppliers directly with production schedules (8). Consequently, timing becomes everything. Therefore, being able to update the working model with speed and accuracy is crucial. The team handling the model must ensure that the information passed on between departments and 3rd parties is accurate every step of the way.

According to the Innovation Scouting Report, data-driven technologies and business models can only truly be scaled when the current silo mentality is overcome (9). As the construction industry goes through its digital transformation, attempts towards holistic building systems for wood-based multi-story developments have emerged. In most cases, the aim is to standardize design solutions that work in a multitude of environments and minimize the complexity in managing all the stakeholders along the value chain. One system under development is from Build-in-Wood (in the following referred to as «BiW»), a European Horizon 2020 project focused on offering high-quality, affordable, and environmentally friendly housing with timber construction. Figure 2.0.5 lists a set of criteria for the BiW building system and contains a couple of illustrations exemplifying its sequential characteristics.

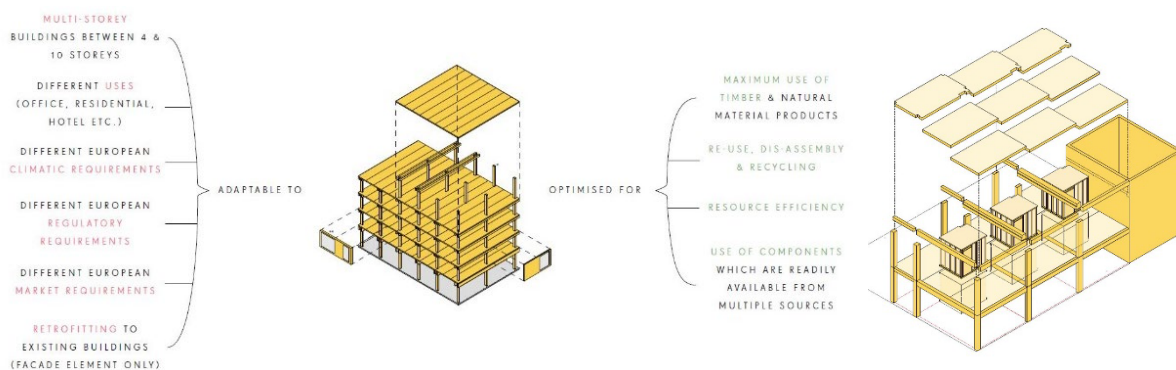


Figure 2.0.5: Left Image: Build in Wood Building System Criteria. Right Image: Installation sequencing.

(Images courtesy of Build in Wood and Waugh Thistleton Architects)



This project has received funding from the European Union's Horizon 2020 research and innovation programme under grant agreement No 862820.

One area of investigation for BiW is the integration of third-party modular components. Among the benefits identified by BiW for using non-structural pods in their system is to shorten the on-site construction program and standardize components and installation processes. During the development of this thesis, the researcher represented Tjiko GmbH as a consultant for wet areas with BiW. This collaboration serves as a good example for the cross-integration of knowledge among trades. On one end, subcontractors providing ETO products can be much wiser when developing their designs and fabrication processes. On the other end, BiW builds consensus on how to best integrate modules and their technical arrangements with the other systems in the puzzle.

3. Research Partner: Tjiko GmbH



Figure 3.0.1: Tjiko Products. (Pictures courtesy of Tjiko)

Tjiko GmbH is a start-up from Rosenheim offering design-to-construction solutions for prefabricated modular bathrooms. Figure 3.0.1 gives a glimpse of finished products at different phases. The firm emerged from the Technische Hochschule Rosenheim in 2017 with a clear vision to pioneer in the efforts to reduce building costs for construction by 50%. The author joined Tjiko as Product Developer in early 2019.

In a multi-story prefab building, the bathroom pod is just a piece in the puzzle. But an important one. Their placements can have a substantial impact on the larger MEP strategy. And from a design perspective, their position and functional features influence the shape and activities of the adjacent spaces. When Tjiko collaborates on the MEP strategy early on and the batch size is a good fit, integrating tangential functional elements into their modules can be advantageous. It reduces the management of different trades and combines steps during the installation stage. Figure 3.0.2 shows a consolidated module of a fully functional bathroom pod with a floor-to-ceiling fenestration, including a built-in kitchen, and a built-in closet unit.

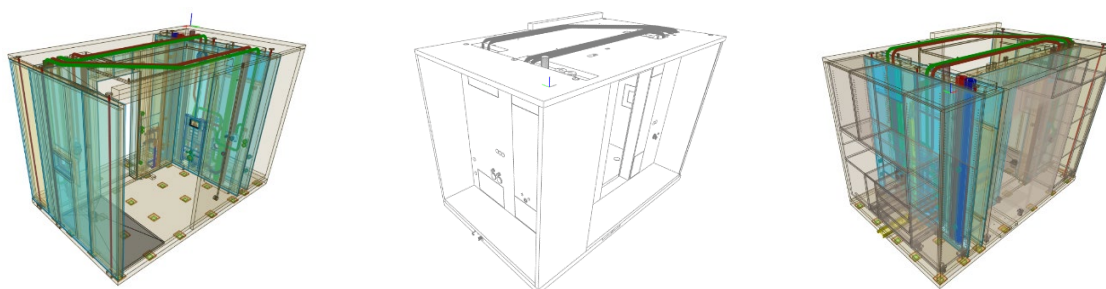


Figure 3.0.2: Multi-functional Module. (Screenshots courtesy of Tjiko)

Tjiko also responds to the fact that bathrooms within the same building may come in a range of sizes, may be standard, accessible, or barrier-free, and come with a variety of washroom assets, accessories, and finishes. Figure 3.0.3 shows a bathroom-pod floor plan with three different options concerning the placement of the vertical service shaft. In a best-case scenario for the production, all modules would be stacked vertically. However, depending on the requirements and orientation of the units within each level, the modules can have multiple door placements, rotated, mirrored, and/or staggered vertically. Therefore, the number of product variations force Tjiko to maintain a highly organized operation to produce small batches efficiently.

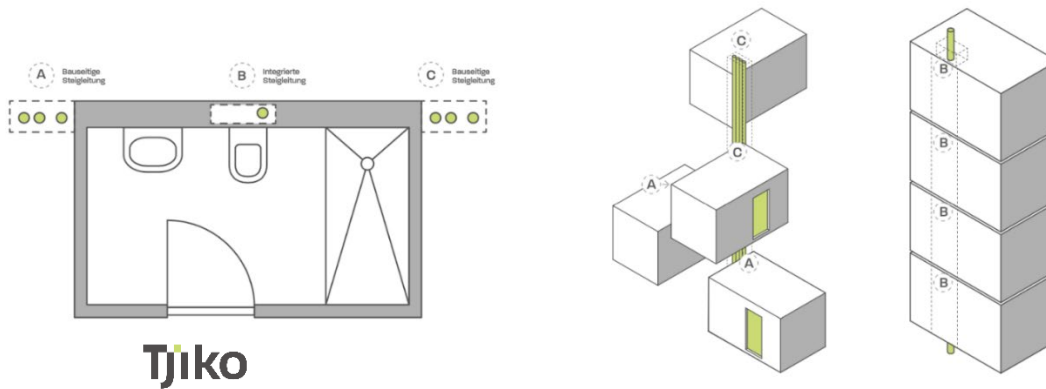


Figure 3.0.3: Tjiko System Integration. Das Tjiko Bad. (Images courtesy of Tjiko)

4. Proof of Concept

The POC called Degrees of Parametrization (also referred to as «D.o.P.» or «D.o.P. System») was carried out with Tjiko from June to December 2020. A strategy for product development was devised to respond to the challenges faced by Tjiko in the planning of bathroom modules for their small batch production. It was noted during the design and product development that offering standardized, partially customized, and fully personalized products was fundamental. According to Merriam-Webster, the definition of *parameterize* is simply «to express in terms of parameters»(10). When designing, determining which aspects or parameters of the product can be personalized by the customer is fundamental. This is a delicate step because every added customer input reverberates across the system and can seriously increase the scope of work. Therefore, maintaining a balance between the default inputs and the customizable inputs is key. In this context, products with a minimal amount of customization choices contain a high degree of parametric inputs that have been automated, or preselected, by the designer. In contrast, custom modules with more selectable variables, by default, have a lower degree of parameterization since those automated steps become manual inputs.

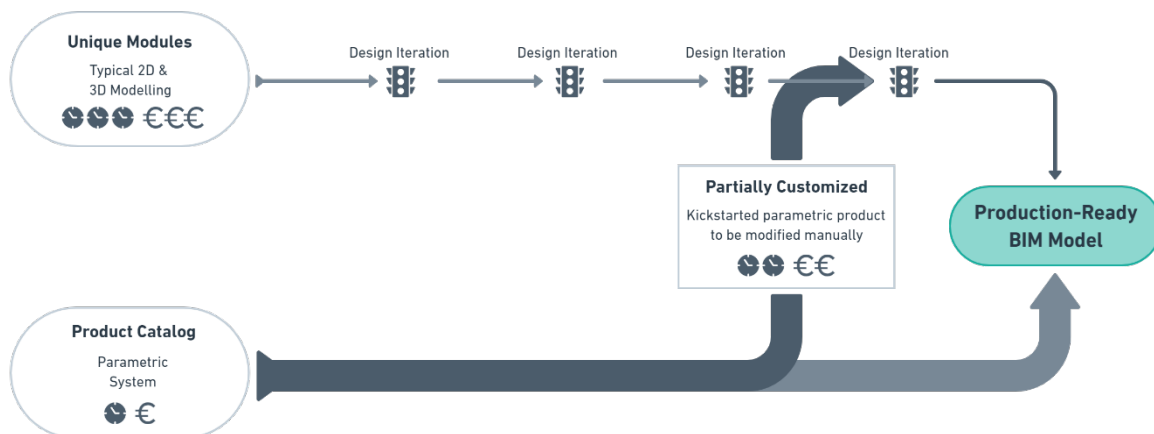


Figure 4.0.1: Tjiko Product offerings. (Diagram by Author)

This POC focused exclusively on the design, development, and execution of all products within the product catalog. Figure 4.0.1 illustrates the three product offerings and implies longer durations and higher costs for delivering small batches of unique bathroom modules compared to standardized modules.

4.1. Das Tjiko-Bad

The product catalog (aka «Das Tjiko-Bad») constitutes the backbone of information for the parametric framework. In short, a customer working with Tjiko can choose between different «models» (bathroom layouts) and «design lines». The design lines include functional and aesthetic items that include the sanitary assets along with the material and color palettes. Once the final dimensions, the design line, and the model type are determined, the documentation of customer inputs is done. From Tjiko's point of view, this format enables the implementation of standards and helps reduce choice overload for the customer. Figure 4.1.1 shows some of the models offered in the product catalog and the «Zermatt» design line.

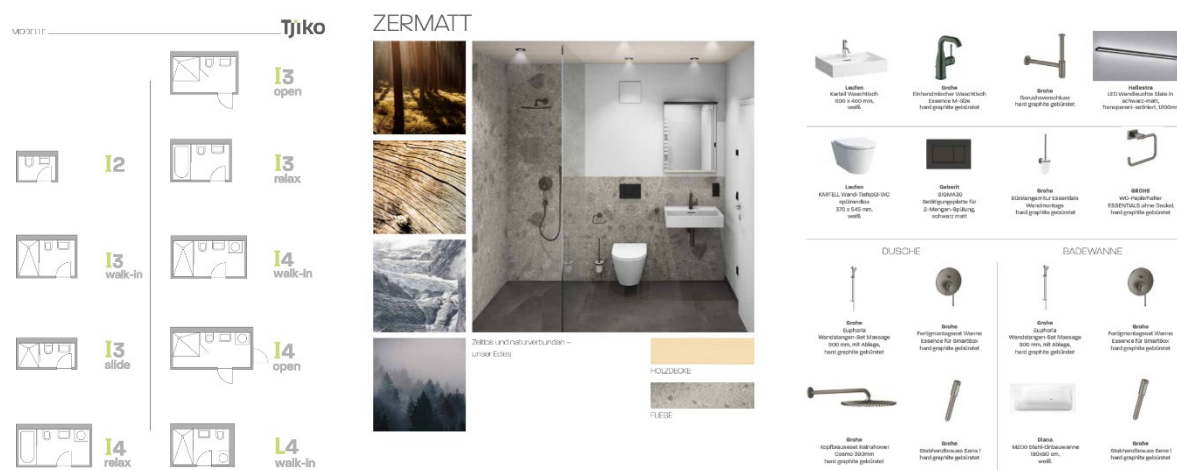


Figure 4.1.1: Das Tjiko-Bad. (Images courtesy of Tjiko)

4.2. Implementation

ModSpecs			
DIMENSIONS (mm)	Model Type	Select Design Line:	
Exterior Width	Product 'A'	Zermatt	
2425	Floor Panel Family	Door	WC
Exterior Length	CLT Type 1	Supplier9_model10001_RSwing_885x2032mm	Supplier24_model4321_400x600mm
3895	Wall A Family	Door Electrical Drilling Template	Radiator
Exterior Height	Wall Type 1	Supplier58_model1010_L1.3.2	Supplier36_model1551_1800x450mm
2350	Wall B Family	Washbasin	Tiles Family
	Wall Type 3	Supplier24_model1234_550x650mm	Supplier12_model54C_600x300mm
	Wall C Family	Shower or Bathtub	Lighting Concept
	Wall Type 2	Supplier22_model1087_1000x1400mm	Supplier62_LED001_AreaBased
	Wall D Family	Shower or Bathtub Fittings	Niche
	Built Up Floor Family	Supplier36_model17890_AP-ShowerSet	Supplier16_model8888_260x400mm
	Built Up Floor Type 2	Washing Machine	Furniture
	Roof Panel Family	Supplier28_model5555_750x850mm	Supplier29_model4185_WM750x850mm
	CLT Type 1	Washing Machine Electrical Drilling Template	
		Supplier58_model1010_SS_1.2	

Table 4.2.1: Left: Example drilling template. Right: Generic set of ModSpecs. (Table by Author)

Some of the programs used for this POC were already part of Tjiko's technology stack. Such as Excel, Autocad, and hsbcad. Revit and Dynamo were chosen to implement computational design workflows. Dynamo is a plug-in that allows designers to create algorithms for a wide array of applications. From data processing to generating geometry (11). The term «ModSpecs» refers to the Excel spreadsheet with the customer inputs. This file is what tells the Dynamo graph what to generate in Revit. Table 4.2.1 shows an example set of ModSpecs. The inputs, in bold, are selected from dropdown menus while the rest of the data in the sheet auto-propagates based on the selected inputs. This format reduces naming variations and errors when running the Dynamo graph. Once the ModSpecs are completed and saved, the design team opens Revit and launches Dynamo. In essence, once the designer runs the Dynamo Graph, the functions specified in Dynamo are manifested in Revit. Figure 4.2.2 shows a screenshot of the Dynamo UI and the graph used to generate the bathroom models in this POC. The 3D model on the right is a .ifc model exported from Revit after running this Dynamo graph. This model is very basic but more than enough for early coordinating and estimating.

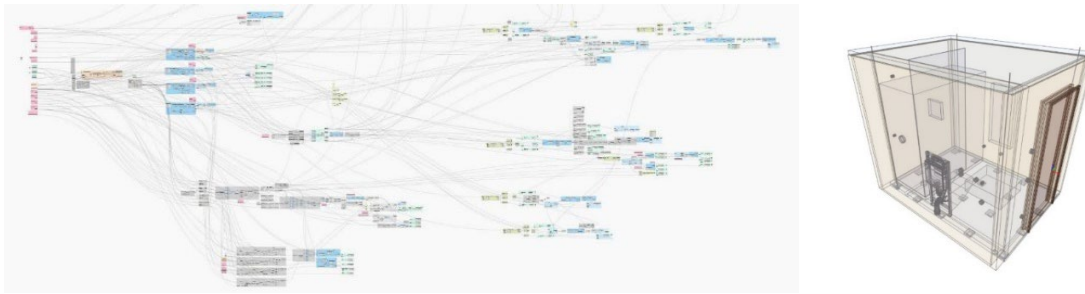


Figure 4.2.2: Left: Design Script 1. Right: .ifc export after running Script 1. (Screenshots courtesy of Tjiko)

Because a project flows from general to specific, subcontractors avoid overinvesting in schematic proposals. Understanding that design is an iterative process, spending too much time on a solution that will likely change, or be replaced by another idea, is unproductive. However, if the Dynamo script could consistently build accurate 3D models in a fraction of the time, then delivering a quick turn-around without overextending resources during the estimation phase could be achieved. If a customer changes the specifications of a product, the team could quickly generate a new one instead of manually editing the previous one. Significantly cutting back on manual 3D modeling.

Only until a letter of intent or a contract is signed, would the Project Manager run a separate sequence of Dynamo graphs that read the existing model's geometry and parameters to apply the corresponding hsbcad TSLs. For example, LED lights, electrical outlets, and asset mounting patterns are translated into box-cuts and void drills and applied to the CLT panels and sheathing layers on the wall elements. In addition, these scripts kickstart the documentation process by creating a set of cross-sections and sheets, placing those sections in the sheets, and populating the Titleblock based on the inputs in the ModSpecs. Seriously reducing tedious and repetitive tasks with a workflow that minimizes mistakes.

Unfortunately, at the time of this POC, hsbcad had not released its hsbStickFrame package for Revit. Therefore, the near-finished Revit model was exported with the hsbcad exporter tool and imported into Autocad with the *HSB_IMPORTMODELX* command. Afterward, a series of manual steps convert the walls and the stick-frame spacing logic is applied. At this point, the project manager can switch into «default mode». Meaning that the process to complete the product and take it to «production-ready» status was carried out by typical 3D modeling in Autocad. Figure 4.2.3 shows a typical WC drilling pattern that would be applied with hsbcad as 'void drills' via Dynamo. The 3D image is from the .ifc model exported from Autocad. This model is shared with the leading party and other technical partners to check for collisions and the integrity of all MEP connections. Lastly, the figure shows a sheet kickstarted with Dynamo.

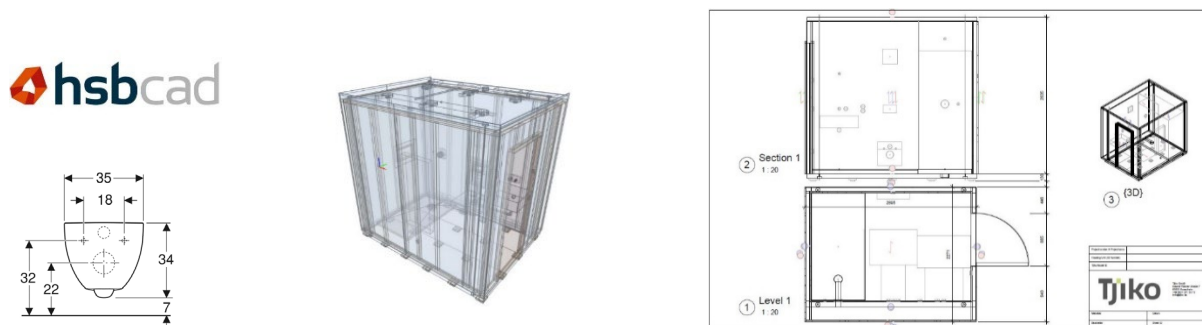


Figure 4.2.3: Left: Mounting pattern translated to hsb drills. (Image courtesy of hsbcad and Geberit, n.d.)

Middle: .ifc export from Autocad. Right: Revit sheet kickstarted by Dynamo. (Screenshots courtesy of Tjiko)

4.3. Results

The D.o.P. System provides a delivery model for standard products that begins in the sales phase. However, the team decided to first test the effectiveness and reliability of the Dynamo graphs on an ongoing project with good fit. Figure 4.3.1 illustrates the start of the POC with the rhomboid labeled ModSpecs and ends with the production data milestone.

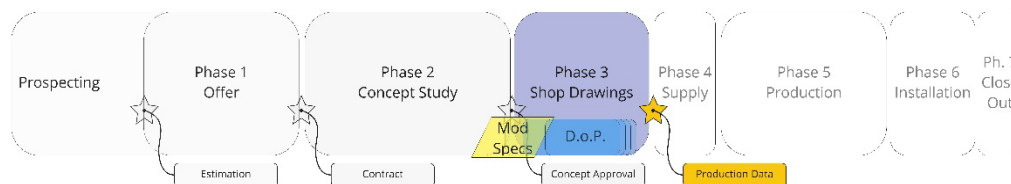


Figure 4.431: POC tested within Phase 3 of the Tjiko PCP. (Diagram by author)

The contracted design was very similar to a standard model. And began by generating the model in Revit and exported it to Autocad. This model ended up substituting the original model used in estimation. Then, the new model went through a typical course of clash detection and MEP updates. Once approved, it was exported as an .ifc file and sent to Tjiko's suppliers (Phase 4). A few weeks later, Tjiko's production received the components and assembled the parts (Phase 5). Figure 4.4.2 shows the stick frame walls and the drilling patterns for the washroom assets, on the left. The middle picture highlights the operations done to the CLT roof panel. And on the right, the pre-assembled modules are split into batches and finished out.



Figure 4.4.2: Prefab walls, CLT panels, and assembled modules from the POC. (Pictures courtesy of Tjiko)

Because this was a partially customized product, it still took the project manager a considerable amount of time to coordinate and finalize the planning. Overall, implementing the D.o.P system just reduced the workload by approximately 15 hours. Nothing revolutionary. However, those 15 hours - that would have been spent manually building the 3D model - were replaced by a workflow that lasted 35 minutes. Approximately 24 times faster. Figure 4.4.3 provides a table, on the right, that delineates the durations of each step in the POC. The bar graph and pie-chart illustrate how despite contributing up to 15% of the total workload, the D.o.P. System took less than 2% of the total planning duration.

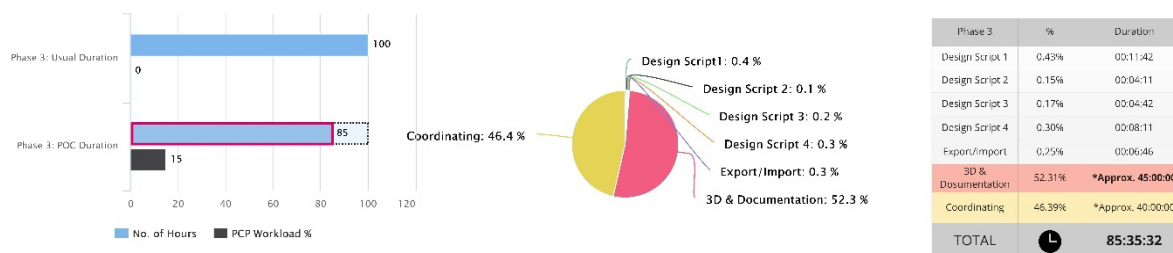


Figure 4.4.3: Step durations in POC. (Tables and charts by author)

5. Analysis

The impact on the total planning time was low. But it was expected. Transferring to AutoCAD and making it unique really slowed down the team. However, if standard products could be sold instead of customized modules, this solution offered great potential. With tools like Dynamo and Grasshopper, developing a highly flexible and customizable product is possible. It's just a matter of proficiency with computational design tools, good systems thinking, and a highly motivated and organized team.

When working with unique product variations, using AutoCAD with hsbCAD allows for the highest range of customizability. But it comes at a cost determined by the feasibility of developing these unique solutions in relation to the batch size in production. Knowing that not all projects consist of low variations and high volumes, improving the feasibility of small batches for production is key for a small organization like Tjiko. A 60% reduction of total planning time was predicted if a standard product was left unaltered. Translating into quicker turnarounds for smaller batch sizes.

5.1. Rewiring

In many cases when a project is completed, its information is archived and forgotten. By comparison, this system is designed to salvage and repurpose the knowledge gained in a project cycle. Figure 5.1.1 shows a rewired L3 model. Which was repurposed from the I3 model used in the POC. The time spent readapting the workflow took approximately 15 hours.

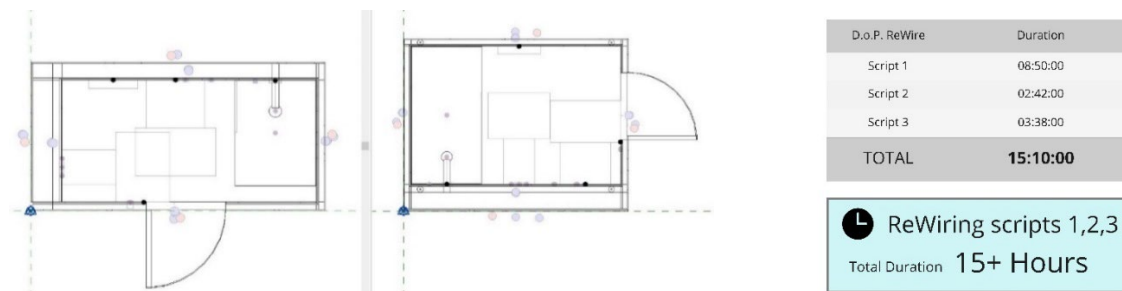


Figure 5.1.1: Left: L3 Model. Right: I3 model. Rewiring duration. (Screenshot courtesy of Tjiko)

If a unique project were to meet certain benchmarks – such as volume and technical recurrences – rewiring the scripts for a personalized solution might make sense. In turn, this new script could be offered as a new model type in the product catalog.

6. Conclusion

This thesis argued that the planning stages themselves, have become the bottleneck for new construction. For companies going through a digital transition, implementing computational design strategies could become the difference between stagnation and growth. According to Bernstein, regardless of how much architects and design professionals are criticized, or wrongly accused, for never stopping the design, the profession will remain at the center of construction. «Design operates at the headwaters of the entire building enterprise, and design information – no matter who might create it – is still the necessary lifeblood of construction. Understanding, controlling, and coordinating how the information assures that a design converts into a built artifact will be our central challenge in a world where digital modeling, machine expertise, high resolution data sets and algorithms become part of the modernized building industry. The tools are certainly available and at our beck and call, we only have to decide to use them (12).»

Publisher FORUM **HOLZBAU**

Bahnhofplatz 1, 2502 Biel/Bienne, Switzerland

T +41 32 372 20 00

info@forum-holzbau.com, www.forum-holzbau.com

Machining and typesetting: Simone Burri, Katja Rossel, Katharina Uebersax

© 2022 by FORUM HOLZBAU, Biel/Bienne, Schweiz

ISBN 978-3-906226-50-7